1-17-2018 10:00 AM

The Production of Pyrolytic Biochar for Addition in Value-Added Composite Material

Douglas Matthew Cuthbertson
The University of Western Ontario

Supervisor
Berruti, Franco
The University of Western Ontario Co-Supervisor
Briens, Cedric L.
The University of Western Ontario

Graduate Program in Chemical and Biochemical Engineering
A thesis submitted in partial fulfillment of the requirements for the degree in Master of Engineering Science

Abstract

Pyrolytic biochar has recently gained attention for its potential value as a carbon sequestering by-product that can be used in industrial applications. While biochar is typically targeted for soil amendment applications, higher value applications such as addition in consumer products and building materials needs to be investigated.

In this study, biochar is produced from three different Canadian feedstocks using three different pyrolysis methods. The biochar is characterized to determine the effects that feedstock selection and pyrolysis conditions have on biochar properties. The biochar is also incorporated into concrete at varying concentrations to create a lightweight and sustainable material. The effect of biochar addition on the mechanical strength, as well as the thermal and acoustic properties of the concrete is studied. Biochar was also added to polymer composites. The carbon microstructure was analyzed, and the effects of biochar on the dielectric properties of the composite material was determined.

Keywords

Biochar, pyrolysis, Miscanthus, Dried Distiller's Grain, concrete, composite, Mechanically Fluidized Reactor

Co-Authorship Statement

Chapter 1

All literature research and writing was performed by the author.

Chapter 2

The FESEM imagery as well as the EDX analysis on the produced biochar was analyzed at the Applied Science and Technology Department (DISAT) at the Politecnico di Torino, Italy, by Mauro Giorcelli, Alberto Tagliaferro, and Massimo Rovere. The production of the biochar as well as all other characterization was performed at the Institute for Chemicals and Fuels for Alternative Resources by the author with the assistance of post doctorates and laboratory technicians.

Chapter 3

The biochar used in concrete production was produced in the ICFAR MFR 100, and characterized by the author. The concrete samples were all prepared by the author in the ICFAR facility, and the density of the samples was measured as well. The compressive strength, acoustical absorption, and thermal conductivity were measured at the Department of Architectural Science at Ryerson University in Toronto by Dr. Umberto Berardi.

Chapter 4

The high temperature, CO_2 activated biochar was produced at ICFAR in the Jiggle-Bed Reactor by a previous PhD student, Anastasia Colomba. Raman spectroscopy analysis, biochar conductivity, and composite permittivity were determined by the DISAT at the Politecnico di Torino by Mauro Giorcelli, Alberto Tagliaferro, Patrizia Savi, Isabelle Bianco, and Massimo Rovere. The predictive method for determining the biochar dispersion in polymers, as well as all consequent testing and analysis was performed by the author.

Acknowledgements

I would like to thank my supervisors Dr. Franco Berruti and Dr. Cedric Briens for bringing me into this project and offering me support and guidance throughout my research. Their time and assistance was crucial in every stage of my research, and I am extremely grateful.

I would like to thank the people who aided me throughout my work:

Clayton Cook, Cody Ruthman and the rest of the UMS for building the equipment I work with, and fixing everything that I managed to break. Thomas Johnston, for his technical assistance on guidance on the various systems I worked with. Venkateswara Reddy Kandlakuti, for his laboratory assistance and for the analytical tests he performed on my material. The ICFAR postdocs and research team, for providing guidance and assistance. I would be nowhere without the support of everyone.

A special thank you to the various research teams around the world. Dr. Umberto Berardi at Ryerson University; Dr. Amar Mohanty and Dr. Manjusri Misra at the BDDC at the University of Guelph; Dr. Alberto Tagliaferro, Dr. Mauro Giorcelli, Dr. Patricia Savi, and Dr. Pravin Jagdale at the Politecnico di Torino. Thank you to all the researchers who performed testing on my material, and invited me to their laboratories and conferences over the years.

Thank you to NSERC, NSERC (Engage) and the Ontario Research Fund (ORF, RE7), for providing the funding for my research and to attend several wonderful conferences, and to SGPS for awarding me with my scholarship. Thank you to Verti-Crete of Toronto and Mr. Phillip di Palma for sponsoring my research and supplying me with the materials to complete my work.

Finally, I would like to thank my family and friends. My parents and grandparents, who have always been my biggest supporters, and who have been there for me through every day of my research. My friends scattered across Canada, for their continuous encouragement. The friends I made at ICFAR, for sharing many wonderful memories. To Avery Weintraub, for lifting me up after my bad days, and for the love and support over the last half year. To Matt Guglietti, for being there for me when I needed it most, and for being the best friend I could ask for. And to all those I forgot to mention, I could not have finished this without the help of the people around me. This thesis is as much yours as it is mine.

Table of Contents

List of Figures

List of Tables

Abbreviations and Nomenclatures

AC: Activated Carbon

BC: Biochar

BET: Brauener, Emmet, and Teller surface area, m^2/g

CEC: Cation Exchange Capacity

CNT: Carbon nanotubes

DDG: Dried Distiller's Grain

CO_2e: Carbon Dioxide Equivalent

EDX: Energy Dispersive X-Ray

EMI: Electromagnetic Interference

EMW: Electromagnetic Wave

ESP: Electrostatic Precipitator

FTIR: Fourier-Transform Infrared

GHG: Green House Gas

HTT: Highest Treatment Temperature, ℃

H/C: Ratio of Atomic Hydrogen to Atomic Carbon

ICFAR: Institute for Chemicals and Fuels from Alternative Resources

ICP: Inductively Coupled Plasma Optical Emission Spectroscopy

MEKP: Methyl Ethyl Ketone Peroxide Catalyst

MFR: Mechanically Fluidized Reactor

MS, AWF: Miscanthus provided by All Weather Farms

MS, Drumbo: Miscanthus harvested in Drumbo, Ontario

MWCNT: Multi-wall Carbon Nanotubes

NRC: Noise Reduction Coefficient

O/C: Ratio of Atomic Oxygen to Atomic Carbon

PP: Polypropylene

PVC: Poly-Vinyl Chloride

RGB: Red-Green-Blue

SEM: Scanning Electron Microscopy

SMD: Sauter Mean Diameter, μ

SPF: Spruce-Pine-Fir Lumber

WC: Wood Chip

wt%: weight fraction, reported as a percentage

A: surface area, m^2

f: frequency, Hz

L: sample thickness, m

R: electrical resistance, ohms

α: sound absorption coefficient, unitless

ε: electrical permittivity, unitless

Ø: pore size, nm

σ: electrical conductivity, S/m

τ: vapour residence time, s

ω: angular frequency, rad/s

Chapter 1

1 Introduction

The research work presented in this thesis investigates the production of pyrolysis biochar and its behaviour when used as a filler in composite materials. This research focuses on the effect of production parameters on the characteristics of biochar, and how these characteristics in turn change the effectiveness of integration with other materials, and the properties of the product composite. A key motivational factor for this work is to find increased value for biochar produced through pyrolysis, and to add sustainable options for the composite production industry. The format used in this thesis is the monograph format.

This chapter covers information on the pyrolysis process and technologies, and biochar production and characteristics. Additionally, it provides some information on composite technologies and the role that fillers play in industry. Finally, it describes the objectives and motivation for the work presented.

1.1 Pyrolysis

The global demand for energy and petroleum based products has generated several problems, many of which have major implications now and in the future. Perhaps the most significant among these problems is the reliance on fossil fuels, through which easily accessible reserves will eventually be exhausted (Lehmann, 2007). In addition, the carbon emissions from the burning of fossil fuels have created an imbalance in the natural carbon cycle, resulting in the ongoing climate change (Schmidt, 2012b). While the materials and energy derived from petroleum are still key for industrial development, more sustainable alternatives are required.

Biomass has been recognized as a highly advantageous renewable energy source, and is gathering attention due to its abundance, positive environmental considerations, and waste reduction potential (Behazin et al., 2016; Jahirul et al., 2012). While the term, "biomass", covers a large range of different materials, it is defined as, "a mass of live or dead organic matter" (FAO, 2009). While very similar to charcoal, the only real difference is that charcoal is primarily used for energy and heat (Lehmann & Joseph, 2009). There are two main methods used to convert biomass into biofuels: biochemical, yielding mostly ethanol; and

thermochemical, typically yielding solid, liquid and gas phase products (Tripathi et al., 2016). Biochemical methods are typically limited by their conversion efficiency, as it does not process all components of biomass, typically needing de-lignified feedstock, whereas thermochemical methods can break down these components (Behazin et al., 2016).

Pyrolysis is just one of many thermochemical conversion methods, however it is gaining popularity as it is the only conversion method that produces liquid, solid and gas products in significant levels (Tripathi et al., 2016). Pyrolysis is the thermal decomposition of biomass in limited or zero oxygen environments (Bridgwater, 2003). An exact description of the pyrolysis process is challenging, as there are various complex chemical and physical transformations occurring during the reaction, such as dehydration, depolymerization, and decarboxylation among others (Kan et al., 2016; Neves et al., 2011). However, biomass pyrolysis is accepted to fall into the three stages of (i) dehydration, (ii) primary decomposition, which involves the breakdown of volatile components within the biomass, forming the main constituents in the range of 200-400 °C, and (iii) cracking and repolymerization, where heavy compounds are broken to form biochar and gas, and vapours that can be condensed to form bio-oil (Kan et al., 2016; Neves et al., 2011).

1.1.1 Pyrolysis Classification

While the pyrolysis process produces a variety of products in solid biochar, liquid bio-oil and gaseous vapours, the relative distribution of products depends heavily on the operating conditions and feed material (Jahirul et al., 2012). Biomass consists of three common components: cellulose, hemi-cellulose and lignin, at varying proportions in different feedstocks, (Ranzi et al., 2008). Each of these factors decomposes and breaks down at different temperatures and rates, which is further complicated by interactions between cellulose and the other two components in different materials (Jahirul et al., 2012; Ranzi et al., 2008). Due to these factors, it is largely difficult to completely predict the production quantity of each of the different materials for different feedstocks or pyrolysis conditions. However, kinetic studies have shown that the different components of biomass decompose at different temperatures and rates during pyrolysis, as shown in Figure 1.1. While the reactions occurring during each stage are complex, and typically require large amounts of kinetic modelling to fully understand, the rate of mass loss for each component gives some insight to the process. At temperatures below

200 °C, the lignin forms a molten phase within the biochar, slowly breaking down through depolymerization and cleavage, however after 350 °C it starts to reform solid material through aromatic condensation (Dufour et al., 2012). The hemi-cellulose and cellulose exhibit much more drastic mass loss rates in the range of 250 to 400 °C (Ranzi et al., 2008). The decomposition of compounds found within the hemi-cellulose and cellulose components typically lead to the formation of non-condensable gases, and the condensable vapours leading to the oil and tars (Jahirul et al., 2012). The biochar is typically composed of the residual lignin, which decomposes then solidifies at higher temperatures (Di Blasi, 2008), and mineral content in the biomass. Due to this, pyrolysis processes can be broken into separate categories which predict typical yields based on temperature, heating rate and residence time, summarised in Table 1.1.

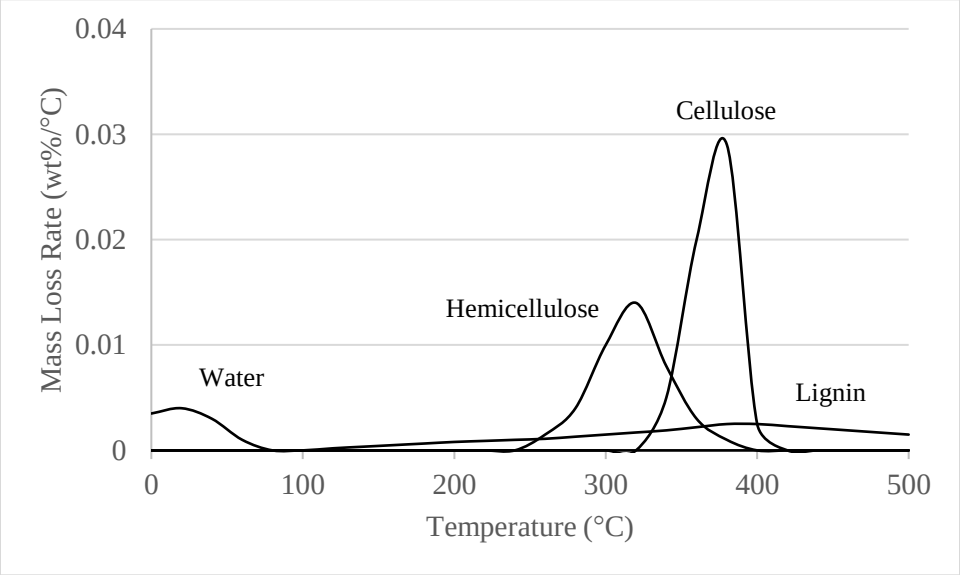

Figure 1.1-Decomposition of individual biomass components with pyrolysis temperature (Adapted from Jahirul et al., 2012)

Slow Pyrolysis

Slow pyrolysis has been the main form of pyrolysis used over the last thousand years, typically used for the production of charcoal (Kan et al., 2016). It is characterized by using lower heating rates (0.1-1 °C/minute), to a temperature in the range of 400-550 °C, and with long residence times of hours to days (Tripathi et al., 2016). Slow pyrolysis is favourable for the production of biochar during reactions, as the long vapour residence time at higher temperatures allows for

secondary reactions to take place, in which cracking of the bio-oil vapours occurs (Cha et al., 2016). During these reactions, the vapours repolymerize on the solid residue within the reactor, which negatively impacts the liquid phase bio-oil yield and quality, while increasing the solid biochar production (Jahirul et al., 2012; Kan et al., 2016).

Fast Pyrolysis

Fast pyrolysis involves the rapid heating of biomass to high temperatures in the range of 500-800 °C, at anywhere from 10-200° C/min, with a vapour residence time in the range of several seconds (Manyà, 2012; Tripathi et al., 2016). The key to fast pyrolysis is that the biomass decomposes at a fast rate to form mostly vapours, the vapour residence time is very short, and the vapours are rapidly quenched. This serves to minimize secondary cracking reactions within the vapours that occur at higher temperatures, and cracking on the biochar particle surface which would serve to reduce the bio-oil yield (Bridgwater, 2012; Bridgwater & Peacocke, 2000). In recent years, bio-oil has been gaining increased attention, as it can be upgraded to produce liquid fuels, specialty chemicals and other products. Due to the potential value of bio-oil, and the high production rates that can be accomplished with fast pyrolysis systems, fast pyrolysis has been gaining popularity (Bridgwater & Peacocke, 2000; K. Wang & Brown, 2017).

Flash Pyrolysis

Flash pyrolysis is quite similar, yet perhaps an improved version, to fast pyrolysis. It is characterized by high reaction temperatures in the range of 900-1200 °C, extremely high heating rates typically around 1000 °C/s, and residence times under 1 s (Kan et al., 2016; Tripathi et al., 2016). The heat and mass transfer of the reaction, as well as reaction kinetics and properties of the biomass play a large role in the quality and distribution of the products in flash pyrolysis (Tripathi et al., 2016). While this process has the potential to yield high levels of liquid bio-oil, limitations exist in the stability of the bio-oil, typically associated with the char and ash present in the liquid. The presence of solids promotes additional reactions, which can increase the viscosity of the liquid (Canabarro et al., 2013).

Table 1.1- Typical operating parameters and products for pyrolysis (Adapted from Jahirul et al., 2012)

Pyrolysis Process	Solid Residence Time (s)	Heating Rate (°C/s)	Particle Size (mm)	Temperature (°C)	Product Yield (%)		
					Bio-Oil	Biochar	Gas
Slow	450-550	0.1-1	5-50	300-700	30	35	35
Fast	0.5-10	10-200	<1	600-1000	50	20	30
Flash	<0.5	>1000	<0.2	800-1100	75	12	13

1.1.2 Pyrolysis Reactors

Similar to the variation in pyrolysis process techniques, there is a large variety of reaction systems that are used for pyrolysis. Pyrolysis is by no means a new technology, with charcoal production existing for thousands of years. It has been thought that humans have produced black carbon sources since they first learned to control fire. The initial black carbon "reactors" were made using wood and other combustible organics in piles or holes in the ground, producing a sort of pit kiln. These wood piles or pits would burn on the exterior, while oxygen would be limited in the base of the pile. Over the course of several hours-to-days, charcoal would be produced from the high temperatures in the "kiln" (Brewer & Brown, 2012). The first reactors built for charcoal production were kilns, utilizing a long residence time and lower heating rate for production (Colomba, 2015). However, as researchers uncovered more about the production of bio-oil and variation in product properties, more specialized reactors have been developed.

The pyrolysis reactor is the heart of any pyrolysis system, and it is essential to choose the appropriate design for any application. The most important factors to be controlled by a reactor are temperature, heating rate, separation and control of vapours and char, and gas cooling (Bridgwater & Peacocke, 2000). Most reactors will vary in the method in which they transfer heat to the system, and the gas-solid contact mode (Colomba, 2015), where no design is deemed the "best", as each has its own advantages and disadvantages (Jahirul et al., 2012). The most common types of reactors are summarized briefly below:

Fixed-Bed Reactors

In fixed bed reactors, the solid fuels move down a vertical shaft, and are contacted by either a counter or co-current gas stream used to heat the system (Bridgwater, 2003). The char and ash can then be collected from the base of the reactor, while the product gas stream exits at the top or

bottom, based on the direction of flow. Fixed bed reactors are usually used for slow pyrolysis, as they utilize long solid residence time and high carbon conservation (Jahirul et al., 2012). It is a proven and reliable technology for fuels that are uniform and with little fines or moisture, and produces a relatively clean gas. However, it is limited by its limited scale up potential, and is usually used for gasification (Bridgwater, 2003).

Fluidized-Bed Reactors

Fluidized beds are characterized by using a fluidizing gas to provide effective mixing throughout a bed. Often, sand is heated in a combustor and is used as a solid bed, which provides effective heat transfer to the biomass, and allows the pyrolysis reaction to take place (Bridgwater, 2012). The bed typically sits atop a distributor plate, and the fluidizing gas, usually an inert gas with no oxygen, is passed through the solid bed and lifts it in a fluid state. This method provides effective mixing and heat transfer, while conveying vapour components out of the reactor and reducing the gas residence time (Anuar et al., 2016). The solid product is then removed from the gas stream, typically through cyclone, scrubbers or ESP, and the gases are cooled to collect oils. Fluidized beds are popular for fast pyrolysis systems, as they provide good heat transfer, control of residence time, and solid-fluid contact; as well as being relatively simple. Two types of fluidized beds are often used: bubbling fluidized beds, where the gases exit after cleaning; and circulating beds, where the hot solids are recycled to a combustor where they are heated through burning of the solid or gaseous by-products (Briens et al., 2008). Circulating beds have many of the same features as bubbling beds, with increased biochar attrition due to higher gas velocities. This results in increased biochar levels in the oil and vapours, but circulating beds have the advantage of higher throughput over bubbling beds (Bridgwater, 2012)

Ablative Reactors

The ablative process is quite different than other configurations. In this design, high pressure is used to hold biomass particles against a hot reactor wall or plate (Bridgwater, 2012). Constant relative movement between the particle and the wall is essential, as to allow the oil collected on the reactor surface to evaporate, and so that the pyrolysis front moves through the particle (Bridgwater, 2003). Through this, the reaction rates are limited by the heat transfer to the reactor, rather than to the particle, and gas is not required. This configuration allows for the use

of large feed sizes, but since the reactor is controlled by the surface area of contact, scale-up is costly compared to more simple designs (Bridgwater, 2003; Jahirul et al., 2012). One common reactor type for ablative processes is the rotating cone reactor. Rotating cone configurations use centrifugal force, forcing biomass and heating mediums towards the outer cone and up the lower wall of the reactor. This results in a high rate of mixing and heat transfer throughout the lower volume of the reactor where the rotation is occurring, as well as good heat transfer at the wall (Hulet et al., 2005). The vapours and gases exit freely, and the sand and biomass mixture pour over the top of the cone. The solids mixture is then sent to combustion, where the char is burned to heat the sand, and the heated sand returns to the cone (Bridgwater, 2003, 2012; Jahirul et al., 2012). While it can be an effective system, effective heat transfer is difficult in large-scale applications, although several larger scale test units have been successfully developed (Hulet et al., 2005; Kan et al., 2016).

Auger Reactors

Auger and screw reactors are relatively uncomplicated systems which do not fall under fast pyrolysis, but rather intermediate pyrolysis (Colomba, 2015). Biomass is pulled through a heated cylindrical tube by means of an auger or screw. Heat can be provided by a variety of mechanisms, such as heated sand or steel balls, or internal passage throughout the reactor using hot fluid to provide heat, which inherently would provide difficulties in scale-up. While vapour residence times can be manipulated, it is difficult to achieve the short times of fluidized beds. However, these reactors can be advantageous for difficult to handle feedstocks (Bridgwater, 2012; Jahirul et al., 2012).

Vacuum Reactors

Vacuum reactors are used for fast pyrolysis processes, and are rather complicated and costly systems. The liquid bio-oil yield achieved is usually in the range of 30-35 %, which is higher than typical fast pyrolysis processes due to the short vapour residence time, while showing higher char yields. However, the creation of a vacuum requires costly vessels and piping to be installed, however the system can be favourable as large particle sizes can be processed, and no gases are required during pyrolysis (Bridgwater, 2012).

1.2 Biochar

Biochar, also known as biocarbon or pyrolytic char, is the solid, carbonaceous residue generated from the pyrolysis process. Similar to charcoal, it has an inherent energy value if combusted, however, it differs in the fact that charcoal is used historically to burn, whereas biochar is used in other applications, such as soil amendment (Lehmann & Joseph, 2009). The physical and chemical characteristics of pyrolysis biochar can vary heavily depending on factors such as feedstock and process temperature. However, biochar gathers interest due to its potential for high fixed carbon levels, large surface area and porosity, and adsorptive capabilities (Kloss et al., 2011; Xie et al., 2014). Biochar is quickly gaining ground due the versatility of potential applications it presents, as highlighted in *55 Uses of Biochar* (Schmidt, 2012) and *Recent advances in the utilization of biochar* (Qian et al., 2015), as well as its carbon sequestration potential (Schmidt, 2012b).

As biochar can vary heavily depending on how it was produced, various studies have worked on developing models to grasp product formation. Despite the variance, there are general trends for product distribution and properties depending on temperature (Neves et al., 2011). Due to this, an understanding of the basic mechanism of biochar formation allows insight into the characteristics that the biochar presents. As biomass is composed of several different constituents (cellulose, hemi-cellulose, lignin, and mineral compounds) which decompose at different temperatures, the largest variation in biochar comes from the selected material (Ranzi et al., 2008; Xie et al., 2014). Next, the heating rate, pyrolysis temperature, and residence time play large roles, as they control the chemical compounds that break down, and whether or not different reactions have time to occur (Neves et al., 2011; Ronsse et al., 2013).

As expected with any process, the product yield is always one of the most investigated aspects of biochar productions. The yield of biochar is heavily dependent of both feedstock and pyrolysis temperature. The initial composition of the biomass plays a large role in the biochar yield, as materials with higher lignin content tend to produce higher yields (Manyà, 2012). This is likely do to the slow rate at which lignin decomposes and then reforms into solid material, as shown in Figure 1.1 (Dufour et al., 2012). The inorganic content, or ash content, also plays a large role in the yield for two reasons, the first being that it stays within the biochar and is concentrated at higher temperatures, the second being it catalyzes biochar formation reactions (Manyà, 2012).

Perhaps obviously, low pyrolysis temperature will favour solids yield, as less volatilization will have occurred. As temperatures increase past 500 °C, the cellulose and hemicellulose have mostly decomposed and the lignin loss rate will begin to slow down. In this temperature range, the biochar will consist largely of fixed, aromatic carbon along with the mineral ash content of the feedstock. (Dufour et al., 2012; Schimmelpfennig & Glaser, 2012). Thus, from a feedstock point of view, high fixed carbon and low volatile matter content will favour biochar production. The process conditions typically associated with slow pyrolysis favour the production of biochar as well (Xie et al., 2014). The lower heating rate ensures that no secondary pyrolysis occurs, and reduces the level of thermal cracking, both of which favour biochar yield, whereas higher heating rates favour fragmentation, increasing vapour and gas yields (Tripathi et al., 2016). The vapour residence time also plays a large role, but it typically gets grouped together with other parameters, making it difficult to paint a clear picture. It makes sense though, that increased vapour residence time would promote the re-polymerization reactions that occur at the biochar surface, and will therefore increase the yield (Manyà, 2012; Tripathi et al., 2016). While there are other factors that can play a role in yield, such as particle size and reactor bed height, the feedstock and temperature typically show the strongest influence, and the range of yields can be seen in Figure 1.2 (Eastern Red Maple, fast pyrolysis), although the yield can vary heavily from what is shown.

The elemental composition of biochar also tends to vary depending on the feedstock and process conditions, however, as the alternative names for biochar imply, carbon makes up most the material. As the pyrolysis temperature increases, the organic matter breaks down, leaving behind aromatic carbon structures (Schimmelpfennig & Glaser, 2012). Through this, as the intensity of pyrolysis continues, the initial hydrogen and oxygen content of the feedstock decrease, while the fixed carbon content of the biochar will increase, even though carbon is still lost during the breakdown of volatile components (Ronsse et al., 2013). Due to this, despite the initial carbon content of the biomass, high temperature pyrolysis (750 °C), will result in biochar with very high fixed carbon contents, and very little volatile matter on an ash-free basis. It has also been found that feedstocks with higher lignin contents tend to have higher oxygen content due to the increased carbon content of lignin than in cellulose and hemicellulose. Additionally, it can lead to an increased aromatic structure within the biochar itself (Nanda et al., 2016).

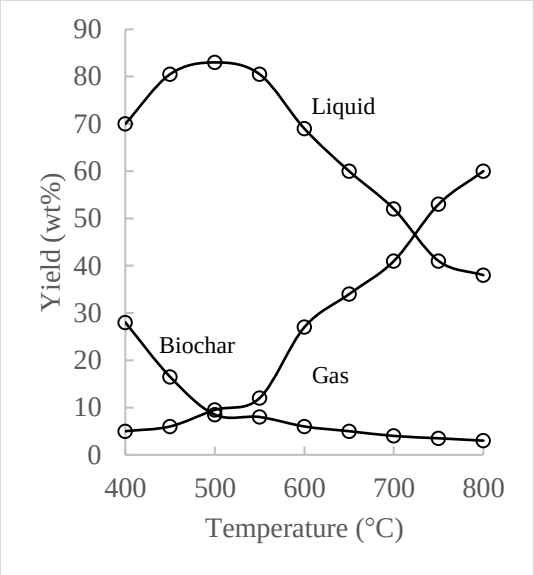

Figure 1.2- Relative proportions of end products from pyrolysis of Eastern Red Maple (Adapted from Scott, Piskorz, Bergougnou, Graham, & Overend, 1988)

The hydrogen and oxygen content diminish readily as the weaker bonds in the more volatile biomass constituents are cleaved, though they can both exist in surface functional groups. The hydrogen content becomes near negligible as the surface groups are broken down, however, oxygen can remain in recalcitrant fractions in the final aromatic rings (Jindo et al., 2014). Understanding of the H/C ratio is important for determining the extent of pyrolysis, and the O/C ratio can be a good indicator of polar surface groups, implying hydrophobicity or hydrophilicity (Schimmelpfennig & Glaser, 2012). Typically, high oxygen contents are typical of lignocellulosic biomass, as well as higher heating rate processes, due to the shorter residence time (Manyà, 2012; Tripathi et al., 2016).

While carbon, hydrogen, and oxygen certainly make up the most of biochar, other elements can be found in the form of chemicals, minerals, and ash. Nitrogen and sulphur can both exist in biochar, largely due to their presence in biomass materials. However, there are conflicting findings on the N and S contents, as they can either be increased or decreased with pyrolysis intensities; their initial biomass concentration seems to be the largest indicator of their final concentration in biochar, with animal waste and wastewater sludge biochar showing the highest levels (Tripathi et al., 2016; Xie et al., 2014). The ash content of biochar consists mostly of the ash contained in biomass, with 95-99% of the ash content remaining. Through this, the ash content appears to rise with temperature, however, it is typically the loss of other material that

causes this (Ronsse et al., 2013). While inorganic materials (Al, K, P, Si, *etc…*) are not necessarily ash, they are often grouped into one category as they do not typically break down during pyrolysis (Manyà, 2012). Where ash can be advantageous or problematic for a variety of reasons, one potential cause for concern comes from the presence of contaminants. Biochar from biosolids and pulp and paper effluents can have inorganic toxicants, such as copper and arsenic, and solid and industrial waste can have high levels of heavy metals (Srinivasan et al., 2015).

The chemical groups that appear on the surface of biochar particles, or surface functional groups, are important in dictating the interactions between these particles and external forces. While some studies have worked on identifying all the groups which can be present through FTIR spectroscopy (Chia et al., 2012; Kloss et al., 2011), some functionalities have shown to have more impact than others. Aromatic surface groups, which appear with C-H bending and stretching, typically results from the lignin aromatic residues, but also from the conversion of cellulose residues (Chia et al., 2012). However, cellulose is not completely carbonized during pyrolysis, as stretching of aliphatic C-H groups can be found, despite decreasing at higher temperatures (Kloss et al., 2011). The alkyl functionalities present in these groups are highly correlated with the hydrophobic tendencies which are shown by biochar produced at lower temperatures (Das & Sarmah, 2015; Kinney et al., 2012). Several oxygen containing groups are often formed on the surface of biochar, typically in the form of ketones, carboxylic acid esters, and anhydrides, which are typically residues of cellulose and hemi-cellulose (Chia et al., 2012; Das et al., 2015). These groups are very important in a variety of industries, as the polar carboxylic and carbonyl groups provide negative charges, and improve the cation exchange capacity of biochar (Kloss et al., 2011), and can represent hydrophilicity in some situations (Gray et al., 2014). However, these groups disappear with increasing pyrolysis temperature. Hydroxyl groups can also be present, typically associated with wood residues, but also thought to arise from water and mineral based -OH groups (Chia et al., 2012). As these groups break down through increasing temperature, they have been found to be important for the pore formation of biochar (Kloss et al., 2011).

One of the most important characteristics of biochar is the surface area, or the area that is available for interactions with exterior elements. The surface area of biochar comes from the porous structure which is created by the volatiles escaping at high temperatures (Srinivasan et al.,

2015). The pores present in biochar are typically composed of micropores (Ø< 2 nm), mesopores (1 nm< Ø< 50 nm), and macropores (Ø > 50 nm) (Colomba, 2015). The pore availability, and resultant surface area, is often the most desirable characteristic of biochar, as it has large implications for a variety of factors such as water retention, adsorption capacity of organic and inorganic pollutants, and polymer-filler matrix interactions to name a few (Das et al., 2015; Jindo et al., 2014; Kan et al., 2016). While different pore sizes may be important for different applications, increasing the surface area of biochar is almost always desired.

The Brauner, Emmet and Teller (BET) surface area is the most commonly used method for reporting the surface area of biochar particles. As with most of the discussed characteristics, the porosity and surface area are largely dependent on the biomass feedstock, pyrolysis temperature, and residence time. Increasing pyrolysis temperature promotes the breaking down of organic compounds within the particles, and allow for fused-ring aromatic carbon structures to form. These structures allow for micropores to develop within the biochar, and subsequently increase the surface area of the material (Schimmelpfennig & Glaser, 2012; Shaaban et al., 2014). The BET surface area will continue to increase with increasing pyrolysis temperature until a plateau is reached in the range of 700 °C, after which the surface area can decrease for certain feedstocks. This is thought to be due to the melting of the ash within the material, filling and blocking access to the internal pores, and also due to the potential deformation or collapse of pores (Ronsse et al., 2013; Schimmelpfennig & Glaser, 2012). Increasing the residence time of the biochar within the system also has a positive effect, widening the pore size by allowing the walls between pores to break down. It also allows for the repolymerization reaction on the particles, creating a rougher surface, which can increase the BET surface area (Shaaban et al., 2014; Tripathi et al., 2016). Some other factors have been thought to increase the surface area, such as decreasing the reactor pressure to promote tar removal (Manyà, 2012), or increasing the heating rate, which can cause fragmentation of the particles (Brewer et al., 2009).

1.2.1 Biochar Applications

While the versatility of biochar may make characterisation difficult, it also provides versatility when it comes to specific applications. Initially used for agricultural purposes, researchers have investigated the use of biochar in a wide range of fields, with positive results in many of them (Schmidt, 2012a). While crude biochar has been implemented in a wide range of purposes, as

highlighted in *55 Uses of Biochar* (Schmidt, 2012a), recent research has looked at using engineered biochar for advanced applications (Qian et al., 2015). While several papers have reviewed the different characteristics and possible applications of biochar (Amin et al., 2016; Manyà, 2012; Nanda, Dalai, Berruti, & Kozinski, 2016; Qian et al., 2015; Srinivasan et al., 2015), the most developed applications will be summarized below.

Soil Improvement

Adding charred wood to improve soil quality is perhaps the earliest known application of "biochar". Soil in the Amazonian region garnered particular interest, as it was found that certain soils had improved fertility and increased humus content when compared to surrounding infertile soils (Schimmelpfennig & Glaser, 2012). The soil, termed *Terra Preta*, was found to contain charred organic material, thought to be gathered from sources such as controlled forest fires, which has since lead to in depth investigation of biochar for soil improvement purposes (Manyà, 2012). In 2006, the International Biochar Initiative (IBI) was launched, as a way of promoting biochar research and commercialization for agricultural purposes, and offering standardization and classification of produced biochar.

Biochar has shown the ability to have positive effects on aspects such as water retention, nutrient efficiency, cation exchange capacity (CEC), microbial activity, and associated GHG and nitrogen emissions (Fryda & Visser, 2015; Manyà, 2012; Qian et al., 2015; Schimmelpfennig & Glaser, 2012). While the reason for increased water retention cannot be attributed to one single reason, it is thought that the porous nature of biochar allows it to retain water during wet periods, and release it during drier conditions (Schimmelpfennig & Glaser, 2012). While a higher surface area may benefit water uptake, it is thought to also enhance the growth of microbial communities in the soil, which are beneficial for nutrient cycling (Qian et al., 2015). The internal pores of the biochar are an ideal place for colonization of microorganisms, providing protection from environment and predators alike (Nanda et al., 2016). There are actually several ways through which biochar promotes nutrient availability, one of which being nutrients dissolved in the water being available to the plants for a longer period of time (Fryda & Visser, 2015). Also, by increasing the CEC of soil, nutrients are prevented from leaching into moving water, and through retention are therefore more available within the soil to plants (Qian et al., 2015).

Perhaps the most encouraging benefits of this application, is the reduction of emissions associated with agricultural activities. Soil appears to be the only storage sight for large quantities of biochar for long-term mitigation of climate change (Nanda et al., 2016) Due to the stability of biochar in soil, in some cases storing carbon in the ground for hundreds of years, and the promotion of CO_2 consumption by healthier plants, biochar acts as a carbon sequestration agent (Manyà, 2012). Carbon sequestration occurs as biochar is stabilizing the carbon that has been taken up by plants and storing it over long periods in the soil, while also helping to promote the growth and uptake of new plants (Roberts et al., 2010) This helps to offset the CO_2 in the atmosphere, and in turn, reduce the effects of global warming (Qian et al., 2015). Since biochar also allows the soil to retain more nitrogen, potential N_2O emissions can be reduced. Additionally, as the soil uses nutrients more efficiently, the need for fertilizer to supply nutrients is decreased. In turn, this results in fewer emissions associated with production, transportation and spreading of these fertilizers (Lehmann, 2008; Manyà, 2012; Qian et al., 2015).

Pollutant Adsorption

As mentioned previously, biochar has shown the ability to retain water and adsorb nutrients for retention within the soil to which it is added. Research has also shown that biochar can be beneficial for removing contaminants in soil, as well as water. The key characteristics of biochar for contaminant adsorption are its surface area, micro-porosity and surface functionality, with acidic functional groups being thought to provide the most adsorption benefits (Qian et al., 2015; Srinivasan et al., 2015).

Studies have shown that biochar is effective for remediation of organic compounds found in soil, and those dissolved in water. Researchers have found that biochar has been able to decrease PAH concentration in sewage sludge, and lowered the hazardous impacts of both pesticides and herbicides in soil (Xie et al., 2014). Also, char has the ability to retain and limit the availability of heavy metals, as biochar can present a high pH and CEC depending on the feedstock (Qian et al., 2015). Several studies have been performed, showing that biochar can reduce concentrations of metals such as Cu, Pb, Cd, and As in waste streams. The different porous structures present in biochar samples allow the char to perform different mechanisms other than adsorption, namely oxidation and reduction, which can reduce toxin mobility (Xie et al., 2014).

Activated and Engineered Carbon

While untreated biochar can be used for contaminant removal, its relatively low surface area can be a limiting factor in its potential application. Typically, activated carbons, which are most commonly used in water and air treatment, have much higher surface areas, in the range of 800-1200 m^2/g (Hamza et al., 2014). While traditional activated carbon has excellent adsorption properties, the high commercial cost along with the impact of using non-renewable materials as a precursor, have lead to investigation into different methods of producing activated carbons (Colomba, 2015; Hamza et al., 2015). Due to this, extensive research has been performed with the goal of modifying biochar to increase the surface area or modify the surface functionality to increase the adsorption capacity.

Typically, modification is done by either chemical or physical modification. In chemical modification, acids or bases are typically used in a one or two step activation process. This typically results in a drastic increase in surface area, as well as an increase in porosity and pore size. Additionally, chemicals allow for the modification of surface functionality, which can increase the affinity of the biochar with certain contaminants. While chemical modification allows for the activation process to be done at a lower temperature than physical modification, the potentially toxic chemicals required, and generated waste streams, can make the method undesirable (Colomba, 2015; Xie et al., 2014). In physical processes, air, steam, or CO_2 at very high temperatures are used in order to remove volatiles and allow reactions to take place, which open clogged pores within the biochar structure (Colomba, 2015; Xie et al., 2014). For example, CO_2 can react with the C in the biochar, forming CO and enhancing the microporous structure of the material (Xie et al., 2014). By using CO_2 at temperatures reaching 900 °C for activation periods as low as an hour, biochar can be activated to show BET surface areas of over 1100 m^2/g, although the biochar precursor still plays a role in potential surface area (Jung & Kim, 2014). Physical processes are often preferred due to chemical methods due to the ease and cleanliness of the process (Colomba, 2015).

1.3 Composites

Polymers are macromolecules consisting of chains of smaller molecules connected through chemical bonds. While this section will not go deeply into a chemical or physical explanation of

polymers, it will briefly discuss the makeup and properties of polymers. The structures of polymers vary heavily, showing different structures (chains, branches, etc…), along with varying molecular weights (Braun et al., 2013b). These polymers can display a wide range of chemical, physical and mechanical properties, which is evident by the wide range of polymers displayed in nature.

Synthetic polymers were first produced in the early twentieth century, and chemists have developed methods to control different aspects of the polymers such as architecture and functionality, customizing polymers to satisfy different needs, such as electrical conductivity or thermal stability (Braun et al., 2013a). With most polymers, mechanical properties are typically the most important to consider for various applications. In linear polymers, the mechanical properties typically improve with increasing molecular weight of the structure, at the expense of drastically increased viscosity when molten during processing. So while polymer science has evolved such that polymers with extremely high molecular weights (10^6 Daltons) can be synthesized, the field has also had to develop advanced processing methods (Shaw, 2012).

Approximately 85% of polymers produced today are thermoplastics (Xanthos, 2010b). Of this, 70% of thermoplastics are made of low cost resins, namely the four polymers: polyethylenes, polypropylene (PP), polystyrene, and poly-vinyl chloride (PVC) (Wypych, 2009; Xanthos, 2010b). The demand for these thermoplastics can be seen by looking around everyday life. The low cost they present has resulted in more thermoplastics being present in cars, appliances and everyday products (Rothon, 2003). Commercial polymers are not typically made of the pure polymer, but rather consist of the material blended with other polymers, or solid additives such as fillers, resulting in composite materials (Shaw, 2012).

It is widely thought that fillers were first added to composite materials in an attempt to decrease the cost (Rothon, 2003). While the fillers may have been cheaper than the polymer initially, the rising cost of synthetic fillers means that this is no longer the case. The addition of fillers into organic polymers results in a polymer-filler matrix, leading to structures throughout the material that drastically effect the properties of the end product (Xanthos, 2010b). So while in some cases, cost reduction can occur, fillers are largely used to improve the mechanical and chemical properties of the material, and sometimes to add different functions to the product (Wypych,

2009; Xanthos, 2010b). The next section will go into more detail about filler properties and how they affect composites.

1.3.1 Fillers

Fillers are solid materials added to polymers in order to improve certain characteristics of the final product (Xanthos, 2010b). Some of the most common and commercially important fillers include calcium carbonate, talc, mica, clay, aluminum trihydrate, and carbon black, among many others (Jancar, 1998). The characteristics of various fillers are different, and the properties of the polymer they are incorporated into play a large role, so it is hard to say exactly what will be affected when incorporating a filler into a composite. Due to this, creating the investigated composite material is one of the only ways to gain insight into the properties of the final product.

The most common production method of thermoplastics is extrusion, with injection moulding being the second most common in industry (Xanthos, 2010b). These methods are still typically used when fillers are being added, however, since it is important to ensure that the filler is dispersed effectively in the polymer, the filler is typically added after the polymer is fully melted (Todd, 2010). Polymers have a much higher thermal expansion coefficient than fillers, leading to a unique interaction at the polymer-filler interface. This interaction is one of the most important parameters in dictating the outcome of the mixture, and is often determined by the surface activity (DeArmitt, 2011; Fröhlich et al., 2005; Rothon, 2003). Adhesion at the surface shows considerable influence on mechanical and stress response, with acid-base interactions showing increased importance (Rothon, 2003). Ultimately, it comes down to the surface functionality of the filler, and the chemistry of the polymer, for determining compatibility. For example, a hydrophilic filler may not be ideal for usage with a hydrophobic polymer, as wettability between the two will be low, resulting in poor mechanical properties (Wypych, 2009).

The other key characteristics for determining the effectiveness of a filler are also important due to their effect on polymer-filler adhesion. The available surface area of a filler allows for increased absorption of polymer to the filler, which can increase the interaction between the two. The increased pore absorption can improve the tensile strength, yield stress, and fractional resistance of the final product, but in some situations can lead to overly brittle and stiff materials

(DeArmitt, 2011). The particle size is often considered one of the most important aspects to control (Peterson, 2012b). Not only does smaller particle size increase available surface area per unit volume, it can allow for tighter packing of the filler in the material (Fröhlich et al., 2005; Murphy, 2001). Conflicting results can arise from different distributions though, as small particles increase the blend viscosity, and can form aggregates which act as fracture initiation sites. On the other hand, larger particles can de-bond from the polymer under stress loads and act as flaws (DeArmitt, 2011; Murphy, 2001; Peterson, 2012b). The filler shape is important, as it has the largest effect on the packing of the material. Fillers come in a variety of shapes, and the aspect ratio, or the ratio of length to diameter, is usually the only defining characteristic (Rothon, 2003).

Aside from these key characteristics, it is hard to say which characteristics are key across the entire composite industry. A lower filler density can allow for final materials which are lighter, which is important in automotive fields (Wypych, 2009). Thermal stability can be important in materials used in high heat applications, and electrical conductivity is necessary in some more recent applications (Wypych, 2009; Xanthos, 2010a). It is safe to say that the ideal characteristics of fillers depend heavily on the desired application of the product composite, and that a cheaper filler is always desirable.

1.3.2 Biochar as a Filler

Biochar has gained interest in recent years due to the potential to apply the material in the growing field of biocomposites; i.e. materials where one or more of the components are biological in origin. This can mean the filler or polymer is made of renewable sources, such as plant fibre, recycled material, or waste crops and oils (Fowler et al., 2006). Incorporating biochar into composites could help reduce the usage of synthetic fillers in these materials, such as carbon black (Das et al., 2015). Carbon black is a non-renewable filler, produced from the treatment and processing of hydrocarbons from the oil and gas industry (Wypych, 2009). Despite the cost of production, carbon black is the most widely used filler in industry, and the oldest active filler as well (Fröhlich et al., 2005). This is due to its common use in the tire industry, along with other automotive applications, which has lead to the expectation that the global carbon black market will surpass $25 billion dollars, as stated by Lucintel and reported by carbonblacksales.com.

Some of the characteristics of biochar that were listed earlier in this chapter give it the potential to be utilized successfully as a filler in certain composites. While the particle size of biochar is typically not consistent across feedstocks and productions methods, it is possible to grind the material down to smaller sizes (Peterson, 2012b). Without grinding though, biochar displays a wide particle size distribution, whereas carbon black is typically uniform in the range of 300 nm (Wypych, 2009). The surface area of biochar allows for stable matrices to develop at the polymer-filler interface, and the hydrophobic nature of biochar give it an advantage in compatibility when compared to other organic fillers such as wood (Das et al., 2015; Kinney et al., 2012). There are some potential drawbacks to the addition of biochar into biocomposites, such as the potential for high ash content which can cause overly brittle and stiff materials (Peterson, 2012a). However, some key features of biochar, such as high thermal stability and potential electrical conductivity, add promise to the field (Ahmetli et al., 2013). Adding this to the renewability and carbon offsetting ability of biochar, and it could be a field with vast expansion possibilities.

1.3.3 Biochar in Concrete

Concrete is a man-made composite material that is made of cement, which acts as a binding material, and a mixture of aggregate and sand, acting as fillers (Li, 2011a). The resulting composite is a stone-like material, and is the most commonly used construction material in the word, with 14 billion tonnes being produced in 2007 (Li, 2011c). There are two main reasons why it is so popular, the first being that concrete has a high compressive strength, making it ideal for uses with high compressive forces, as well as good water and thermal resistance. This makes it ideal for use in applications like buildings, bridges, and roads, while requiring very little maintenance. The second factor is the low cost and availability of materials, requiring low energy input compared to other materials (Li, 2011a).

It is very important to understand the chemistry and physical interactions involved in concrete production to predict how effective it will be in different applications. Due to the complex nature of the reactions taking place within the cement, this review will not go in to depth about the cement, but will briefly explain the mechanism through which cement, and in turn concrete, is produced. Portland cement is the most commonly found cement in concrete. It is produced by firing a mixture of limestone (or chalk) and clay (or shale), along with other additives, in a rotary

kiln at around 1500 °C (Moir, 2003). The result is a fine powder consisting mostly of CaO, SiO_2, Al_2O_3, SO_3, and Fe_2O_3. As water is added to the cement powder, it forms a paste which acts as a binder and coater within the concrete (Li, 2011a). The hydration of cement involves reacting the anhydrous components in the cement with water to create hydrated ones. The hydrated components take up more space than their non-hydrated counterparts, and in turn form an interlocking mass. So long as the material is sufficiently hydrated, the lower the water to cement ratio, the higher the compressive strength of the concrete will be, and the concrete will have a higher resistance to penetration (Moir, 2003). However, keeping a low water to cement makes the fresh concrete difficult to work with, and as such, enough water needs to be added to make the concrete workable, but without compromising the mechanical properties.

The cement paste binds together the aggregate material within the concrete, as well as any other materials such as rebar, acting as a glue for the materials. It also coats the filling materials in the concrete while the material is still wet, and any additional cement paste acts as a lubricant, making it easier for the aggregate and materials to flow (Li, 2011b). The aggregate makes up around 75% of the concrete volume, and as such it plays an important role in the final properties of the final concrete product. While there is no chemical reaction between the cement paste and the aggregate, the aggregate is more than just an inert material and provides benefits beyond cost reduction. The aggregate helps control shrinking and leaking of cement paste, and influences factors such as stiffness, density, and wear resistance of the final material (Li, 2011b).

The introduction of biochar into cementitious and concrete based materials comes from two main reasons. The first is the improvement of concrete composites through the addition of fillers and additives. While chemical additives have been added in the past to improve things like workability and setting time, inert materials, particularly nanoscale materials, are being investigated to improve key characteristics such as compressive strength and hardness. Different powders have been used, such as silica, fly ash, glass, limestone and slag, in order to try and produce high performance materials (Ferro et al., 2014).

The second reason, as with most applications, is for environmental benefit. As mentioned earlier, concrete is the most commonly used building material in the world, with over 14 billion tons of concrete being produced and used per year (Li, 2011c). While the aggregate and water

used (around 80% of the mass of concrete) come with relatively little associated CO_2 emissions, the production of cement uses around 4 GJ of energy and 0.8 to 1 tons of CO_2 per ton of cement (Li, 2011c). This is in addition to the fuel and emissions associated with concrete mixing, transport, and installation. It stands to reason that any means of reducing the environmental impact of concrete production and utilisation should be investigated. It has been discovered that industrial wastes can be added into concrete mixtures, which has been found to not only reduce waste levels, but can even show improvements to the concrete material itself (Li, 2011a). It seems expected then, that biochar could be used as an additive in the concrete industry, to help reduce waste and carbon levels, and even to show improvement to the building material itself.

As mentioned earlier in this section, biochar has the potential to reduce the net greenhouse gas emissions by sequestering atmospheric carbon. A life cycle analysis performed by Roberts et al. (2009), found that biochar has the potential to reduce net greenhouse gas emissions by up to 870 kg CO_2e per dry ton of feedstock (Roberts et al., 2010). In addition, the biochar can be saturated with CO_2 before it is added to the concrete for additional biochar sequestration, at up to 300 kg CO_2 per tone of dry feedstock (Wei et al., 2012).

As with the other applications, biochar also has several characteristics that can improve the quality of cementitious composites. Firstly, as particles within the size range of nano to micro scale can have a large impact on the mechanical properties of concrete, the first improvements would come from the effect of the small particle size that biochar can present. The use of carbon-based nano-particles has been found to offset the brittle behaviour of cement that is associated with an increase in strength by improving the ductility of the composite (Restuccia & Ferro, 2016). The size of sand used in concrete can play a large role in the fracture toughness of a cement composite, where reducing the size or loading level can increase the fracture strength to ideal levels. Due to this, modifying loading levels or particle size could allow for biochar to be used to tailor the brittle behaviour of concrete without compromising mechanical strength (Shin et al., 2015). In addition to the effects of particle size, the absorptive and adsorptive properties of biochar play an important role as well. The water retention of biochar allows it to absorb the water used in the initial mixing, which means that the evaporation loss of water can be reduced with the addition of biochar (Choi et al., 2012). More importantly, the water retained by biochar during initial mixing is released during the hardening of the concrete, promoting secondary

hydration reactions, thereby having a positive effect on the mechanical properties of the concrete (Choi et al., 2012; Gupta & Kua, 2017). In addition, the use of nano-particles can increase the hydration process speed (Restuccia & Ferro, 2016). While other nano- or microparticles may also improve the mechanical properties of concrete, the lightweight nature of biochar can allow for decreases in the overall density of concrete, which will have advantages in transportation costs.

Outside of the mechanical properties of the cement composites, some of the favourable properties of biochar can be transferred to the matrix which supports it: its low thermal conductivity, high chemical stability, and low flammability (Gupta & Kua, 2017). The low thermal conductivity of biochar is due to the presence of various pores throughout the particle (Brewer et al., 2009), which break thermal bridging within concrete. This is key for increasing insulation and therefore heating and cooling energy requirements within buildings (Gupta & Kua, 2017). In addition to heat insulation, biochar provides excellent humidity insulation when used in walls and buildings. The pores in biochar allow it to store moisture in the air, regulating the humidity levels within 40- 75 % (Schmidt, 2013). This has large health implications, as it can prevent asthma and other respiratory illnesses brought on by dry air, as well as mould growth caused by damp air (Gupta & Kua, 2017; Schmidt, 2013).

While biochar may have properties similar to charcoal, in that it is combustible in the presence of oxygen, studies have found that biochar itself is not a flammable material. In a study on the combustion front propagation of biochar, biochar produced through slow pyrolysis showed no combustion front propagation, whereas fast pyrolysis chars showed slightly higher propagation, though not enough to be considered flammable. Through this, it was found that the level of volatiles and fixed carbon influence the combustion properties, and a low H/C ratio is important for reducing flammability (Zhao et al., 2014).

Concrete itself is not a flammable material, and is generally considered to perform well in the presence of fire or extreme heat. However, in the presence of high temperatures, concrete can still undergo a loss of strength as well as spalling (Cather, 2003). Spalling is the structural deformation and breaking up of layers of concrete as it is exposed to fire, and is caused by several factors such as aggregate fracturing, particles expanding, and evaporation of trapped

water (Hertz, 2003). Due to this, biochar may have positive effects by maintaining structure in the presence of high temperatures, and retaining free water to prevent evaporation.

Lastly, biochar offers chemical stability within concrete. Stability is an important factor when applying additives to concrete and asphalt, as they are susceptible to degradation reactions and oxidation. Since these reactions can compromise the quality of the building material and result in harmful products, it is important to know that these reactions will not be triggered by additives, to result in durable materials (Gupta & Kua, 2017). Similar to the application in soil, the stability of biochar depends largely on the fixed carbon level of the material, and the lack of reactive surface groups on the biochar. As discussed previously, the surface functional groups of biochar largely depend on the feedstock that is chosen, and the pyrolysis temperature as these groups will disappear with higher treatment temperatures (Kloss et al., 2011). Due to this, a biochar with a low O/C ratio will have lower reactivity, and as a result will be less likely to cause or promote reactions within concrete and asphalt (Gupta & Kua, 2017).

1.4 Objectives

The objectives of this thesis are:

1) Develop large scale production methods for creating larger quantities of consistent and predictable biochar from a range of feedstocks.

While research has been performed on pyrolysis reactor technology, most studies produced biochar in a small lab-scale configuration or purchased the biochar from another facility. The production technique plays a dominant role in the final biochar characteristics, so it is important to understand the trends in properties of biochar produced in large scales, and how to produce the desired properties consistently for industrial applications.

2) Produce and characterize biochar from different waste materials that are abundant in Canadian industry to determine the range of characteristics that can be present and used in industrial applications.

While biochar has been gaining lots of research attention in recent years as potential soil amendment and fertilizer, more valuable applications must be investigated to drive pyrolysis

forward as a prominent method of producing alternative energy and chemicals. Additionally, the utilization of waste materials which would potentially end in a landfill or stockpiled somewhere will promote the carbon sequestration associated with biochar.

3) Create charcrete using a common commercial concrete recipe, to determine the effects of adding biochar to cementitious composites.

Studies have began to investigate the use of biochar as an addition in cementitious composites (Ahmad et al., 2015; Choi et al., 2012; Restuccia & Ferro, 2016). However, most research has focussed on mixtures involving biochar in pure cement powder, or with a small amount of fine sand added to create mortar. This study aims to understand how the addition of biochar will affect key properties of commonly found concrete, such as its thermal conductivity and sound absorption.

4) Determine the carbon microstructure of biochar created from different Canadian industrial feedstocks and find the electrical conductivity of the biochar produced at varying temperatures, and the permittivity of composites produced with this biochar.

Biochar can show similar carbon structure to that of graphene materials and carbon black at a lower cost, and recent studies have focused on developing composites using biochar for electrical purposes (Ahmetli et al., 2013; Behazin et al., 2016; Nan et al., 2015; Quaranta et al., 2016). To optimize the cost effectiveness of these electrical composites, a wider range of biochar feedstocks need to be investigated for potential electrical properties.

5) Develop a quick and cost-effective method for determining how biochar will distribute in polymer-composites.

One of the key factors that determines how well a filler will behave in a polymer is the dispersion of the filler throughout the material. Poor distribution can result in poor mechanical properties, as areas with packed fillers will be susceptible to stresses. Electrically conductive fillers require networks to be formed throughout the material (Wypych, 2009). Therefore, it is ideal for having a method of determining how well a filler will disperse in a polymer without the time intensive and costly process of making the composite.

1.5 Scope of Thesis

- Chapter 2 discusses the reactor systems and feedstocks used to produce the biochar that is used in this thesis. The different methodologies are compared in terms of product yield, and the characteristics of the biochar produced in terms of chemical and physical characteristics.
- In Chapter 3, biochar is added to concrete to produce a lightweight, green building material. The effect of the biochar addition at different loading levels on the compressive strength, acoustic reduction, and thermal properties is analyzed.
- In Chapter 4, the effects of biochar addition on polymer composites are studied. The carbon microstructure and electrical conductivity of the biochar are analyzed. A method for predicting the distribution of biochar when added to composites is developed, and the electrical shielding properties of the polymer composites are determined.
- Chapter 5 covers the final conclusions and recommendations.

Chapter 2

2 Biochar Production and Characterization

This chapter describes the feedstocks chosen for this research and the different biochar production methods that were employed for the thesis. Additionally, the analytical methods used to test the biochar will be discussed, as well as the characteristics of the biochar that was produced.

2.1 Introduction

The increasing global demand for energy and petroleum based products has presented several hurdles which need to be overcome, such as decreasing oil reserves and an imbalance in the natural carbon cycle leading to climate change (Donaldson et al., 2013; Schmidt, 2012b). This has lead to interest in being placed in renewable, more sustainable alternatives being developed. Of these alternatives, biomass has been recognized as a highly advantageous feedstock due to abundance, positive environmental attributes, and waste management potential (Behazin et al., 2016; Jahirul et al., 2012). Biomass is defined as, "A mass of live or dead organic matter" by the Food and Agricultural Organization (FAO, 2009), and is very similar to charcoal except that charcoal is primarily used for burning (Lehmann & Joseph, 2009). This covers a wide range of materials, such as wood, plants, and foods. While raw biomass does not have much value for energy or chemical applications, several conversion methods have been developed to convert biomass into products.

Pyrolysis is the thermal decomposition of biomass in a limited or zero oxygen environment, at temperatures ranging from 350- 650 °C (Bridgwater, 2003). While there are several different thermal conversion methods for treating biomass, pyrolysis is one of the most popular methods since it produces solid (biochar), liquid (bio-oil), and gas phase products (Tripathi et al., 2016). While bio-oil has gained the most attention over the last 30 years due to its potential to replace petroleum for energy and chemicals, biochar has recently started gaining the attention of researchers. Biochar is the solid, high carbon residue remaining after the evacuation of volatile components during pyrolysis (Lehmann & Joseph, 2009). While biochar can have a wide range of characteristics, it is typically characterized by high fixed carbon levels, high specific surface

area and pore volume, and good adsorptive properties (Kloss et al., 2011; Xie, Reddy, Wang, Yargicoglu, & Spokas, 2014). While initially investigated largely for application as a soil amendment, recent research has looked at using engineered biochar for a wide range of industrial applications (Qian et al., 2015; Schmidt, 2012a). A more in-depth review of pyrolysis and biochar can be found in Chapter 1.

One of the most important aspects of the biochar industry is the versatility in characteristics that can be seen in the material. The biomass selected, the reaction process used, and the temperature can all play large roles in determining the final properties of the biochar. Due to this, significant research has been done to investigate the effects of different pyrolysis processes, and several comprehensive reviews and studies have been performed discussing reactors, temperature, and other variables (Bridgwater & Peacocke, 2000; Jahirul et al., 2012; Kan et al., 2016; Manyà, 2012; Tripathi et al., 2016). While a variety of biomasses found around the world have been investigated for biochar purposes, this study aims to highlight those found abundantly throughout Canada. Miscanthus, wood, and dried distiller's grain (DDG) were selected for investigation, as each represents a different biomass type of potentially high economic impact.

Miscanthus, which comes in a variety of strains, is a perennial grass introduced to North America and Europe, which stands anywhere from 2 to 4 meters tall (Scurlock, 1999). According to Ontario's Invasive Species Awareness Program (www.invadingspecies.com), Miscanthus is an invasive species, in that it spreads quickly and grows in dense packs, leading to negative impacts on the surrounding vegetation. However, this creates an advantage for Miscanthus to be grown as an energy crop: a low-cost, low-maintenance plant that can be used to make biofuels (Brosse et al., 2012). The effects of pyrolysis of Miscanthus has been investigated in several studies. One study found Miscanthus pyrolyzed at 600 °C for 10 minutes had a surface area of 51 m^2/g, and a carbon content of 85.1% (Kwapinski et al., 2010). Another study found that Miscanthus pyrolyzes at 500 °C with a 27 % yield of biochar that is ideal for soil applications due to its high carbon content (79%) and surface area (180 m^2/g) (Lee, Eum, et al., 2013).

While wood is an extremely well-known feedstock for biochar production, this study aims to find more value in waste or recycled materials. One of these sources is waste wood from

construction projects, used for building, renovation and demolition projects. In a report published in 2006, it was estimated that 875 000 tonnes were disposed of by Canada in 2002 (Natural Resources Canada, 2006). This presents an ideal feedstock for biochar production as most of this material ends in landfills. The lumber used in buildings is typically SPF (spruce-pine-fir), and is made of a combination of different softwood species found throughout Canada, according to Canada Wood (canadawood.org). This would lead one to expect that the biochar should have properties similar to those of the base woods used. However, certain preservatives used to treat wood (Cu, As, Cr) could be maintained within the material, which could result in the biochar having increased levels of certain heavy metals (Lucchini et al., 2014; Zelinka & Stone, 2011). Despite little research being done on converting waste construction and demolition wood to biochar, one study has shown that biochar from waste wood (particle board, plywood, and demolition wood) produced at 480 °C had high fixed carbon (>88%), and low ash contents (<3%) (Mitchell et al., 2013). This corresponds well to other studies preparing biochar from each wood on their own, namely pine (Ronsse et al., 2013; Xie et al., 2014).

DDG is as a co-product of bioethanol production from corn, consisting of the leftover grain once the starch has been fermented (Wood et al., 2014). Since the DDG consists mainly of proteins, fats, and fibres, it has typically been used as livestock feed. However, with the increase in production of bioethanol using fermentation, much more DDG has been produced in recent years, making it a potential feedstock for biochar production (Xu et al., 2011). Another factor is that corn with high levels of mycotoxins, such as vomitoxin, is unsuitable for consumption, and the mycotoxin will be concentrated in the DDG (National Hog Farmer, 2017). DDG differs from other feedstocks used for pyrolysis in that it is not a lignocellulosic material, rather a cereal made of around 55 % carbohydrates, 30% protein, and 10 % fat, and the rest minerals (Liu, 2011). Despite that, studies have still attempted to find biochar characteristics of the grains. One study found that biochar from brewer's grain produced at 700 °C had a high production yield (53.3 %), however the ash content of the material was quite high and the surface area did not reach the levels that should be expected for high temperature pyrolysis (32 m^2/g). However, the authors found that the biochar could still be used as a precursor for biochar used for capturing NH_4^+ -N (Zhang & Wang, 2016). Another study showed similar trends for the DDG biochar, showing that at 600 °C, the yield was still high (29.2%), and the biochar had relatively low carbon content (61.48%) (Wood et al., 2014).

This study aims to investigate the varying characteristics of biochar produced from three different Canadian feedstocks. Additionally, the change in biochar properties from different pyrolysis systems and increasing temperatures will be analyzed. The goal of this research is to both analyze the biochar characteristics, such that production methods can be made to specifically meet needed properties for industrial applications, and to produce biochar with a wide range of properties such that the impacts of individual characteristics on different material properties can be determined.

2.2 Materials and Methods

For the experiments in this study, three feedstocks were chosen from different suppliers. The selected feedstocks were based on two key factors, the first being that all three feedstocks are abundant in Canada. The second being that each feedstock represents a different "category" of feedstock. That is, the wood chips are a forestry residue, the Miscanthus an agricultural residue, and the distiller's grain an industrial by-product.

The wood chips were supplied by BRQ in Trois Rivieres, Quebec. The wood is a collection of construction waste material collected from the Trois Rivieres region. Two different harvests of Miscanthus (*Miscanthus sacchariflorus)* were chosen, the first being collected from Drumbo, Ontario (shortened to MS, Drumbo), and the second was provided by All Weather Farms Inc, in Port Ryerse, Ontario (shortened to MS, AWF). The dried distiller's grain was supplied by IGPC Ethanol Inc., in Alymer, Ontario. The wood chips and Miscanthus were both ground in a hammermill to pass an 840 µm screen before pyrolysis.

2.2.1 Experimental Set-up

The fast pyrolysis experiments were carried out in the Pyrolysis Pilot Plant. The Pilot Plant is a pilot scale reactor, originally designed to handle fluidization reactions using pre-heated nitrogen, which has been modified for continuous, mechanically fluidized experiments. Biomass can be fed to the reactor using either a side mounted screw feeder, or the ICFAR biomass "slug injector" feeder. The slug injection feeder uses a solenoid valve to allow a small amount of biomass to fall into a tube, after which a short and powerful blast of nitrogen pushes the material into the reactor (Berruti, 2013). A mechanical mixer is present at the bottom of the reactor, and

heat is provided through a combination of band heaters and induction. The main aspects of the reactor are shown in Figure 2.1.

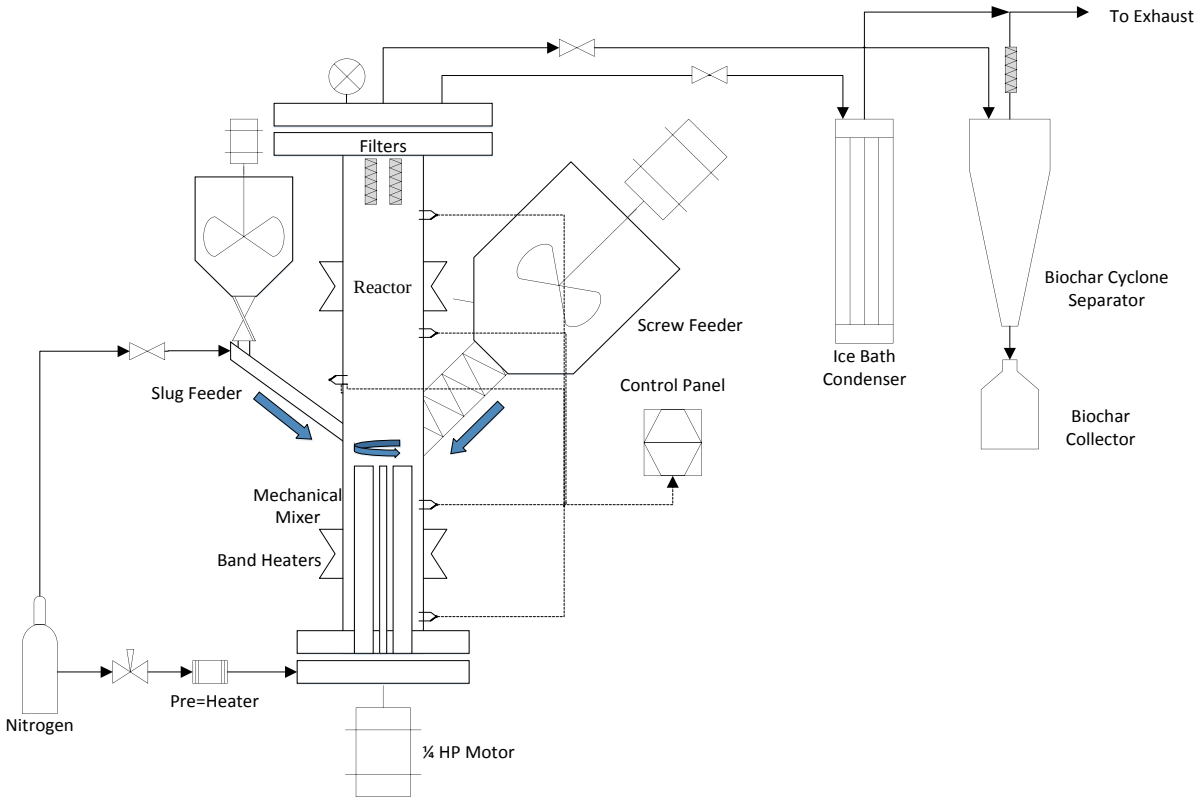

Figure 2.1-Flow Diagram for the Pyrolysis Pilot Plant

By using mechanical mixing instead of fluidization, the need for a heating medium (such as sand) is negated. This means that pure biochar can be produced and extracted through the modified continuous extractor near the bottom of the reactor. Thus, the pre-heated nitrogen can be used to control the vapour residence time within the reactor. Vapours exit the reactor through tubes at the top of the reactor, before passing through a 2.9 L condenser in an ice bath and exiting through the exhaust, or an electrostatic precipitator followed by a condenser train.

The unmodified reactor is made of stainless steel 316, with an inner diameter of 7.62 cm, a wall thickness of 0.55 cm, and a height of 58.4 cm, giving a volume of 2.9 L. It is labelled unmodified as the continuous extraction extension was not used in these experiments. The reactor has two joints: a lid, a flange with a diameter of 25.4 cm, and the bottom of the reactor, a flange with a diameter of 12.7 cm. Heat is provided using 4 Watlow MI Ceramic band heaters each providing 950 W, with fiberglass insulation wrapped around the reactor and flanges to

minimize heat loss. Five thermocouples are placed throughout the reactor in order monitor and control power output through the band heaters, connected to Honeywell Temperature controllers. Nitrogen is passed through a pre-heater before being supplied to the reactor through a perforated plate at the base of the reactor. A pressure gauge is connected to the top of the reactor to monitor pressure, with a 15 PSI safety release valve. The material is mixed using a mechanical agitator powered by a ¼ horsepower electrical motor. Biomass is fed using one of two options, the first being a screw feeder, mounted to the side of the reactor at a 45° angle, where an agitator and screw are powered by a ¼ horsepower electrical motor into the reactor. The second option is the ICFAR biomass "slug injection" feeder, which feeds biomass from a hopper through a 5/8" pipe connected at a 45° attached to the side of the reactor. The biomass falls from the hopper through a pneumatically controlled pinch valve, which can be set to open at different time intervals (around 5 seconds) for a short time interval (less than one second). The biomass falls into an injection tube, which is then forced into the reactor through a nitrogen pulse, along with a continuous nitrogen stream which keeps biomass from settling in the tube (Berruti, 2013).

The vapours exit the reactor through two 0.5" pipes at the top of the reactor, with steel mesh placed over the exits to keep particles from entering the condenser. In order to continuously extract biochar from the system, an extension was built at the bottom of the reactor, as shown in Figure 2.2. The extension is made of carbon steel, with an inner diameter of 7.62 cm and a height of 18cm, bringing the total reactor volume to 3.38 L. The biochar is pulled through a 1.5" pipe attached halfway up the extensions by a screw, powered by an air motor, and falls into a 1.4 L collection system which can be replaced quickly through cam and groove couplings as shown in Figure 2.2. The extension is heated by a 1.8 kW induction system wrapped around the exterior of the pipe, with the temperature controlled by a thermocouple hooked up to a laptop with data acquisition software.

The biochar can also be collected using an elutriation system. A one inch pipe exits from the top of the reactor, before reducing to a 0.5" line. The line exits into a collector, made of 3" pipe, with an inlet pipe entering at an angle to create a cyclone, where the biochar will hit the wall and fall to the bottom of the collector. The vapours then exit through a straight line before passing through a steel mesh filter and leaving through the exhaust. The biochar can be collected by removing the bottom half through the use of cam-and-groove couplings.

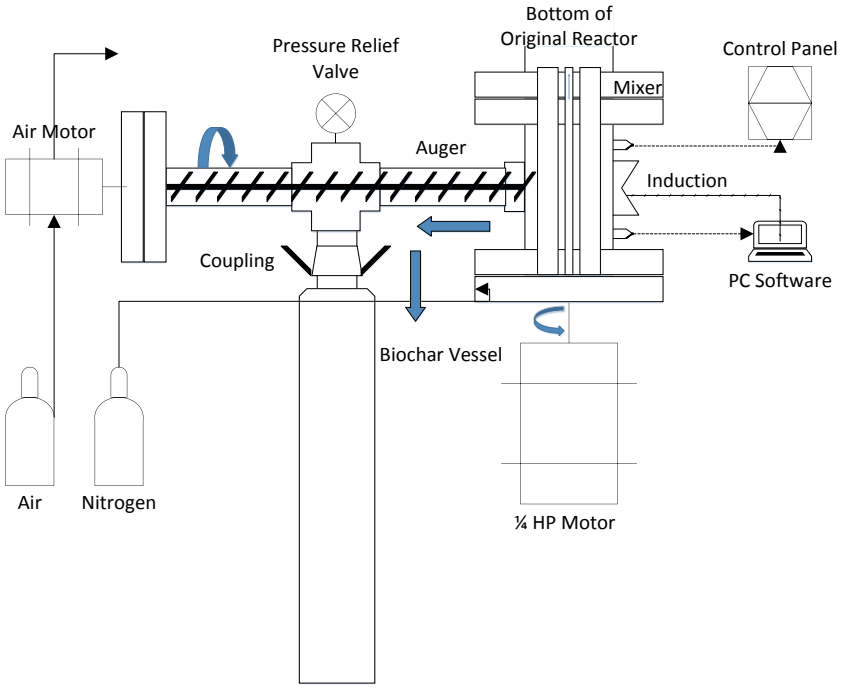

Figure 2.2-Continuous extraction modification for the pyrolysis pilot plant

2.2.2 Pyrolysis Experiments

It is worth noting that for all experimental trials conducted, while bio-oil was collected from the condensers, it was not analyzed as part of this study, and a mass balance was not performed on the systems.

Unmodified Pyrolysis Pilot Plant Experiments

For these experiments, the bottom extension and char extractor modifications were not used. The reactor was first heated to the desired temperature by setting the control points on the reactor panel (see Table 2.1), and heating to the desired temperature would take anywhere from 30 to 45 minutes. During pre-heating, the nitrogen flow was set to 9 SLPM which had been used in experiments by other researchers, and the nitrogen pre-heater was set to 350 °C (superficial gas velocity of 0.06 m/s), and the mechanical mixer was turned to 25 RPM to help distribute the heat. Approximately 300 g of Miscanthus was then added to the screw feeder hopper by the use of a funnel. The exhaust lines from the reactor were connected to an electrostatic precipitator (ESP) and condenser train, with the ESP set to 15 kV. Once the reactor was pre-heated, the nitrogen flow-rate was set to the desired flow rate to achieve a 3 second residence time.

The feed motor was then set to 40 RPM (1 kg/h for Miscanthus and wood), and biomass was fed to the reactor. The reaction was allowed to proceed for 40 minutes, the time which it took to feed all the material, after which the feeder was turned off. The exhaust line was then turned off using two ball valves connected to the lines, and the char elutriation line was opened. The mechanical agitator was turned off, and the nitrogen flow was set to the maximum the flowmeter could read at 82 SLPM (0.58 m/s), in order to elutriate the biochar from the reactor and into the collector. This was carried out for 20 minutes, at which point, the elutriation line was closed, the condenser lines were opened again, and the reactor was either shut down, or another batch was started depending on the run. The set of pyrolysis experiments carried out under this operation method is shown in Table 2.1. The temperature range was selected as 350 °C is the lower limit typically seen in pyrolysis, and 550 °C is the heating limitation of the reactor.

Table 2.1-List of runs and operating conditions for unmodified pilot plant experiments

Run	*Feedstock*	*Temperature (°C)*	*τ (s)*	*Biomass Fed (g)*	*Batches*	*Feed Time (min)*
1	MS, Drumbo	550	3	867	2	40
2	MS, Drumbo	550	3	761	3	40
3	MS, Drumbo	500	3	385	1	40
4	MS, Drumbo	500	3	300	1	40
5	MS, Drumbo	500	3	211	1	40
6	MS, Drumbo	450	3	477	3	40
7	MS, AWF	500	3	838	3	40
8	MS, AWF	450	3	297	1	40
9	MS, AWF	400	3	897	3	40
10	MS, AWF	350	3	548	2	40

Continuous Pyrolysis Experiments

For the continuous experiments, the extension for char extraction was attached to the bottom of the reactor. The exhaust lines were connected to a single condenser in an ice bath for the run. The reactor was first heated by setting the temperature controls on the reactor panel to the desired temperature, and by setting the induction control to the desired temperature. During pre-heating, the mechanical agitator was turned on to 30 RPM, and the nitrogen flow was set to the desired flowrate for the run. It is worth noting that for the first few runs, the nitrogen was pre-heated to 350 °C and set to higher flowrates, but for the remainder of the runs was left cold and set anywhere between 5 and 8 SLPM to assist the mechanical agitator, while the gas temperature

was undetermined. This was because the higher flowrates of nitrogen were causing the biochar to be lifted from the bed in previous experiments.

For runs using the screw feeder, the biomass was then fed to the feeder using a funnel at the top of the hopper, and the feed motor was set to 40 RPM (1 kg/h for Miscanthus and wood) once the reactor was at temperature. For the pulse feeder, the biomass was added to the hopper using a funnel, and the hopper agitator was turned on. Once the reactor temperature was reached, the continuous nitrogen flow to the slug feeder was turned on. The ball valve on the line from the feeder to the reactor was opened, and the program used to control the solenoid valve was started, resulting in a feed rate of approximately 800 g/hr of distiller's grains.

Once the feeding had started, the reaction continued for 45 minutes, as it was discovered the continuous reactions needed slightly longer pyrolysis time. At this point, the feeder was turned off, and the air supply to the air motor was turned on at a regulated pressure of 25-40 PSI. After 4 minutes, the air motor was turned off. If the collector was full, it would be replaced by releasing the cam-and-groove couplings, capping the collector, placing it in a water bath to quench the biochar, and replacing the collector with another. At this point, another batch could be run. The complete list of runs completed in this operation method is shown in Table 2.2.

Slow Pyrolysis Experiments

The slow pyrolysis experiments were carried out in a small scale, batch mechanically fluidized reactor (MFR). The reactor has a height of 12.7 cm and diameter of 9.1 cm, giving a volume of 0.83 L. The reactor is made of stainless steel 316, and wrapped in carbon steel wire in order to increase the induction efficiency. The reactor is mixed using an internal blade mixer which is connected to a 1/4 HP electrical motor. The reactor is filled by removing the bolts holding onto the lid and filling the reactor with biomass (approximately 80 g of Miscanthus), before reattaching the lid and connecting the motor to the mixer shaft. The reactor is heated using the same 1.8 kW induction system and controlling program as the pilot plant extension, with the temperature recorded by a thermocouple placed within the bed of the reactor. The reactor configuration is shown in Figure 2.3.

Table 2.2-List of experiments and operating conditions for continuous pyrolysis experiments

Run	*Feedstock*	*Temperature (°C)*	*τ (s)**	*Feeder*	*Biomass Fed (g)*	*Feed Time (min)*
1	MS, AWF	550	8.7	Screw	1437.5	45
2	MS, AWF	550	8.7	Screw	1500	45
3	MS, AWF	550	11.6	Screw	866.5	45
4	MS, AWF	450	7.0	Screw	903.5	45
5	MS, AWF	450	7.0	Screw	1868.5	45
6	MS, AWF	450	11.6	Screw	1062.5	45
7	MS, AWF	350	7.0	Screw	1492	45
8	MS, AWF	350	7.0	Screw	974.5	45
9	Wood Chip	550	10.0	Screw	977.5	45
10	Wood Chip	550	10.0	Screw	1496	45
11	Wood Chip	450	10.0	Screw	1814.5	45
12	Wood Chip	450	8.7	Screw	973.5	45
13	Wood Chip	350	8.7	Screw	1678.5	45
14	Wood Chip	350	8.7	Screw	874	45
15	DDG	500	14.0**	Pulse	1602	45
16	DDG	500	14.0**	Pulse	617.5	45
17	DDG	500	14.0**	Pulse	1875	45
18	DDG	400	14.0**	Pulse	1539	45
19	DDG	400	14.0**	Pulse	1410	45

* The residence time is calculated assuming the nitrogen reaches reactor temperature
** The residence time is calculated using the nitrogen feed, ignoring the nitrogen from the pulse feeder

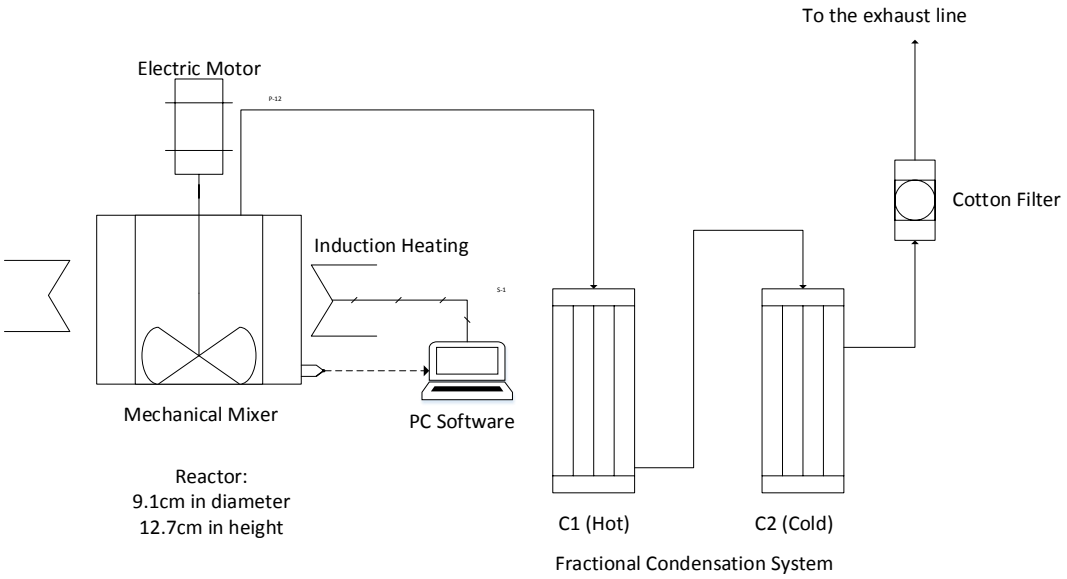

Figure 2.3-Small Mechanically Fluidized Reactor

To start the reaction, the computer software controlling the induction system is turned on, and the set-point temperature is entered. The mixer is turned on, spinning in a "washing machine" method, where it spins one way for several seconds, stops, and then begins to spin the other way. The exhaust vent fume hood is turned on, to create a pressure differential within the reactor to remove the vapours. The vapours exit through a tube in the center of the reactor, before passing through a condensation train (only the cold condenser was used for these experiments), and exiting through the exhaust line. Once the set point temperature was reached (around 2 hours), called the highest treatment temperature (HTT), the reactor was kept at temperature for 5-10 minutes in order to ensure complete pyrolysis. After this, the induction was turned off, and the reactor was allowed to cool. The bio-oil could be collected by removing the condenser, and the biochar was collected by removing the lid and collecting the material. A complete list of runs and operating conditions is shown in Table 2.3. The average and fastest heating rates were uncontrolled and were determined by the rate at which the system heated. The differences in HTT were due to limitations of the system depending on the amount of insulation used, with 500 °C being the highest temperature achievable in the system.

Table 2.3- List of experiments and operating conditions for slow pyrolysis experiments

Run	*Feedstock*	*HTT (°C)*	*Average Heating Rate (°C/min)*	*Fastest Heating Rate (°C/min)*	*Pyrolysis Time (min)*	*Biomass Fed (g)*
1	MS, AWF	350	3.8	12.4	109	72
2	MS, AWF	327	2.7	11.8	124	74
3	MS, AWF	500	5.1	13.1	110	75
4	MS, AWF	480	3.8	14.0	123	74.5

Thermal Treatment

To further study the characteristics of the biochar produced from dried distiller's grain, experiments were conducted to treat previously produced biochar at 600 °C. The term thermal treatment was used as opposed to pyrolysis, as these were the only experiments in which previously produced biochar was introduced to higher temperatures. In order to do this, a muffle furnace was used, after being modified to purge the furnace chamber with nitrogen for the duration of the experiment. The distiller's grain biochar used in this experiment was collected from the ICFAR MFR-100 (shortened to MFR-DDG), a large scale, continuous, mechanically

fluidized reactor capable of processing 100 kg/hr of biomass. The biochar was produced at around 480 °C.

300 grams of biochar was loaded into a stainless-steel container, which was placed into the muffle furnace. The nitrogen purge was open providing 1.42 LPM of nitrogen over the biochar container and into the furnace chamber. The muffle furnace was then turned on and heated to 600 °C, which was selected as it is a 100 °C step from the highest DDG pyrolysis temperature in previous experiments. The temperature was maintained for an hour, at which point the furnace was turned off. Nitrogen flow was maintained until the reactor reached a low enough temperature where there was no risk of biochar combustion. A list of experiments is listed in Table 2.4. Once again the heating rate was a nature of the system parameters.

Table 2.4- List of experimental runs for thermal treatment

Run	*Feedstock*	*Temperature (°C)*	*Heating Rate (°C/min)*	*Hold Time (min)*
1	MFR-DDG	600	14.6	60
2	MFR-DDG	600	14.6	60
3	MFR-DDG	600	15	60
4	MFR-DDG	600	16	60
5	MFR-DDG	600	16.9	60

2.2.3 Analytical Methods

Proximate Analysis

Proximate analysis is used to determine the quantity of volatile matter, fixed carbon, and inorganic ash contained in the sample by weight. The analysis was carried out following a modified method set by ASTM D1762-84. Approximately 1 g of material was placed in a porcelain crucible, and placed in an oven at 105 °C for at least 2 hours to determine the dry weight of material. A lid was then placed over the crucible, which was then placed in a muffle furnace at 950 °C for 11 minutes. The volatile matter was calculated as the mass fraction lost after this step. The samples were placed in a desiccator to cool, then placed in the muffle furnace at 750 °C for at least 6 hours. The remaining material was calculated as the dry ash content of the biochar. The fixed carbon of the sample was found by subtracting the volatile content and ash content from the dry mass of material. The volatile matter, fixed carbon, and ash are all reported on percent dry weight basis, and as an average of biochar produced at that temperature.

The ash calculated yield of the pyrolysis experiments is the theoretical yield based off an ash balance from the feedstock and the biochar. This is based off of the assumption that most of the inorganic content of the feedstock will remain in the charred material (Ronsse, van Hecke, Dickinson, & Prins, 2013). It was calculated as shown in the equation below.

$$Ash\ Calculated\ Yield\ (wt\%) = 100\ \% * \frac{Ash_{Feed}(wt\ \%)}{Ash_{Biochar}(wt\%)}$$

Elemental Analysis

The C, H, and N contents of the samples were determined using the Thermo Scientific FlashEA 1112 analyzer. Measurements were recorded in triplicate to ensure reproducibility of the results. Oxygen was determined by difference of C, H, N and the ash content.

Surface Area and Pore Volume

The BET surface area, external surface area, pore volume and average pore size was determined using a TriStar II 3020 BET Surface Area and Pore Analyzer from Micrometrics. Prior to analysis, the samples were degassed using nitrogen at 105 °C for 1 hour, and at 300 °C for a minimum of 5 hours. All results were calculated using a 55-point analysis. The surface area was determined using the Brauner, Emmett, and Teller (BET) method.

Particle Size Analysis

The particle size analysis was carried out using a Sympatec Helos/BF Particle Size Analyzer. The Helos systems uses laser diffraction to determine the particle size distribution of samples in accordance with ISO 13320-1 standards.

Metals Analysis

The inorganic content of the materials was determined using inductively coupled plasma optical emission spectrometry (ICP-OES) analysis. Before analysis, the sample is washed, by taking a known weight of sample and adding to it 9 mL of 69% HNO_3 and 2 mL of HCl. The mixture is heated to 170 °C for 15-20 minutes, before 2-3 mL of 30% H_2O_2 is added and the solution heated for 5-10 minutes. Once cooled, the solution was passed through a Whatman No. 41 filter paper

and rinsed using Milli-Q water. Once the solution was made, a blank was prepared using the same procedure. The washed sample and blank was then analyzed by Varian Vista-PRO CCD Simultaneous ICP-OES against known calibration standards, and the results calculated from there.

Scanning Electron Microscopy (FESEM) and EDX Analysis

FESEM analysis was performed by the Applied Science and Technology Department (DISAT) at the Politecnico di Torino, Italy. A ZEISS SUPRA^{TM} 40 Field Emission Scanning Electron Microscope was used in order to analyze the structure of the biochar particles. Additionally, the microscope is equipped with an Energy Dispersive X-Rays detector (EDX, Oxford Inca Energy 450) for elemental detection on the surface of the particles. FESEM imaging was performed on the biochar produced in the continuous pyrolysis experiments.

2.3 Results

2.3.1 Production Yields

In Table 2.5, the results of the unmodified Pyrolysis Pilot Plant runs are shown. The biochar yield from the reactor was much lower than expected. This is largely due to particles being entrained in the exiting vapour stream, where biochar would be carried to the filter screen and through in some cases. As well, the biochar collection method of elutriating the particles resulted in biochar collecting in lines, and being passed through the system into the exhaust line.

In Figure 2.4, it becomes clear that the later runs using the Miscanthus from All Weather Farms resulted in a biochar yield from the reactor approaching the theoretical yield based off of the ash balance. While bother actual yields were relatively similar, that ash calculated yield of the MS, Drumbo was much higher than that of the MS, AWF. This is because the ash content of the MS, AWF biochar was much higher than the MS, Drumbo biochar, despite having a lower initial ash content (Table 2.11). This implies that some of the inorganic materials in the Drumbo feedstocks were lost at higher pyrolysis temperatures, or that there is non-homogeneity in the material. The reason for the actual yield being lower than that ash calculated yield is that some of the biochar is lost in collection, or is swept into the condenser system.

Table 2.5- Production results for unmodified pyrolysis experiments

FEEDSTOCK	PYROLYSIS TEMPERATURE (°C)	BIOMASS FED (g)	BIOCHAR YIELD (WT%)	ASH CALCULATED YIELD (%)
MS, DRUMBO	550	867	12.4	29.9
MS, DRUMBO	550	761	15.0	32.0
MS, DRUMBO	500	385	19.0	31.5
MS, DRUMBO	500	300	16.0	32.8
MS, DRUMBO	500	211	17.8	39.4
MS, DRUMBO	450	477	17.2	39.6
MS, AWF	500	897	19.2	19.4
MS, AWF	450	548	19.4	21.1
MS, AWF	400	838	17.6	20.3
MS, AWF	350	297	19.5	34.7

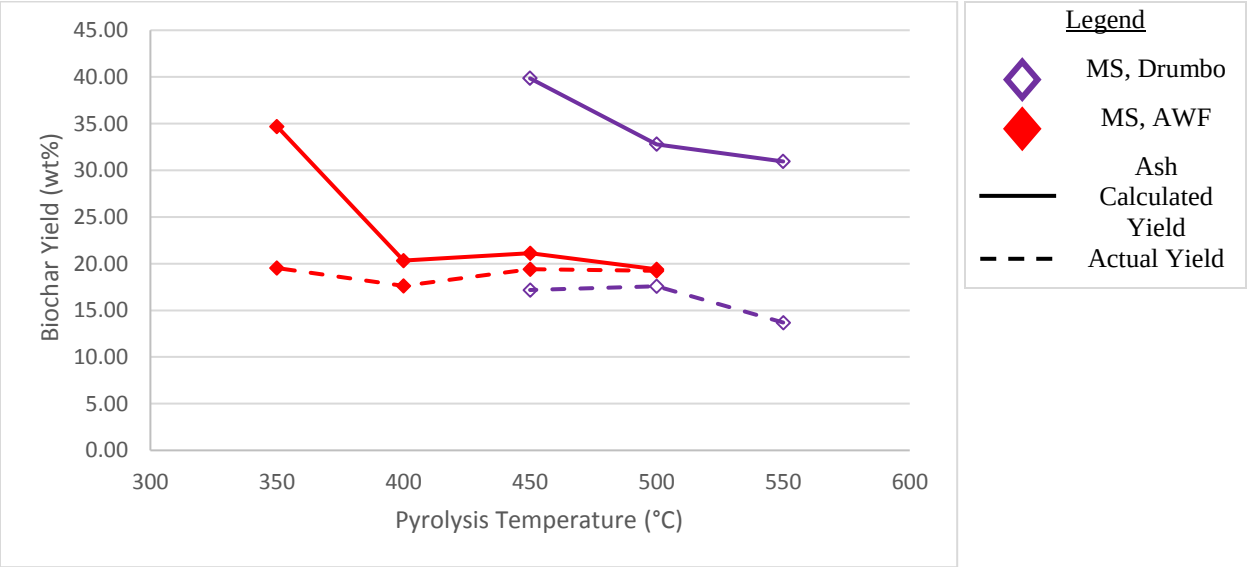

Figure 2.4- Theoretical vs actual yield for Miscanthus biochar in unmodified pyrolysis experiments

Continuous Pyrolysis

From Table 2.6, the collection yield for both the Miscanthus and wood chips are fairly constant between duplicated experiments. Issues still came up around the vapour exit plugging, which would result in yields shifting slightly due to vapour condensation in the biochar collection auger. The distiller's grain presented problems in processing due to the nature of the feedstock.

At elevated temperatures, the grain melts into a wax like material, which once hardened, is extremely difficult to break up. This resulted in the residue building up around sections of the reactor, such as feeder lines, thermocouples, and around the walls of the reactor, making it difficult to collect and properly analyze the yield. It is possible that this caused the volatiles in the material to stick with the biochar, resulting in the higher yields at lower temperatures.

Table 2.6- Production results for biochar from continuous pyrolysis

FEEDSTOCK	PYROLYSIS TEMPERATURE (°C)	BIOMASS FED (G)	BIOCHAR YIELD (WT%)	ASH CALCULATED YIELD (%)
MS, AWF	550	1438	11.1	24.3
MS, AWF	550	1500	15.5	19.7
MS, AWF	550	867	7.9	19.6
MS, AWF	450	904	19.3	20.2
MS, AWF	450	1869	16.3	20.4
MS, AWF	450	1063	18.8	18.7
MS, AWF	350	1492	20.0	38.9
MS, AWF	350	975	26.7	32.2
WOOD CHIP	550	978	18.8	50.4
WOOD CHIP	550	1496	22.4	22.0
WOOD CHIP	450	1815	25.0	49.1
WOOD CHIP	450	974	26.5	36.1
WOOD CHIP	350	1679	26.2	119.9
WOOD CHIP	350	874	28.0	87.2
DDG	500	1602	28.0	36.3
DDG	500	618	7.9	47.3
DDG	500	1875	13.1	34.3
DDG	400	1539	50.9	53.7
DDG	400	1410	32.1	44.4

The ash calculated yield of the fast pyrolysis experiments were less comparable than that of the unmodified reactor experiments. While the Miscanthus behaved in a consistent manner, both the wood chips and grains were less reliable. This comes down largely to the feedstock, which will be discussed more in the proximate analysis results. The graph in Figure 2.5 supports this, where once again the yields for Miscanthus compare well compared to the other two feedstocks.

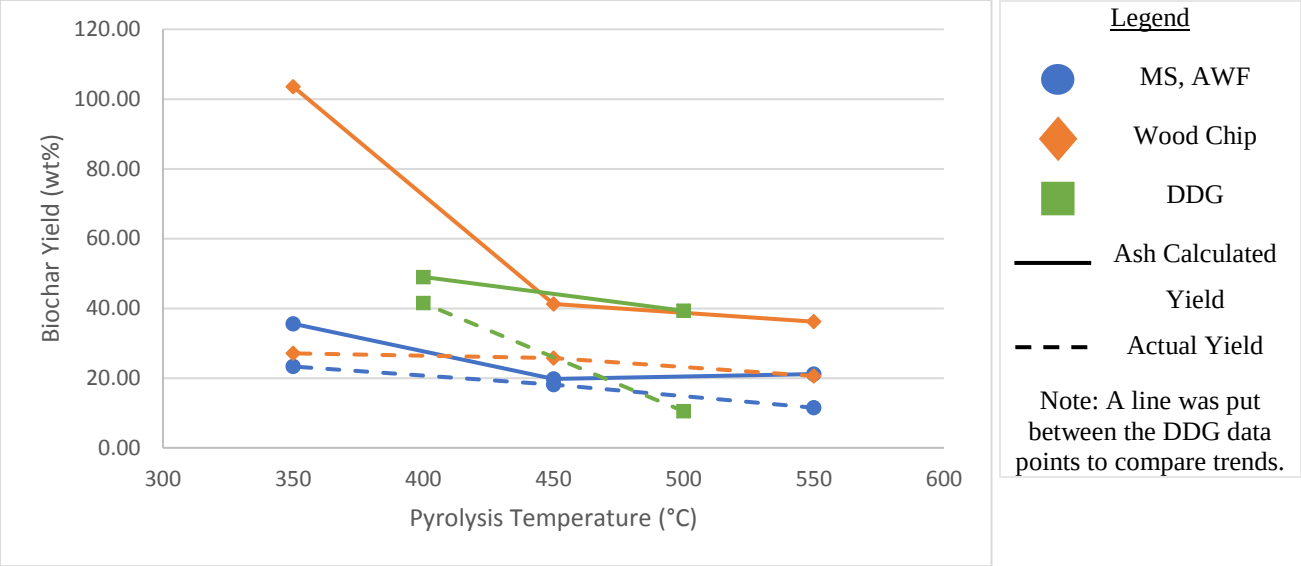

Figure 2.5- Ash calculated yield vs actual biochar yield for continuous pyrolysis experiments

It can be seen that the ash calculated yield for the wood chip biochar was above 100% at 350 °C, which is a result of the ash content of WC350 being lower than the original feedstock. While this could be caused by inorganic materials vaporizing, the sudden increase in ash content with higher temperatures implies that the non-homogeneous nature of the feedstock results in this yield.

Slow Pyrolysis Experiments

The results of the slow pyrolysis experiments are shown in Table 2.7. It can be seen that the yield in these experiments was higher that the previous experiments, which can be attributed to a) slow pyrolysis having a higher yield than fast pyrolysis, and b) that it is easier to collect all the biochar from a batch system. In addition, the actual yield and ash calculated yield are identical, showing how much more effective the collection efficiency is for the small-scale system.

Table 2.7- Production results of the slow pyrolysis experiments

FEEDSTOCK	HTT (°C)	BIOMASS (G)	BIOCHAR YIELD (WT%)	ASH CALCULATED YIELD (WT%)
MS, AWF	500	75	23.4	23.2
MS, AWF	480	75	22.4	21.6
MS, AWF	350	72	24.5	23.6
MS, AWF	327	74	27.5	26.1

Thermal Treatment Experiments

The results of thermal treatment experiments are shown in Table 2.8. The yield in these experiments is so high since biochar was used as the feedstock, and had already been exposed to pyrolysis conditions. From this table, it is clear that the actual yield is slightly lower than the ash calculated yield, which could be due either to the nature of the experiments, or that the grain is not a typical lignocellulosic feedstock and may not behave as biochar does typically. This will be discussed further in the proximate and elemental analysis sections.

Table 2.8- Production results for the thermal treatment experiments

FEEDSTOCK	HTT (°C)	BIOMASS (G)	BIOCHAR YIELD (WT%)	ASH CALCULATED YIELD (WT%)
MFR-DDG	600	301	74.2	79.0
MFR-DDG	600	301	79.9	91.2
MFR-DDG	600	303	80.4	85.6
MFR-DDG	600	303	81.0	85.8
MFR-DDG	600	300	81.5	87.6

Comparison of yields among reactors

Since the Miscanthus from All Weather Farms was used in three different reactor set-ups at similar temperature ranges, we can compare the yield across the three units for a comparison. Figure 2.6 shows the actual biochar yield for the unmodified, continuous, and slow pyrolysis experiments. The yields for both the unmodified and continuous experiments are similar, which is to be expected as they both came from the same reactor, which just different extraction methods. As well, the slow pyrolysis yields were higher than the fast pyrolysis yields over the same temperature range which is discussed above. It can be seen that the pyrolysis at 550 °C has a large drop in yield compared to the two experiments at 500 °C.

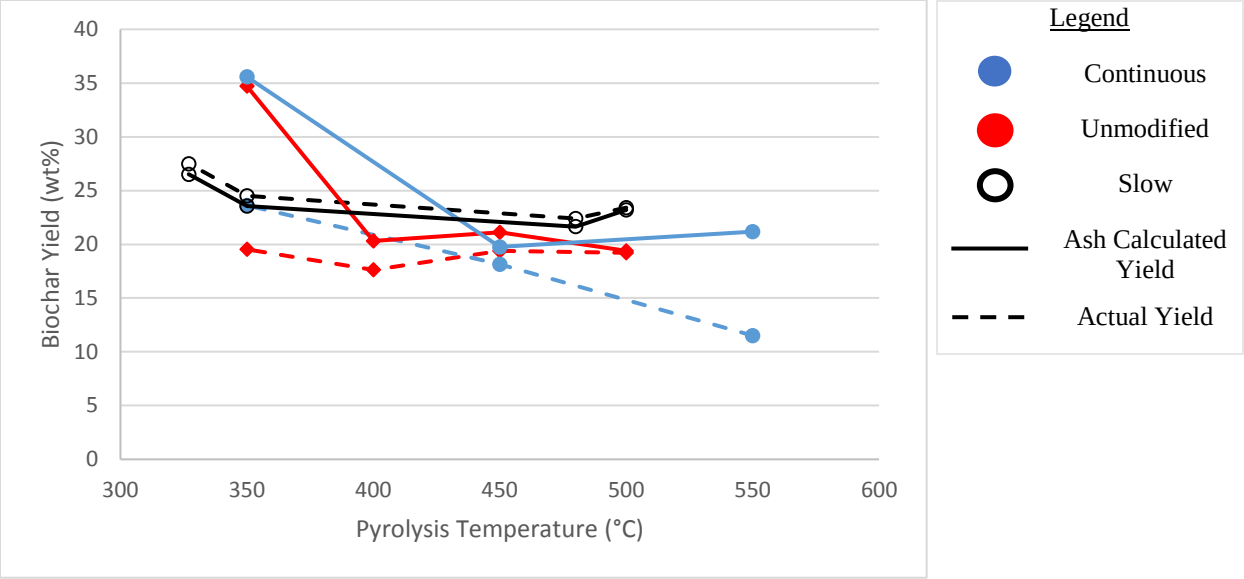

Figure 2.6- Ash calculated and actual yields for biochar produced from MS, AWF for the three different reactor systems

2.3.2 Biochar Characterisation

The proximate and elemental composition of the feedstocks can be seen below in Table 2.9. The different feedstocks shown have a wide range of characteristics, which heavily influence the biochar characteristics. The wood chips clearly have the highest ash content, which is not consistent with the ash content of wood from pine, spruce, and fir (Kloss et al., 2011; Nanda et al., 2013; Suliman et al., 2016; L. Wang & Dibdiakova, 2014), possibly due to its origin as waste from construction sites. The wood waste will have been in contact with a variety of minerals and different metals used in buildings and projects, as well as preservatives and coatings which will have leached metals into the material. It was found that the wood chips were very non-homogeneous when compared to the other feedstocks. Taking samples from different areas of the batch could vary the chemical characteristics of the material, resulting in biochar with non-consistent characteristics.

The Miscanthus samples are slightly different, having the expected elemental analysis of Miscanthus crops (Mimmo et al., 2014). The volatile matter of the crop is higher than other agricultural residues, but one advantage is as a grass, it appears to have a low ash content (Lee et al., 2013; Nanda et al., 2013). Miscanthus has the highest oxygen content of all the samples.

Table 2.9- Composition of feedstocks used in experiments

	Proximate Analysis (wt%)				Elemental Analysis (wt%)			
FEEDSTOCK	**MOISTURE**	**VOLATILES**	**FIXED CARBON**	**ASH**	**C**	**H**	**N**	**O**
MS, Drumbo	5.5	81.9	14.9	3.2	45.2	5.9	1.2	44.5
MS, AWF	7.7	86.6	11.2	2.2	44.7	6.0	0.2	47.0
Wood Chips	9.0	75.1	12.9	12.0	43.2	5.7	0.1	39.0
DDG	9.9	82.0	12.8	5.2	43.8	6.9	4.9	39.2

Finally, the composition of the distiller's grain is rather interesting. Even though it differs from the other feedstocks in that it is not a typical pyrolysis feedstock as it is a starch residue, it still contains similar proximate and elemental compositions. Table 2.10 shows the metal content of each of the different feedstocks. The results show a few key things about the materials. The grain had very high concentrations of inorganic materials typically associated with nutrients (K, Mg, Na, and P) as well as sulphur. No metals were especially prominent in Miscanthus, with Ca and K being in the largest concentrations.

Table 2.10- ICP analysis for the feedstocks used in experiments

METAL (MG/KG)	**MS, DRUMBO**	**MS, AWF**	**WOOD CHIP**	**DDG**
Al	89	111	1083	0.31
Ca	1586	1746	12791	218
Cu	3.7	5.4	8.6	4.4
Fe	187	181	2011	53
K	2349	1588	1499	8716
Mg	471	330	1074	3470
Mn	23.8	39.2	110	12.3
Na	124	241	392	1950
Ni	0.9	0.32	8.9	0.32
P	271	369	114	8405
Pb	<2.5	<2.5	16.7	<2.5
S	304	313	605	7288
Si	566	684	684	50.2
Zn	10.2	16.3	13.2	50.3

The wood has very high concentrations of certain metals (Al, Ca, Fe, Ni, and Pb) compared to the other feedstocks. The high Ca, Al, and Fe content is commonly seen in wood, and they are commonly in abundance depending on the area of the tree the wood is taken from (L. Wang & Dibdiakova, 2014). More alarming is the high content of acid insoluble ash in the wood (consisting of 77% of the total ash content), which comes largely from silica and sand content. This is unsurprising, as The Centre for Construction Research and Training lists over 20 sources of silica dust on construction sites (https://plan.silica-safe.org).

Proximate Analysis

The results of the proximate analysis for the unmodified pyrolysis biochar can be seen in Table 2.11. The results are averaged between the tested batches, with the full set of results shown in Appendix A (Table A.1). A steady increase in the fixed carbon content of both biochars can be seen, which is expected with a decrease in the volatile matter of the samples. The ash content also increases steadily, whereas the Miscanthus from All Weather Farms has a higher ash content despite the feedstock having a lower ash content than the Miscanthus from Drumbo.

Table 2.11- Proximate analysis for biochar from unmodified experiments

BIOCHAR	VOLATILE MATTER (WT%)	FIXED CARBON (WT%)	ASH CONTENT (WT%)
MS, DRUMBO 550	18.4	71.3	10.4
MS, DRUMBO 500	22.5	67.8	9.8
MS, DRUMBO 450	32.1	59.9	8.0
MS, AWF 500	24.1	62.8	13.1
MS, AWF 450	28.8	59.2	12.0
MS, AWF 400	31.0	56.5	12.5
MS, AWF 350	47.2	45.5	7.3

The results of the proximate analysis for the continuous pyrolysis biochar is shown in Table 2.12, with the full results in Table A.2.

Table 2.12- Proximate analysis of continuous pyrolysis experiments

BIOCHAR	VOLATILE MATTER (WT%)	FIXED CARBON (WT%)	ASH CONTENT (WT%)
MS, AWF 550	17.8	71.8	10.2
MS, AWF 450	29.0	60.2	10.9
MS, AWF 350	42.8	51.1	6.1
WOOD CHIP 550	18.1	38.2	43.8
WOOD CHIP 450	24.4	46.6	28.6
WOOD CHIP 350	36.7	52.0	11.4
DDG 500	36.3	47.4	14.3
DDG 400	54.7	35.0	10.4

As, well the trends can be seen in Figure 2.7.

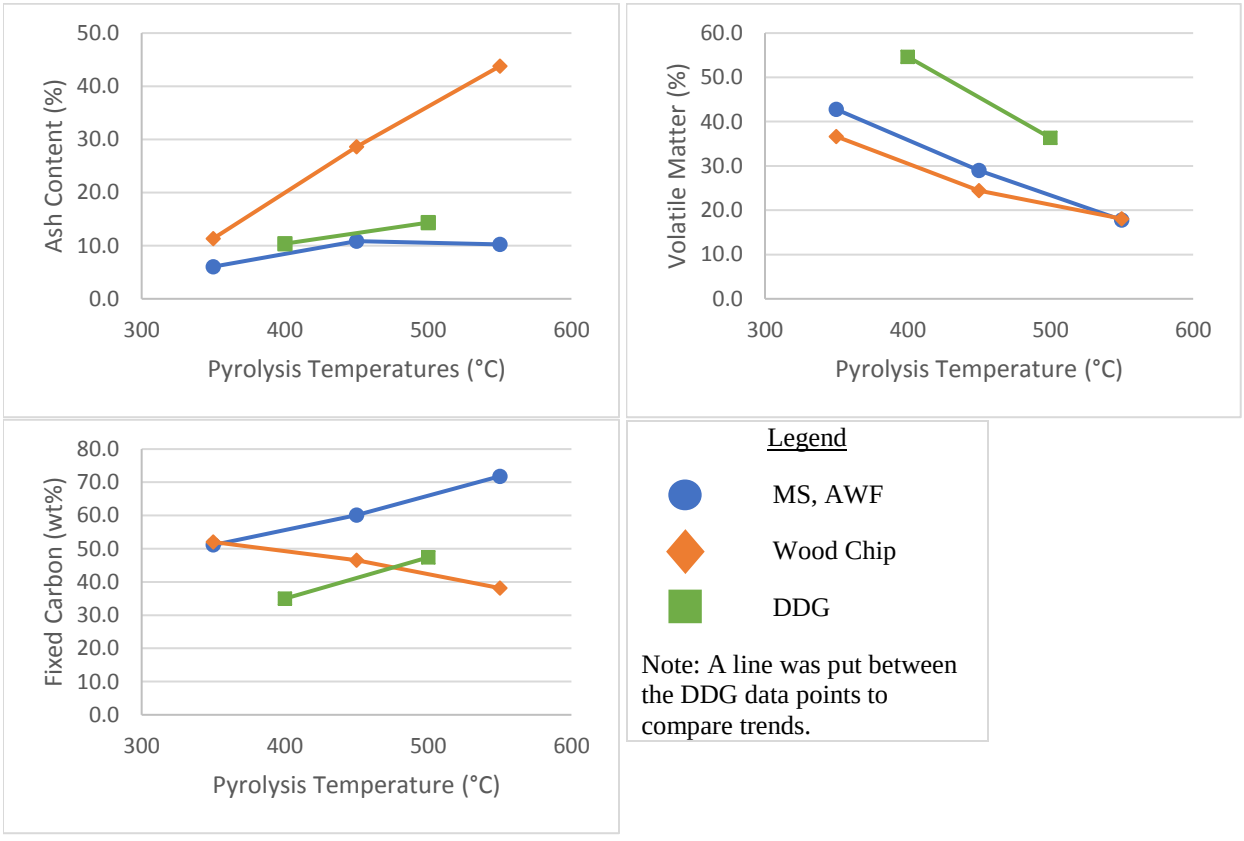

Figure 2.7- Proximate analysis trends for continuous pyrolysis experiments

From these trends, it can be seen that both the Miscanthus and distiller's grain follow similar trends of decreasing volatile matter and increasing fixed carbon with production temperature. While none of the samples reach very high fixed carbon levels of around 90%, the ratio of

volatile to fixed carbon is good. However, the wood chip biochar displayed non-typical behaviour, with both volatiles and fixed carbon decreasing with temperature, with the ash content of the biochar seemingly taking over most of the material. Literature values for wood and waste-derived wood show smaller amount of ash content in biochar (Mitchell et al., 2013), however, the high amount of silica contamination resulted in the very high ash content as discussed previously in the chapter. This large ash content provided inconsistencies in the characterisation of the wood biochar, and since fixed carbon is calculated as a difference of the volatiles and ash, the decreasing values may be due to inconsistencies in silica content.

Table 2.13 shows the proximate analysis for the biochar produced through the slow pyrolysis experiments.

Table 2.13- Proximate analysis for biochar produced from slow pyrolysis experiments

BIOCHAR	VOLATILE MATTER (WT%)	FIXED CARBON (WT%)	ASH CONTENT (WT%)
MS, AWF 500	7.5	81.4	11.0
MS, AWF 480	6.9	81.3	11.7
MS, AWF 350	13.9	75.2	10.8
MS, AWF 327	17.8	72.5	9.7

The results of the slow pyrolysis are very interesting when compared to the other Miscanthus biochar. The volatile matter is extremely low, where even the biochar produced at 327 °C has a lower volatile matter content and higher fixed carbon than MS, AWF 550 from the fast pyrolysis experiments. This shows the influence of pyrolysis time in producing biochar with high degrees of carbonization.

The results of the thermal treatment are shown in Table 2.14, to show the extent of carbonization from the 600 °C pyrolysis. The treated biochar follows the expected trend, and the experiments in the muffle furnace had the desired effect on the biochar by improving the fixed carbon content of the material.

Table 2.14- Proximate analysis of the biochar produced from the thermal treatment experiments

BIOCHAR	VOLATILE MATTER (WT%)	FIXED CARBON (WT%)	ASH CONTENT (WT%)
INITIAL BIOCHAR	44.3	41.2	14.5
MFR DDG 1	20.1	61.6	18.4
MFR DDG 2	16.2	67.9	15.9
MFR DDG 3	16.7	66.4	16.9
MFR DDG 4	17.0	66.1	16.9
MFR DDG 5	16.4	67.0	16.6

Elemental Analysis

Elemental analysis was run on the Miscanthus samples from Drumbo, however, due to limited material produced from the reactor, the unmodified pyrolysis biochar from All Weather Farms Miscanthus did not go through analysis. The results are in Table 2.15, which show the carbon content increasing with increasing temperature, but with similar values between 500 and 550 °C.

Table 2.15- Elemental analysis on biochar produced from unmodified pyrolysis.

BIOCHAR	C (WT%)	H (WT%)	O (WT%)	N (WT%)	O/C	H/C
MS, DRUMBO 550	74.7	3.1	10.8	1.1	0.11	0.49
MS, DRUMBO 500	73.8	3.1	11.8	1.6	0.12	0.5
MS, DRUMBO 450	68.1	3.8	19.0	1.1	0.21	0.66

The Van Krevelen diagram is a convenient method used to visualise the changes in atomic O/C ratio and atomic H/C ratio. The changes in oxygen and hydrogen content comes from dehydration reactions, dehydrogenation, and decarboxylation (Hammes et al., 2006). These ratios can show the degree of carbonization through the thermochemical reaction, and the changes can show which decompositions may be dominant during pyrolysis (Schimmelpfennig & Glaser, 2012). The Van Krevelen diagram can be seen in Figure 2.8, which shows the extent of carbonization through the pyrolysis actions. All three biochar samples show drastic decreases in both ratios from the feedstock, however, both the biochars at 500 and 550 °C show little change, implying that very little oxygen and hydrogen containing groups left as volatiles between these temperatures.

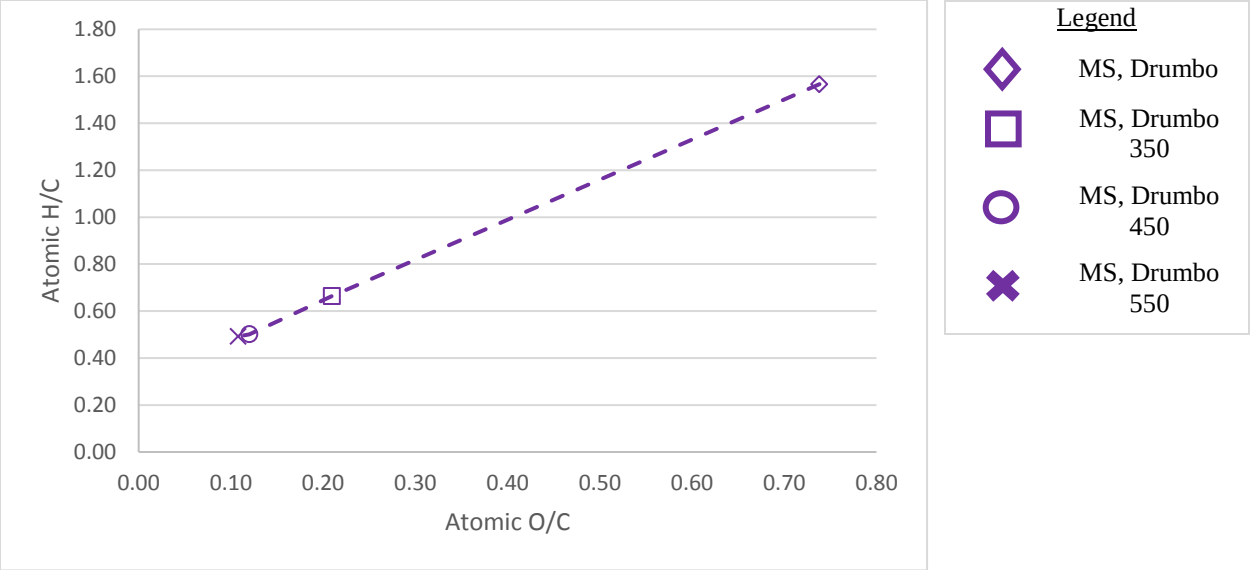

Figure 2.8- Van Krevelen diagram for biochar produced from unmodified pyrolysis experiments

The biochar produced from the continuous pyrolysis experiments is highlighted in Table 2.16.

Table 2.16- Elemental analysis on biochar produced from continuous pyrolysis

BIOCHAR	C (WT%)	H (WT%)	O (WT%)	N (WT%)	O/C	H/C
MS, AWF 550	76.5	3.2	9.8	0.4	0.10	0.50
MS, AWF 450	67.2	3.9	17.6	0.4	0.20	0.70
MS, AWF 350	66.6	4.4	22.6	0.4	0.25	0.79
WOOD CHIP 550	48.5	2.0	5.7	0.1	0.09	0.49
WOOD CHIP 450	59.0	3.0	9.2	0.1	0.12	0.61
WOOD CHIP 350	63.0	4.3	21.2	0.2	0.25	0.82
DDG 500	60.1	4.3	14.8	6.5	0.18	0.86
DDG 400	58.7	5.4	18.8	6.8	0.24	1.10

The trends for carbon and oxygen for each biochar can be seen in Figure 2.9. The original composition of the feedstock is shown in the diagram to show the full extent of pyrolysis on the carbonization of the material. The trends show that carbon content of all three feedstocks show the same trend of increasing at low pyrolysis temperatures. The Miscanthus shows the largest increase in the end, where the distiller's grain carbon content appears to level off slowly. The carbon content of the wood chip biochar shows the same trend as the fixed carbon, increasing slightly before dropping off as temperatures reach 500 °C. This once again implies that the impurities in the wood affect the material in such a way that there is little fixed carbon that

would remain with further pyrolysis. The oxygen content of all three materials decreases as expected, implying the loss of oxygen containing functional groups on the particle surface.

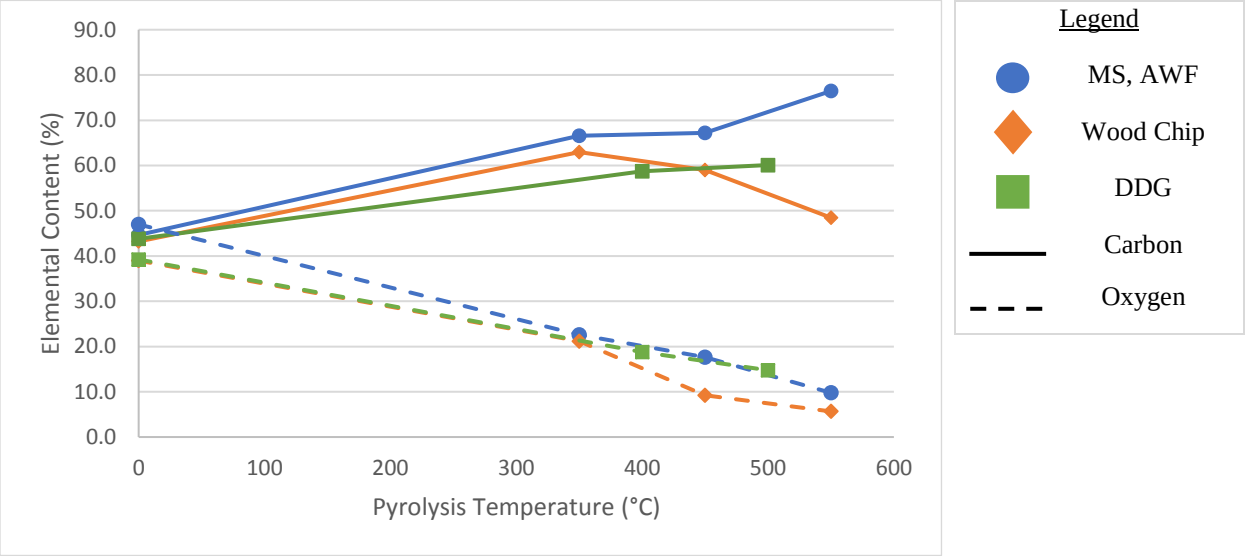

Figure 2.9-Carbon and oxygen content of biochar produced from continuous pyrolysis experiments

The Van Krevelen diagram in Figure 2.10 shows the trend of oxygen and hydrogen groups leaving at the same rate. The feedstocks are shown in the red circle, showing all three have high atomic ratios. The lowest H/C ratios of the biochars occur at 550 °C, although they never reach the lower values of 0.2 used to indicate strong carbonization. The general straight trend may be due to the dominance of dehydration reactions for these biochars.

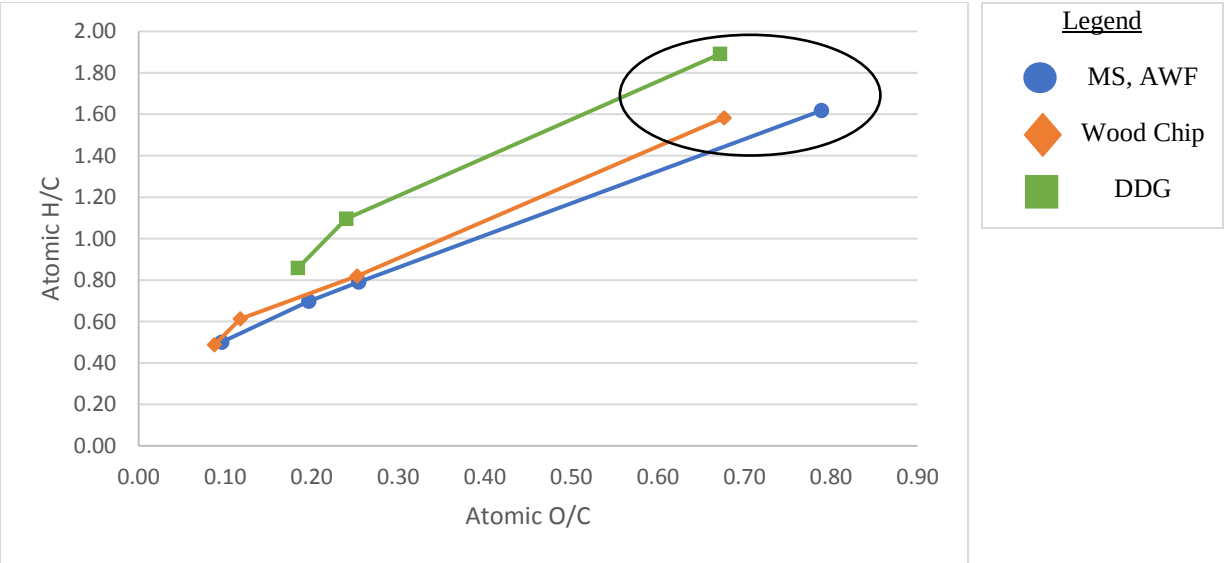

Figure 2.10- Van Krevelen diagram for the continuous pyrolysis biochar, with the feedstocks shown in the circle

The elemental analysis of the slow pyrolysis biochar can be seen in Table 2.17. This table shows that despite the lower production temperature, the carbon content of the biochar is higher than that of the fast production systems. Furthermore, the oxygen content decreases to near negligible levels, especially at 480 °C, which was from the experiment with the longest run time. This shows that prolonged high temperature pyrolysis results in very little volatile matter, and consequently, very little oxygen.

Table 2.17-Elemental composition of biochar produced from slow pyrolysis experiments

BIOCHAR	C (WT%)	H (WT%)	O (WT%)	N (WT%)	O/C	H/C
MS, AWF 500	76.8	1.6	2.8	1.3	0.03	0.25
MS, AWF 480	79.8	1.9	0.0	1.5	0.00	0.29
MS, AWF 350	75.3	2.8	10.1	1.0	0.10	0.44
MS, AWF 327	73.7	3.1	12.3	1.2	0.12	0.51

The Van Krevelen diagram for the slow pyrolysis experiments is shown in Figure 2.11, along with the biochar from Miscanthus from the other two pyrolysis experiments for comparison. This figure shows that while the slow pyrolysis biochar had a much higher degree of carbonization than the other two experiments, all the Miscanthus biochar sat along the same line of reduction. This implies that the rates of decarboxylation and dehydrogenation were the same for all three, but that the longer residence time further reduced the hydrogen and oxygen content.

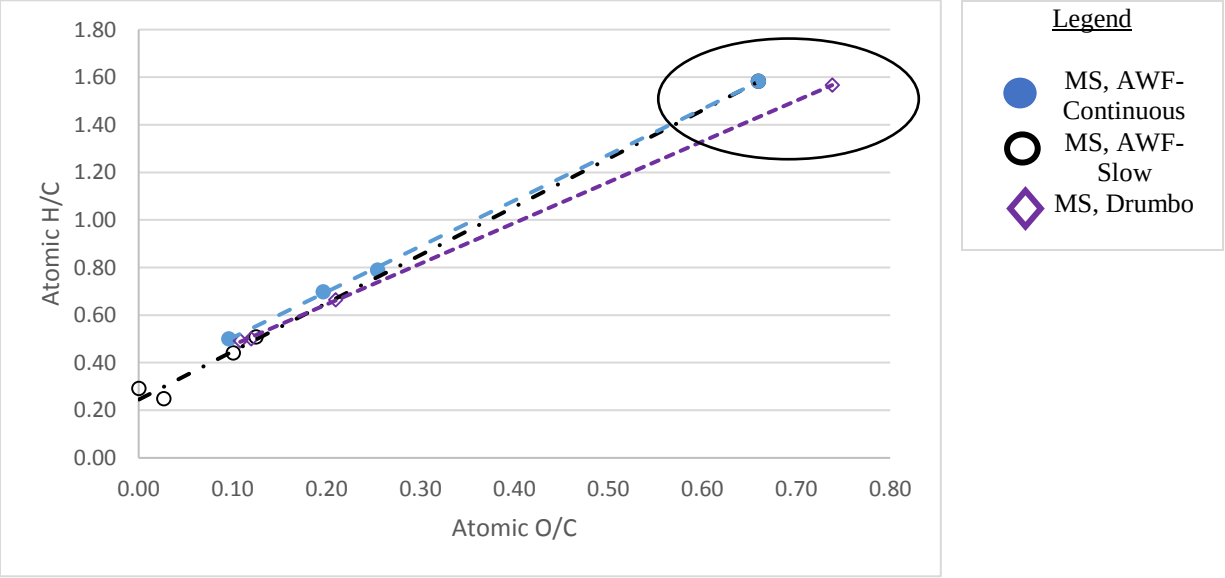

Figure 2.11-Van Krevelen diagram for Miscanthus biochar from three experimental methods

As well, Table 2.18 shows the elemental results of the thermal treatment experiments.

Table 2.18- Elemental Analysis for biochar produced from thermal treatment experiments

BIOCHAR	C (WT%)	H (WT%)	O (WT%)	N (WT%)	O/C	H/C
INITIAL	62.7	3.6	12.2	7.0	0.15	0.69
MFR DDG 1	59.8	1.9	13.4	6.6	0.17	0.38
MFR DDG 2	57.1	1.7	19.4	5.9	0.25	0.36
MFR DDG 3	61.6	1.9	13.2	6.4	0.16	0.36
MFR DDG 4	63.0	2.0	11.8	6.4	0.14	0.38
MFR DDG 5	64.2	2.0	10.6	6.6	0.12	0.38

The carbon and oxygen content of the biochar shows no change from the initial biochar, despite the decrease in volatile matter content of the material. These results continue the trend shown in Figure 2.9, where the carbon content of the biochar produced from distiller's grain seems to approach a plateau at around 60 %. They also correspond to results from a study in which pyrolysis of DDG at 600 °C resulted in a carbon content of 61.48 %, although the ash was much higher (Wood et al., 2014). The stable O/C ratio implies that while volatiles are escaping the biochar, no further decarboxylation is taking place, while the H/C content does decrease. This would imply that more fat and protein is exiting, and that the oxygen is present in minerals.

Surface Area and Pore Volume

The BET results of the different pyrolysis experiments showed very little surface area, possibly due to the constraints of the BET equipment used for the analysis. The analyzer used for this equipment uses nitrogen for adsorption, which results in poor analysis for materials consisting of micropores (Sweatman & Quirke, 2001). Since non-activated biochar typically has a large micropore volume, this means that the low surface area values may come from difficulties in analysis, or from high quantities of volatiles and ash blocking pores.

The surface area and micropore volume of the biochar produced in the slow pyrolysis experiments is shown in Table 2.19. This table shows that the surface area of the biochar increases with increasing HTT. The surface area of the sample produced at 480 °C is higher than the biochar produced at 500 °C, however the sample had a slightly longer pyrolysis time (123 min compared to 110 min). This also shows through the volatile matter content in Table 2.13.

Table 2.19- BET analysis for slow pyrolysis biochar

BIOCHAR	BET SURFACE AREA (m^2/g)	MICROPORE VOLUME (cm^3/g)
MS, AWF 327	4.6	0.0013
MS, AWF 350	149	0.0958
MS, AWF 480	350	0.138
MS, AWF 500	275	0.126

In Figure 2.12, the surface area of the biochar is plotted vs the volatile matter content of the sample.

This shows a relationship between the surface area of the biochar and the volatile matter. This could explain the lack of surface area values for the other pyrolysis experiments, as they had a higher volatiles content, which may result in clogging of the biochar pores.

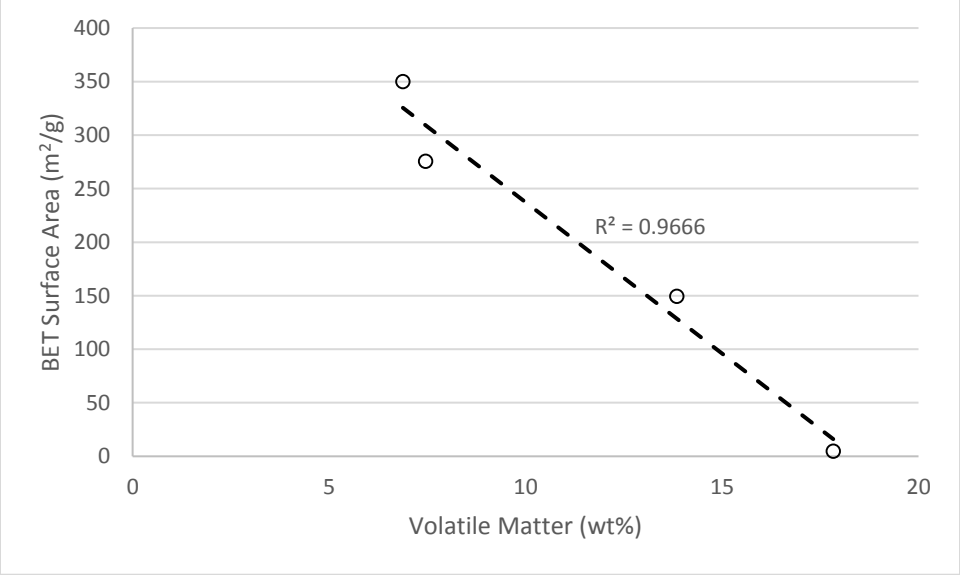

Figure 2.12- Surface area as a function of volatile matter content for slow pyrolysis biochar

Particle Size

The particle size of the biochar produced from the two reactor technologies was analyzed to determine the effect of the mixing on the particle size. In Table 2.20, the sauter mean diameter (SMD) of the unmodified pyrolysis biochar and the slow pyrolysis biochar are shown.

Table 2.20- Sauter mean diameter of Miscanthus biochar for unmodified pyrolysis (left) and for slow pyrolysis (right)

UNMODIFIED PYROLYSIS TEMPERATURE (°C)	SMD (µm)	SLOW PYROLYSIS TEMPERATURE (°C)	SMD (µm)
500	93.6	**500**	98.0
450	101.4	**480**	82.6
400	71.5	**350**	73.5
350	141.1	**327**	57.0

This shows that the biochar produced by slow pyrolysis in the MFR has a smaller particle size than the biochar produced by the pyrolysis pilot plant. This indicates that the mixing in the MFR results in a smaller average particle size, which could be a result of the washing machine style mixing that is used, the volume taken up by the mixer, or the longer pyrolysis time. It has been shown in literature that the aromatic condensation that occurs in pyrolysis can impact the overall particle size, so the increased fixed carbon of the slow pyrolysis biochar could also be the reason (Downie, Crosky, & Munroe, 2009).

Metal Content

The metal contents of the biochars produced are discussed in this section. While all of the same metals as those presented in the feedstock were analyzed, only those that stand out are highlighted. In Figure 2.13, the metal content for the biochar produced from MS, Drumbo in the unmodified pyrolysis experiments are highlighted. While most of the metals followed the expected trend of increasing at the same rate as the ash content, several metals decreased as pyrolysis temperature increased, with silicon and sulphur even decreasing to levels below that of the initial feedstock. This could possibly be attributed to the metal compounds being water soluble and exiting with moisture, or melting and vaporizing at higher temperatures. Potassium was still the most prominent metal in the biochar as in the feedstock.

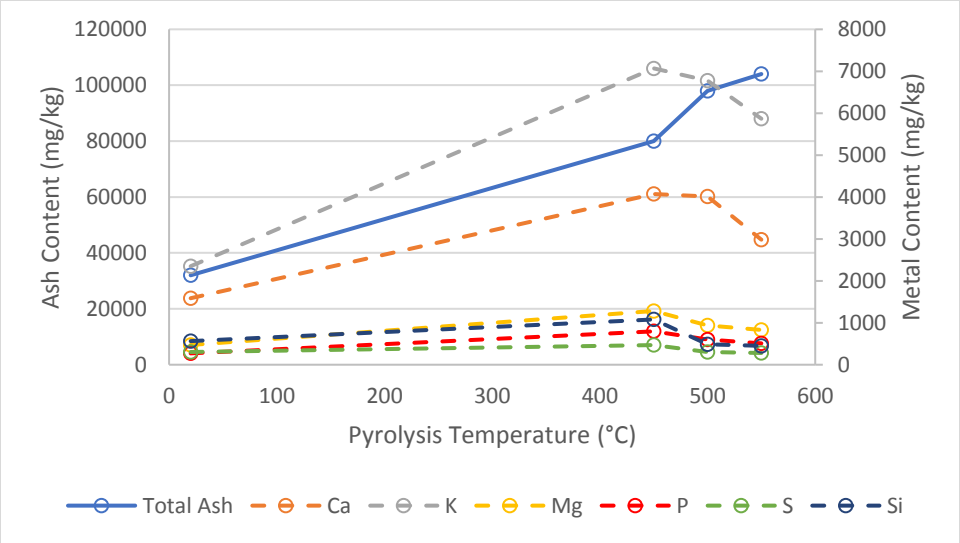

Figure 2.13- Trends in metal content for MS, Drumbo biochar produced in unmodified pyrolysis experiments

Figure 2.14 shows the metals of interest in the MS, AWF biochars produced in the unmodified experiments. As shown in this graph, the potassium follows the same trend in both Miscanthus biochars, albeit at different temperatures. However, the potassium content of the AWF biochar is higher in these biochars, and calcium is the most abundant metal. Of special interest is the zinc and silicon, which reach their highest concentrations at 350 °C. Even if the amount of silicon and zinc oxides remained the same, the concentration would increase as the volatile matter exits the biochar, indicating that both compounds vaporize as pyrolysis temperature is increased.

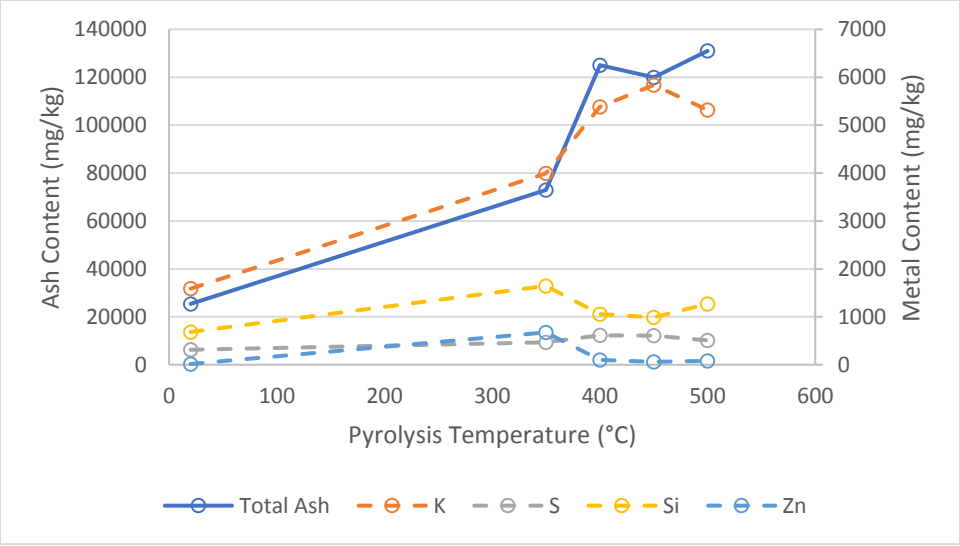

Figure 2.14- Trends in metal content for MS, AWF biochar produced in unmodified pyrolysis experiments

Table 2.21 shows the metal content of the biochars produced from the continuous pyrolysis experiments. The metal contents of the wood chips increase at an extremely high rate, similar to the total ash content. Calcium and iron make up a large quantity of the metal, but also worth noting is that the wood has high copper, lead, and manganese content compared to the other feedstock. This is likely due to the use of preservatives and leaching effects from different construction applications. The distiller's grain has high levels of metals associated with nutrients and vitamins, such as potassium, magnesium, sodium, sulphur, and phosphorus as expected from a feedstock. Outside of the metals expected in minerals, nothing stands out as unusual.

The Miscanthus biochar follows the same trends as the unmodified pyrolysis biochar. Most of the metals are found at the same levels, except for iron and magnesium which are more abundant in the continuous pyrolysis biochar. Similar to the grains, the Miscanthus biochar consists of metals essential for growth, just in lower concentrations, however there are low levels of lead which may come from the water it uptakes.

Table 2.22 compares the metal content of the Miscanthus biochar produced in the slow pyrolysis experiments to the same AWF Miscanthus produced in the unmodified pyrolysis experiments. It can be seen that while several of the metals have the same concentrations and the same temperature trends, the calcium, phosphorus, magnesium, sulphur, and silicon follow opposite trends, and are present at much lower concentrations in the slow pyrolysis experiments. This shows that the pyrolysis residence time plays a large role in the presence of certain metals, potentially due to factors such as water solubility or melting temperature.

SEM Imagery

The SEM images for the Miscanthus samples (MS, AWF 350, 450 and 550) produced from the continuous pyrolysis experiments are shown in Figure 2.15. The lower magnification images show that same grain structure of each of the biochar samples, with more visible structure in the high temperature sample. It can be seen with the higher magnification that the pore structure of the material starts to develop with a honeycomb appearance, however with plenty of material still present within the pores. This is likely why the BET analysis showed little surface area.

Table 2.21- Metal content of biochars produced from continuous pyrolysis experiment

	Miscanthus, AWF			*Wood Chips*			*DDG*	
Temperature	**350**	**450**	**550**	**350**	**450**	**550**	**400**	**500**
Ash (mg/kg)	61,000	109,000	102,000	114,000	286,000	438,000	104,000	143,000
Al	297	657	234	1817	3327	4480	11.1	45.6
Ca	5178	6723	6439	18865	32172	40592	402	803
Cu	11.4	10.5	10.3	13.7	23.9	30.0	3.5	2.3
Fe	766	1942	1618	3594	6815	11112	101	231
K	4213	5247	5350	3249	4081	4223	19035	22374
Mg	1748	1482	2172	1644	3063	3853	6397	8166
Mn	74.9	117	88.4	205	286	303	24.2	37.4
Na	254	493	302	609	958	1153	4307	6103
Ni	4.9	11.6	4.0	21.1	27.6	47.4	1.1	1.9
P	1181	1033	1661	242	326	349	17199	23864
Pb	<2.5	4.7	4.1	22.4	28.8	40.3	<2.5	<2.5
S	311	434	254	872	1216	1582	7672	8250
Si	931	1044	488	1253	695	464	99.0	166
Zn	39.1	56.5	60.2	38.2	56.4	75.8	107	165

Table 2.22- Metal content of Miscanthus biochars produced from slow pyrolysis compared to those produced from unmodified pyrolysis experiments

	MS, AWF-Slow				*MS, AWF- Unmodified*			
Temperature	**327**	**350**	**480**	**500**	**350**	**400**	**450**	**500**
Ash (mg/kg)	97,000	108,000	117,000	110,000	73,000	125,000	120,000	131,000
Al	486	490	716	721	269	667	536	673
Ca	5577	4839	4399	4373	4411	6560	6109	6142
Cu	15	12.6	10.1	41.3	11.5	11.9	15.3	14.2
Fe	732	717	902	1118	503	1009	731	1094
K	4600	4650	4225	4126	3993	5380	5839	5314
Mg	904	700	520	521	855	1255	1194	1144
Mn	87.4	70.5	52.9	47.7	97	135	127	111
Na	681	608	695	768	472	607	698	615
Ni	4.66	4.95	10.5	16.8	2.1	5.2	11.7	4.1
P	1332	1105	919	907	738	1177	1344	1246
Pb	2.58	2.64	2.72	4.55	0.0	4.3	0.0	4.2
S	413	325	152	206	470	613	606	509
Si	518	505	555	420	1645	1055	989	1269
Zn	52.4	50.4	28.6	19.2	675	101	62	81

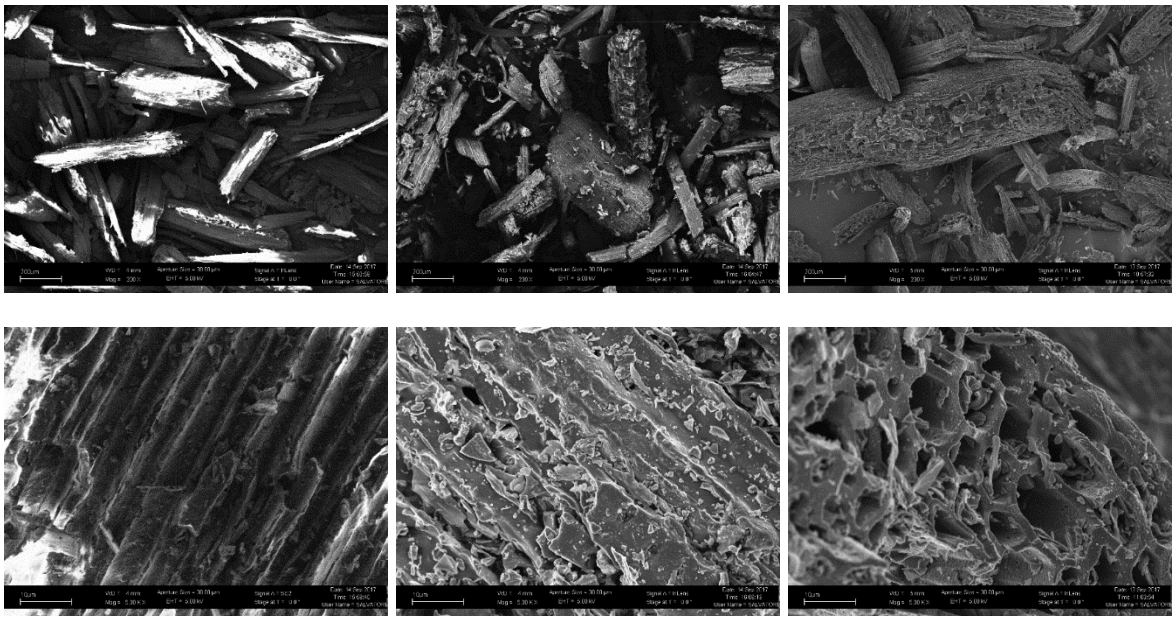

Figure 2.15- SEM Images for MS AWF 350 (left), MS AWF 450 (middle), and MS AWF 550 (right). Top: Magnification of 200 x, Bottom: Magnification of 5.00 kx

The SEM images for the wood chip biochar (WC 350, 450, and 550 can be seen in Figure 2.16. At lower magnification, the wood chip biochar shows similar structure to the Miscanthus, with grain like particles. However, at higher magnification, pore formation can be seen in all the biochar samples. In both the 350 and 450 °C samples, small pores approximately 5 µm across can be seen spread out across the particle. At 550 °C, a clearly defined pore structure can be seen with slightly larger pores organized across the fracture surface. The SEM images for the distiller's grain is shown in Figure 2.17. From the images at lower magnification, the biochar particles appear to be a mixture of shard-like clusters. At higher magnification however, no pore structure seems to be visible within the char particles.

The EDX results for the biochar samples can be seen in Table 2.23. It seems that carbon and oxygen dominate near the surface of particles, which would be expected due to the carbon content of the material and the presence of oxygen containing functional groups. There were small amounts of inorganic material in the Miscanthus and Wood biochar, mainly Mg and K for Miscanthus and Ca for the wood. This is unsurprising as they were some of the most prominent metals in these sample from the ICP analysis. The DDG had much more abundant inorganic materials present, such as K, S, Na, and P. This just shows the prevalence of these materials as the volatile matter escapes the biochar particle.

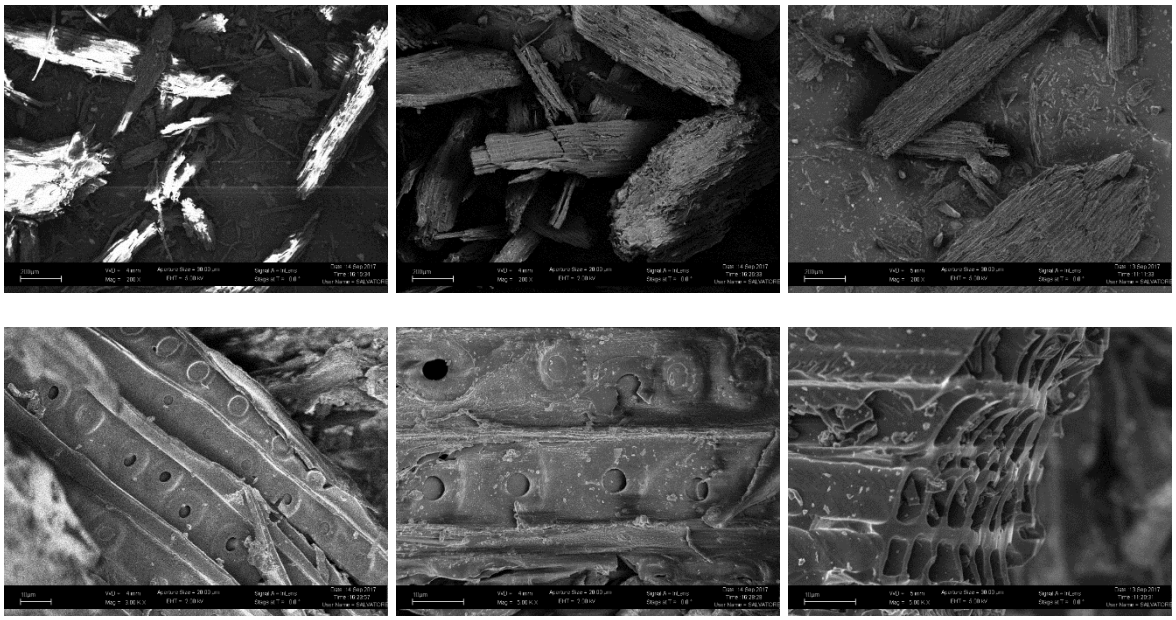

Figure 2.16- SEM Images for WC 350 (left), WC 450 (middle), and WC 550 (right). Top: Magnification of 200 x, Bottom: Magnification of 3.00 kx for left image, 5.00 kx for middle and right

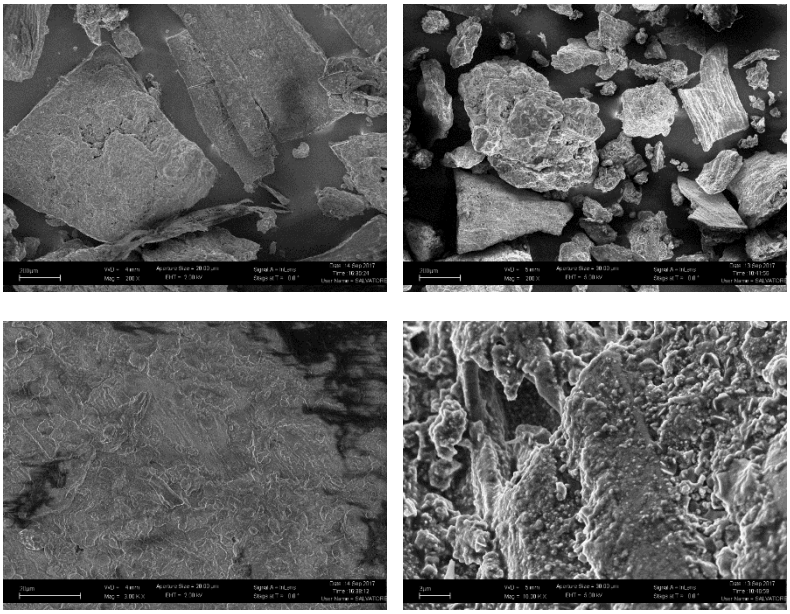

Figure 2.17- SEM images for DDG 400 (left) and DDG 500 (right). Top: Magnification of 200x. Bottom: Magnification of 3.00 kx for left image, 10.00 kx for right image

Table 2.23- EDX analysis results for continuous pyrolysis biochar

	Miscanthus, AWF			*Wood Chips*			*DDG*	
Temperature	**350**	**450**	**550**	**350**	**450**	**550**	**400**	**500**
C (wt %)	74.6	72.31	73.9	68.95	66.93	72.2	51.48	53.74
O	25.14	23.19	19.11	28.44	26.4	22.92	40.92	27.56
Mg		0.13	2.33	0.15	0.34		0.98	1.47
K		2.04	1.67	0.31	1.16	1	2.73	8.99
Si	0.2	1.2		0.57	0.56	0.82		
Ca	0.07	0.72	3	1.58	3.79	2.18		
Fe		0.28			0.52	0.38		
Al		0.15				0.29		
S					0.28	0.2	1.25	2.77
Na							0.89	1.89

2.4 Conclusions

Biochar was produced using four different pyrolysis reactor configurations from three different North American feedstocks: Miscanthus, wood chips, and dried distiller's grain. It was found that the biochar yield from Miscanthus was very similar in both the fast pyrolysis set-ups using the unmodified and continuous pyrolysis experiments, and the yield was highest using the Mechanically Fluidized Reactor for slow pyrolysis. The wood chips had a similar trend in yield with increasing temperature as the Miscanthus, and while the DDG was in the same range, the yield seemed to decrease at a more drastic rate. High temperature treatment on DDG char gave an 80% yield.

From the fast pyrolysis experiments, the Miscanthus biochar showed the largest increase in fixed carbon, reaching 71.3 % and 71.8 % for the unmodified and continuous experiments respectively, with the volatile matter decreasing to 17.8 % for the continuous experiments. The results for the slow pyrolysis was much more drastic, with the fixed carbon reaching 81.4 % and volatiles decreasing as low as 6.9%. The wood chip biochar appeared to be dominated by the ash content, which reached 43.8 %, reducing the amount of fixed carbon in the process. The distiller's grain showed no advanced signs of carbonization with the fixed carbon only reaching 47.7 % at 500 °C, and 67.9 % with further treatment to 600 °C.

While all of the fast pyrolysis experiments showed reductions in the oxygen content of the biochar, temperature seemed to be the largest influence, with 550 °C dropping the O/C ratio as low as 0.09. The DDG char showed signs again that pyrolysis did not provide carbonization as the O/C ratio did not appear to have significant change between 500 and 600 °C. Once again, the slow pyrolysis experiments showed the most drastic changes in oxygen and hydrogen content, with O/C and H/C ratios reaching lows of 0.0 and 0.25 respectively. Additionally, the slow pyrolysis biochar was the only biochar showing increases in surface area, with the BET surface area reaching 350 m^2/g in the most improved biochar.

The metal content of the Miscanthus and DDG feedstocks showed no unexpected inorganic content, with most of the dominant metals increasing with pyrolysis temperature. However, the slow pyrolysis Miscanthus biochar showed some of the more abundant metals decreasing with increasing pyrolysis temperature such as K, Mg, and Ca. Since the wood is recycled from construction projects, it is expected that it would have certain contaminants. The wood biochar was contaminated with unusual heavy metals such as Pb, Cu, and Cr. However, the wood is largely dominated by common metals found in wood such as Ca and Fe, but these inorganics do not do explain the extremely high ash content of the feedstock and biochar.

The scanning electron microscope images provide more evidence of the extent of carbonization and aromatic condensation of the biochar. Both the Miscanthus and wood chip biochar showed grainy biochar structures, with the development of pore structure being seen at the highest pyrolysis temperatures. However, the imaging of the DDG biochar brings up more concerns about the aromatic condensation of fixed carbon, as the images show no signs of pore formation or aromatic rings.

In conclusion, both of the fast pyrolysis systems produced biochar with very similar characteristics, but since the continuous configuration allowed for higher production levels, it appears favourable over the unmodified system. Additionally, the slow pyrolysis experiments allowed for the extent of pyrolysis to be pushed further, but due to the small batch size of the reactor it is limited in the ability to produce biochar for commercial applications. Despite this, biochar with a wide range of characteristics was produced, such that biochar can be produced with desired proximate and elemental properties.

Chapter 3

3 Charcrete: Using biochar as a carbon sequestering additive in building materials

In this chapter, the production of a biochar/ concrete mixture, called charcrete, is analyzed. The recipes used in the production of the charcrete, as well as the analytical methods for characterising the charcrete, are discussed.

3.1 Introduction

Concrete is a composite material resembling stone, made of cement powder, aggregate material, and water. While cement is a powder in its raw form, when mixed with water it forms a paste which binds together filling materials, before undergoing a hydration reaction and hardening (Moir, 2003). Concrete is the most commonly used building material in the world, which is due to two key factors, the first being that the raw materials are readily available and relatively inexpensive as compared to other building materials. The second is that the defining characteristics of concrete is the compressive strength of the cured material, making it ideal for support based roles like damns, pavement, and building support (Li, 2011a).

The popularity of concrete is expected to continue, with the demand increasing due to the constant development of new infrastructure. As with all current technology, the question comes up as how to make concrete more sustainable and environmentally friendly (Li, 2011c). Over 10 billion tons of concrete is produced worldwide each year, so by sheer volume concrete has a large impact on the environment. On top of the energy required for production and transportation, large quantities of natural resources are consumed. Perhaps more importantly, approximately one ton of CO_2 is released per ton of cement powder produced, resulting in the concrete industry accounting for 7% of global greenhouse gas emissions (Li, 2011c; Meyer, 2009). However, the large volume of concrete consumed by industry gives the potential for a high impact on sustainability if greener alternatives can be found.

One of the most common methods for reducing the environmental impact of concrete is by adding recycled materials to the concrete mixture. For example, several industrial waste materials have been successfully introduced as filler materials, such as fly ash, waste glass, and

blast furnace slag (Li, 2011a). These materials have been extensively researched, with fly ash, perhaps the most popular recycled filler, having been implemented in recipes at concentrations up to 60%. The introduction of the fine particles can also help improve mechanical strength, by causing a secondary hydration reaction, which further improves the curing of concrete, and through the filler effects of small particles, similar to fine aggregate (Ferro et al., 2014). While there are disadvantages to using these waste products (longer curing time and inconsistency in composition of fly ash), it goes to show that there are several advantages to using recycled materials in concrete (Meyer, 2009).

It has been proposed to use biochar as an additive for concrete, due to its ability to sequester atmospheric CO_2 (Gupta & Kua, 2017). A life cycle analysis performed on biochar found that biochar can potentially reduce greenhouse gas emissions by 870 kg CO_2e per ton of dry feedstock (Roberts et al., 2010). In addition, biochar has several characteristics that can lead to increased performance of concrete. As a material with a low bulk density, biochar has the potential to drastically decrease the density of hardened concrete (Schmidt, 2013). Additionally, the porosity and high pH of biochar results in it having high water retention, which can lead to it absorbing free water while mixing. This water is released as the hydration reaction continues and the available moisture decreases, which leads to secondary hydration and additional curing of the concrete (Choi et al., 2012). Consequently, this can reduce the workability of the fresh concrete mixture.

Recently, a few studies have been conducted to investigate the addition of biochar to cement mix and mortar (cement and sand). One study found that 5% hardwood biochar added mortar showed improvements in compressive strength, with the strength decreasing at higher levels (Choi et al., 2012). In addition, it was discovered that the addition of hazelnut and peanut shell biochar improved both the compressive strength as well as the flexibility of the concrete (Restuccia & Ferro, 2016). This goes against typical concrete behaviour, where an increase in compressive strength results in more brittle material, with lower tension resistance and fracture toughness. Carbonized bamboo fibers were also added to cement, which resulted in a more tortuous crack path being shown through the concrete leading to a higher amount of energy being required to fracture the material (Ahmad et al., 2015). Both these studies have shown that these small particles act similarly to fine aggregate, forcing crack paths to either go around the

particles, or through the particle, which leads to strong concrete with more ductility and durability (Ahmad et al., 2015; Restuccia & Ferro, 2016).

It has also been suggested that biochar can have positive effects in terms of electrical, acoustic, and thermal properties of biochar. Porous concrete containing voids and interconnected pores is very effective in sound absorption. Acoustic waves that enter these pores are dissipated by having their acoustic energy converted to heat through refraction and interference (C. Zhao et al., 2014). Porous concrete developed with other recycled material has been investigated thoroughly, where studies have shown that using coal bottom ash created a highway noise barrier concrete meeting the same standards as the traditional concrete used in these applications (Arenas et al., 2015). The high quantity of pores present in biochar may assist in the absorption and dissipation of sounds waves, meaning biochar/ concrete (charcrete) composites could be used in sound reduction applications.

Lastly, the low thermal conductivity and low flammability of biochar present different advantages for insulation or in case of fire. The low thermal conductivity is due to the presence of various sized pores throughout the material. When used in materials, the pores help to break up thermal bridging within the material, and help to provide insulation, which could result lower energy costs for charcrete used in buildings (Gupta & Kua, 2017). For example, in 2010, buildings accounted for 32% of total global final energy usage, with space heating accounting for 32% of total building energy consumption (Berardi & Naldi, 2017). There are several effective insulating materials on the market, such as polystyrene and ploy isucyanurate, with some of them even being made of recycled materials like fiberglass and cellulose (United States Department of Energy, n.d.). Despite the abundance of effective materials present in industry, the ability to increase the effective thermal capacity of a building through the addition of carbon-sequestering biochar would help lead to reduced energy usage and GHG emissions.

The low flammability of biochar can help to reduce the risks of damage done to concrete in the case of fire and extreme temperature. While concrete is not a flammable material, and is generally considered to perform well when exposed to fire, concrete can still undergo strength loss and spalling under heat (Cather, 2003). Spalling is the breaking up of layers of concrete when exposed to fire, and is down to several factors such as aggregate breaking, particle

expansions, and water vaporization leading to pressure build-up (Hertz, 2003). The excellent behaviour of biochar when exposed to high temperature can help to reduce the damage done to concrete, by maintaining particle structure and retaining free water to prevent evaporation.

Despite the research being done on using biochar in cement mixtures, there is little to no research being done on adding biochar to industrial concrete (cement, sand, and aggregate). This chapter aims to determine the effects of using biochar at various loading levels in concrete, to determine its performance in terms of mechanical, thermal, and acoustic properties.

3.2 Materials and Methods

The concrete samples were prepared using a standard recommended recipe for most personal applications. The cement used was 30 HE Portland Cement from Keystone Cement Company in Bath, PA, which has an air content of 8.52 % and a 28-day compressive strength of 43.13 MPa. As reported by Keystone Cement, the cement was tested and certified to meet the latest requirements of CSA-A-3000-08. The sand used was 4253919 concrete sand from CBM Aggregates from their Hillsburgh pit. The aggregate size distribution is shown below in Table 3.1.

Table 3.1- Particle size distribution of concrete sand

Sieve/Test	Tests	Average	St Dev	Target	Specification
9.5mm	3	100.0	0.00	100-100	100-100
4.75mm	3	97.1	0.86	95-100	95-100
2.36mm	3	86.0	1.70	80-100	80-100
1.18mm	3	74.9	1.45	50-85	50-85
0.6mm	3	57.4	0.60	25-60	25-60
0.3mm	3	25.9	1.74	20-30	10-30
0.15mm	3	7.2	0.81	0-10	0-10
75um	3	2.29	0.351	0-3	0-3
Pan	3	0.00	0.000		

The aggregate used 6053145- HL3 gravel from CBM Aggregates, supplied by their McNally pit. The aggregate size distribution is shown in Table 3.2. The cement, aggregate, and sand were all provided by our industry sponsor, Verti-Crete of Toronto in Bolton, Canada.

Table 3.2- Particle size distribution of aggregate

Sieve/Test	Tests	Average	Target	Specification
5/8" (16mm)	5	100.0	100-100	100-100
0.530" (13.2mm)	5	99.5	96-100	96-100
3/8" (9.5mm)	5	71.6	50-73	50-73
#4 (4.75mm)	5	7.0	0-10	0-10
#8 (2.36mm)	5	1.9	0-8	0-8
#200 (75um)	5	0.0	0-1	0-1
Pan	5	0.0		

Both sand and aggregate were added at a 3:1 ratio of the cement weight (i.e. 3 kg of sand and 3 kg of aggregate to 1 kg of cement). The concrete was prepared by first mixing the sand into the cement powder in a 5-gallon bucket, followed by the aggregate, and mixing until thoroughly distributed. Water was then added to the mixture at a ratio of 0.5:1 of the cement weight (for the plain samples). Release oil was sprayed on the molds in order to help remove the concrete once it was cured.

Four different moulds were used to create the concrete samples for appropriate testing:

1. A 30 cm x 30 cm x 3 cm square.
2. A 15 cm x 15 cm x 2 cm square.
3. A 10 cm diameter x 2 cm disc.
4. A 5 cm x 5 cm x 5 cm cube.

All of the samples produced were poured into the first three moulds. However, only the samples with low loading levels of biochar (<=3 wt%) were poured into the cubical molds to determine the changes in compressive strength.

Once the mixture was thoroughly mixed, it was slowly added to the largest mold first, filling approximately a third of the volume before tapping the edges to remove any air bubbles that may have been trapped within the cement. After the mold had been filled, it was further tapped to bring the water to the surface of the concrete, and a trowel was used to spread the concrete evenly across the top of the mold, scraping any excess concrete off the top. After that, the small square, cylindrical, and cubical molds were filled in the same fashion. The samples were

allowed to cure for at least two days before being released from the molds. After that, they cured for the remainder of the time in the ICFAR pilot plant under ambient conditions.

It was determined through trial and error that the ideal recipe to fill the four molds was: 1.3 kg cement, 3.9 kg sand, 3.9 kg aggregate, and 0.65 L of water. The activated carbon used was GC 12x40 S from General Carbon, which is a granular activated carbon made from coconut shell. The material properties are shown in Table 3.3.

Table 3.3- GC 12x40S activated carbon properties

Specifications	
Mesh size - 12x40, %: Less than No.12, %: Greater than No. 40, %:	90 (min) 5 (max) 5 (max)
Iodine No., mg/g:	1100 (min)
Surface Area, m^2/g:	1100 (min)
Hardness, %:	98 (min)
Ash Total, %:	4.0 (max)
Moisture, % (as packaged):	5.0 (max)
Typical Density, lbs./cu.ft.: g/cc:	29-33 0.46-0.53

Three different biochars were used. The first (BC1) is produced from dried distiller's grain pyrolyzed in the ICFAR Mechanically Fluidized Reactor (MFR) at 500 °C. The second (BC2) was produced by treating the first biochar in a muffle furnace purged with nitrogen at a temperature of 600 °C. The third biochar (BC3) used in one sample is a Miscanthus biochar (MS, AWF) produced in the ICFAR Pyrolysis Pilot Plant at 450 °C. The proximate characteristics and density of the three biochar sets are shown in Table 3.4.

Table 3.4- Properties of biochar used in concrete production

BIOCHAR	VOLATILE MATTER (%)	FIXED CARBON (%)	ASH CONTENT (%)	BULK DENSITY (G/L)
BC1	44.3	41.2	14.5	600
BC2	17.2	65.9	16.9	633
BC3	35.3	56.8	7.9	100

The carbon samples were incorporated into the concrete mixture by replacing either sand or aggregate while mixing the fresh concrete (for example 1.3 kg cement, 3.6 kg sand, 3.9 kg

aggregate, 0.3 kg carbon). Since both activated carbon and biochar have high water retention, additional water was added as necessary to maintain workability. Tables 3.5 and 3.6 show the list of samples prepared.

Table 3.5- List of concrete samples prepared using activated carbon

SAMPLE	ACTIVATED CARBON (WT%)	WATER TO CEMENT RATIO	FILLER REPLACED
STANDARD	0	0.5	N/A
AC-1	9.5	1.0	Sand
AC-2	11	1.3	Aggregate
AC-3	5	0.8	Sand
AC-4	5	0.7	Sand
AC-5	10	0.8	Sand
AC-6	7	1.3	Sand
AC-7	30	2.5	Aggregate
AC-8	30	2.5	Sand

Concrete Density

The density of the concrete was determined by measuring both the volume of the samples as well as the mass. The volume was calculated by measuring each dimension of the block in four places using a digital caliper accurate to 0.01 mm, and averaging the four values for each dimension.

Compressive Strength

The compressive strength of the concrete samples was determined by Professor Umberto Berardi at the Department of Architectural Science at Ryerson University in Toronto, Canada. The compressive strength of the samples was determined following the procedure detailed in CSA 23.2- 8A, in Section 12. The samples used in this were the 5 cm cubes. Any loose sand grains or imperfections were removed from the surfaces in contact with the bearing blocks of the loading machine. The surface was then ground down such that the surface did not depart from a flat plane by more than 0.05 mm. The cube was then placed between the bearing blocks, and the load was increased at a constant and smooth rate. The compressive strength was calculated as the maximum load maintained by the concrete cube, divided by the cross-area across which the load was supplied.

Table 3.6- List of concrete samples prepared using biochar

SAMPLE	BIOCHAR USED	BIOCHAR WEIGHT %	WATER TO CEMENT RATIO	FILLER REPLACED
1	BC1	5	0.67	Sand
2	BC1	5	0.83	Aggregate
3	BC1	10	1.08	Sand
4	BC1	10	1.25	Aggregate
5	BC1	15	1.50	Sand
6	BC1	15	1.67	Aggregate
7	BC1	12	1.17	Sand
8	BC1	12	1.46	Aggregate
9	BC1	1	0.54	Sand
10	BC1	1	0.50	Aggregate
11	BC1	2	0.56	Sand
12	BC1	2	0.63	Aggregate
13	BC1	3	0.71	Sand
14	BC1	3	0.71	Aggregate
15	BC1	5	0.83	Sand
16	BC1	5	0.71	Aggregate
17	BC3	1	0.75	Aggregate
18	BC2	1	0.65	Sand
19	BC2	1	0.73	Aggregate
20	BC2	2	0.65	Sand
21	BC2	2	0.62	Aggregate
22	BC2	3	0.65	Sand
23	BC2	3	0.67	Aggregate

The load bearing machine used was a hydraulic type meeting the requirements of CSA A3005-13, in section 4.3.12. The equipment is capable of reporting the load applied within an accuracy of 1.0%.

Sound Absorption Coefficient

The acoustic testing was performed at the Department of Architectural Science at Ryerson University in Toronto, Canada. The sounds absorption coefficient was determined following the procedure as highlighted by ISO 10534-2 at normal incidence (International Organization for Standardization, 2001). The measurements were performed using a Kundt's tube with the following dimensions: 10 cm internal diameter (corresponding to an upper frequency of 2000

Hz), 56 cm length, with two microphones placed at a distance of 5 cm (for a lower frequency limit of 200 Hz). To limit the effects of disturbances in measurements, four measurements were performed for each sample, with the absorption results being the average of the four tests.

The Noise Reduction Coefficient (NRC) was calculated in order to compare the concrete samples to other sound reducing materials. The NRC is the average of the sound absorption coefficients at 250, 500, 1000, and 2000 Hz, and is calculated as follows (C. Zhao et al., 2014):

$$NRC = \frac{\alpha_{250} + \alpha_{500} + \alpha_{1000} + \alpha_{2000}}{4}$$

Where α s the sound absorption coefficient. The NRC is then rounded to the nearest 0.05.

Thermal Conductivity

Thermal conductivity measurements were carried out at the Department of Architectural Science at Ryerson University in Toronto, Canada. A NETZSCH HFM 436/3/1E instrument was used to perform the testing following ASTM C518 standards (ASTM Int., 2015). A calibration specimen was used from the U.S. National Institute of Standards and Technology. The 30 cm x 30 cm x 5 cm specimens were placed between two thermally enrolled plates with a 20 °C temperature gradient (the mean temperature is the average of the two temperatures). Once equilibrium is reached, the apparatus uses the steady-state one dimensional heat flux to calculate the thermal conductivity using Fourier's law of heat conduction with 1% error accuracy.

3.3 Results and Discussion

Concrete Production

Most of the samples were produced without issue, except for the blocks with high levels of activated carbon or biochar. For example, in sample AC7 and AC8 (at 30 wt% activated carbon) the samples were very brittle and the large blocks broke when removing them from the mould. Biochar samples 5 and 6 had the same problem, which is why samples 7 and 8 were produced at 12 wt% biochar, and only the large blocks were produced at this loading level.

It was noted that the required water to maintain workability of the concrete was increased as the biochar levels increased within the concrete sample. This is likely due to the water being absorbed by the material, and the additional water required (on top of the amount needed for 0.5 water to cement ratio) is shown in Figure 3.4. This implies that the excess water required for workability increases almost linearly with the amount of biochar added to the cement mixture, implying that it directly related to the water being absorbed by the biochar. The slope shows that 978.6 mL of water excess needs to be added per kg of biochar.

In order to determine the amount of water biochar would absorb, a test was performed to see how much water must be added to the material before free water could be seen, or until a paste was formed in the case of cement. The results of the test are shown in Table 3.7, where it can be seen that 650 mL of water needs to be added per kg of biochar to see any free water appear. Also, when cement alone is used, a water to cement ratio of 0.4 is required to see any free water, which corresponds to the fact that only a 0.36-0.42 water to cement is needed for hydration, with up to 0.45-0.5 needed for workability (Li, 2011b). When 1.5 grams of biochar is added to cement, the water to cement ratio for free water increases to 0.48, which shows that even a small amount of biochar increases the water demand of the cement. Despite that, the ratio of excess water needed to biochar decreases slightly from the value shown in Figure 3.1, which is likely due to the smaller amount of sample used and the lack of aggregate and sand reducing workability.

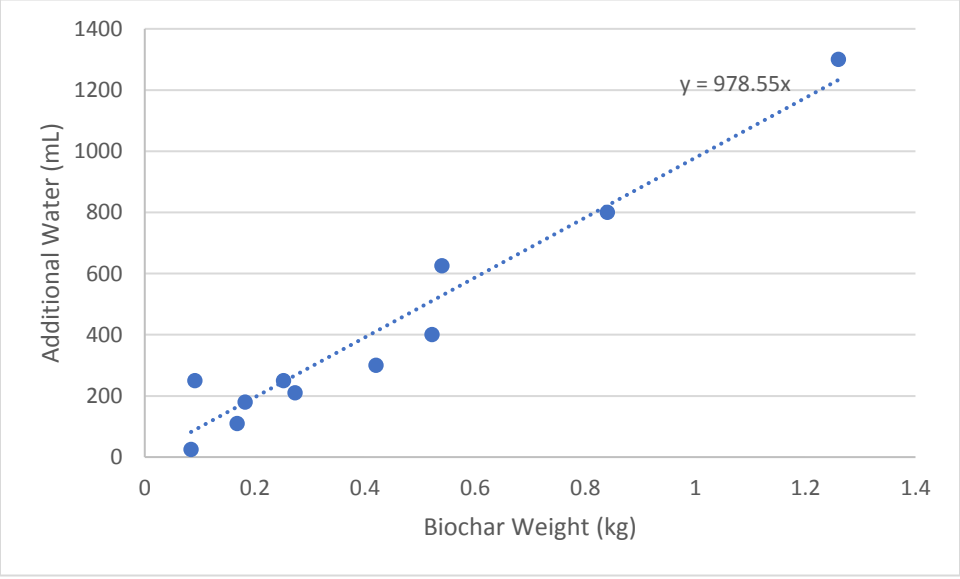

Figure 3.1- Excess water required for workability as a function of biochar weight

Table 3.7- Water required for visible free water for raw concrete materials

MATERIAL	TOTAL MASS (g)	VOLUME WATER (mL)	ADDITIONAL WATER TO BIOCHAR (mL/g)	WATER TO CEMENT RATIO
BIOCHAR (BC1)	10.01	6.35	0.63	N/A
CEMENT	9.99	3.97	0	0.4
87% CEMENT/ 13% BIOCHAR	11.44	4.78	0.53	0.48

Concrete Density

The density of the concrete samples prepared with high loading levels of carbon is shown in Figure 3.2. It can be seen that the addition of biochar and activated carbon decreases the overall concrete density in a near linear fashion. At early levels, both carbon sources decrease the density at the same rate, implying that the carbon bulk density is the most important factor, as the differences in surface area or fixed carbon do not seem to make a difference. At higher levels, the biochar seemed to have a slightly better effect in lowering the density, however, the concrete only accepted up to 15 % biochar by weight. On the other hand, the activated carbon could be added at around 30 % by weight before the concrete was too brittle to handle. Due to this, it appears that both biochar and activated carbon decrease the concrete density at the same levels, with a minimum density of around 1400 kg/m^3. This is promising, as it means that biochar could be used to produce concrete falling under the lightweight category of 1200 to 1800 kg/m^3 (Li, 2011a). It also shows that it does not seem to matter which filler is replaced, which means that the recipes could be fine tuned for other characteristics and still have the same density effect.

Figure 3.3 shows the concrete density with low levels of biochar added, at concentration up to 5 % by weight. This shows that at lower levels that concrete density does not decrease in such a linear fashion as the higher loading levels. Despite this, once the concentration reaches high levels (5%), all of the samples appear to begin decreasing at the same rate. This graph also confirms the thought from the higher loading levels, where the bulk density really seems to play the largest role in decreasing concrete density as the BC3 with the very low density shows the most obvious rapid decrease in concrete density. The full set of concrete density results can be seen in Table A.3.

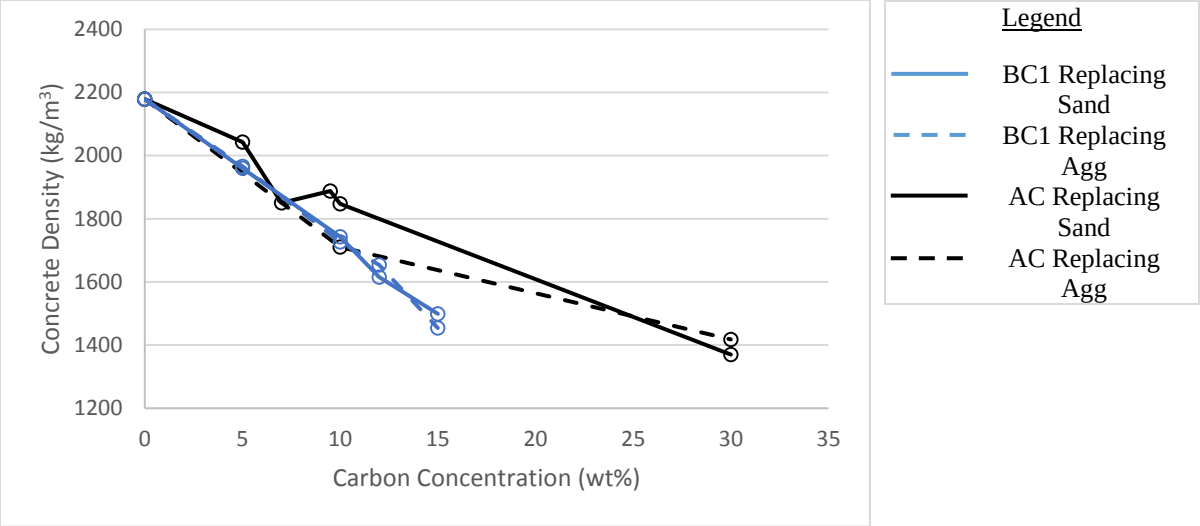

Figure 3.2- Concrete density with the incorporation of high levels of carbon (<=15 wt%)

It is worth noting for these experiments that the standard concrete samples had a concrete density of 2179 kg/m^3, compared to the normal reported concrete weight of 2400 kg/m^3. This difference would make a large impact on the density trends, as a large deviation in density would be present. Despite this, these results prove that concrete can be made lighter without the need to add large levels which could potentially compromise the concrete strength.

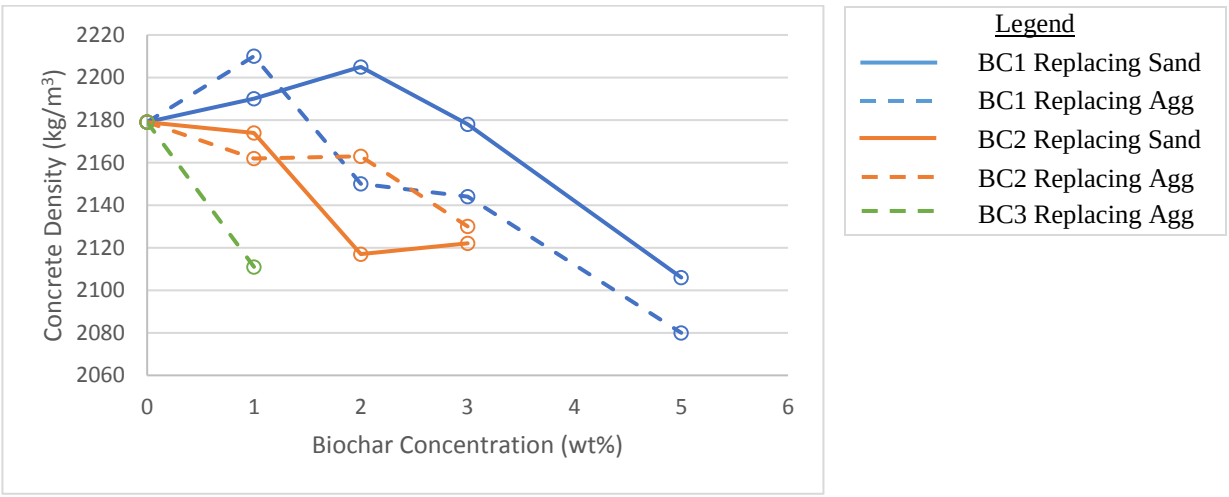

Figure 3.3- Concrete density with the incorporation of low levels of biochar (<=5 wt%)

Compressive Strength

The compressive strength of the charcrete samples can be seen in Table 3.8, and the trends can be seen in Figure 3.4. From the table, it can be seen that the compressive strength of the plain concrete mixture was only 17.1 MPa, which is considerably lower than the specified

compressive strength of the cement at 43.13 MPa. This would even put the concrete in the low-strength concrete classification (Li, 2011a), however the National Ready Mix Concrete Association states that concrete ranges from 17 MPa for residential uses and up to 70 MPa for specific purposes (National Ready Mix Concrete Association, 2003). It is unknown why the range of samples fall on the lower end of the spectrum, but it could be due to the water to cement ratio being higher than normal as was needed to work the concrete into the small moulds. It could also be linked to the lower concrete density.

Table 3.8- Compressive strength of tested samples

MATERIAL	BIOCHAR WT%	WATER/CEMENT	COMPRESSIVE STRENGTH (MPa)			
STANDARD	0	0.6	17.1			
	Replacing Sand			*Replacing Aggregate*		
	Biochar wt%	**Water/ Cement**	**Compressive Strength (MPa)**	**Biochar wt%**	**Water/ Cement**	**Compressive Strength (MPa)**
BC1	1	0.7	11.3	1	0.6	15.6
	2	0.6	18.5	2	0.6	11.4
	3	0.58	21.3	3	0.62	21.9
BC2	1	0.65	19.9	1	0.73	18.4
	2	0.65	12.6	2	0.62	16.2
	3	0.65	18.2	3	0.67	13.7
BC3				1	0.7	14.5

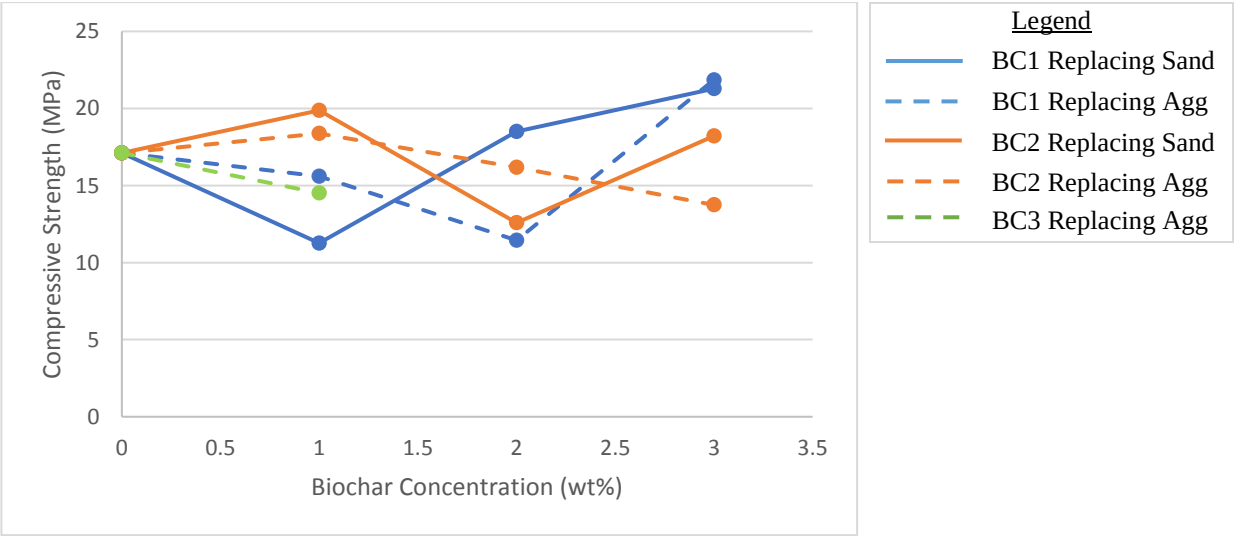

Figure 3.4- Compressive strength as a function of biochar concentration in concrete

From Figure 3.4, it can be seen that there is a slight upward trend in the compressive strength with the different concentrations of biochar added to the concrete. Additionally, it does not seem to matter if the sand or the aggregate is replaced, as both sets of data for each biochar tend to intersect. BC1 showed a small increase in both sets of data at 3 wt %, reaching 21.9 MPa at a maximum, however the lower concentrations show decreases, implying that the trend may be non-significant. Perhaps surprisingly, BC3, consisting of Miscanthus biochar with a smaller particle size, showed a decrease in compressive strength, albeit with a smaller sample size, which could be due to the increase in water to cement ratio as compared to the standard.

This goes against the results using carbonized hemp in cement mixtures, where the compressive strength increased for up to 1 wt% biochar before decreasing slightly (Ferro et al., 2014). However, other results using hardwood biochar showed increases at up to 5 wt% in mortar, so there seems to be no common trend in strength, which may be down to different recipes and biochar used (Choi et al., 2012). The most important takeaway from these results are that the biochar samples at lower concentrations do not compromise the compressive strength. This implies that the other advantageous properties of charcrete can be sought after without compromising the concrete itself, however, more repeat samples need to be produced and analyzed to fully predict the concrete strength.

Sound Absorption

The sound absorption coefficient of four different concrete samples over the tested frequency range can be seen in Figure 3.5. This shows that the addition of biochar and activated carbon had a noticeable impact on the sound absorption across the entire frequency range. This is due to the added material creating interconnected pore networks in the concrete, in which sound enters and is dissipated as heat energy. Even more encouraging is that biochar seemed to have the same effect as the activated carbon in this regard, with both the 10 and 15 wt% samples showing near identical curves as that of the concrete with the 7.3 wt% activated carbon. While this could be due to the higher concentrations of, it would be expected that the considerably higher surface area and associated porosity would have provide the activated carbon with higher sound absorption properties. Since sound dissipation requires interconnected pore networks throughout

the concrete material, it is possible that the increased porosity of the activated carbon has little effect in further improving the porosity of the concrete (C. Zhao et al., 2014).

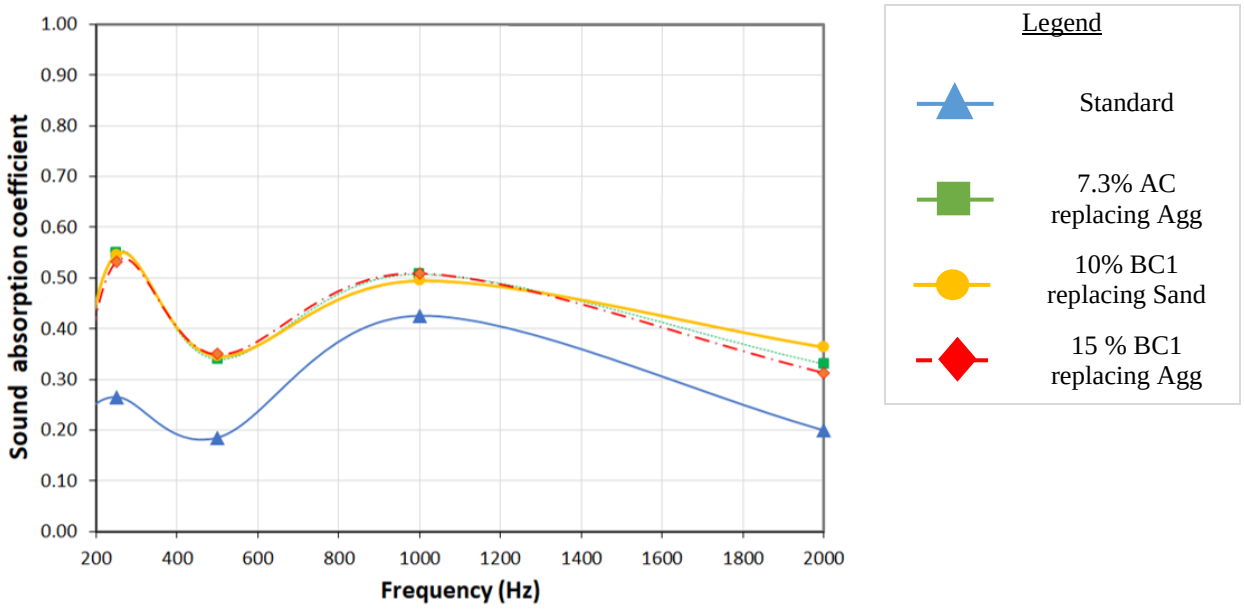

Figure 3.5- Sound absorption coefficient of different concrete samples

The NRC for the concrete is shown in Table 3.9. This further confirms that the sound absorption is the same for all three of the samples with carbon fillers. A material is usually considered to be a sound absorber if it has an NRC of greater than 0.35 (CertainTeed Corporation, 2011). While these results show that biochar addition can have a large effect on the sound absorption of concrete, other studies aimed at improving the acoustic performance have shown larger NRC values using expanded aggregate, implying that larger values could potentially be achieved (C. Zhao et al., 2014).

Table 3.9- Noise Reduction Coefficient for the concrete samples

CONCRETE SAMPLE	FILLER	MATERIAL REPLACED	NRC
STANDARD	None	None	0.25
1	AC	Sand	0.45
2	BC1	Aggregate	0.45
3	BC1	Aggregate	0.45

Thermal Conductivity

Table 3.10 shows the temperature dependant thermal conductivity of five charcrete samples containing varying levels of biochar, using BC1. The biochar has a positive effect on increasing

the insulating properties of the concrete. This is once again due to the pores that are added to the material with the addition of biochar, as well as the low thermal conductivity of biochar that break up thermal bridging through the material (Berardi & Naldi, 2017). From this it can be seen that the sample containing only 1% biochar by weight had the lowest thermal conductivity, and consequently the highest thermal resistance of all the samples. The sample with 5% biochar showed a spike in the thermal conductivity of the material, but since the conductivity seemed to drop off at higher loading levels, it may be due to an irregularity in the samples. Also, as shown in Figure 3.6, the thermal conductivity is consistent across the temperature range, except the samples show higher thermal conductivities at lower temperatures. This implies that the concrete has lower insulation properties in colder conditions. At higher biochar loading levels, there does not seem to be a large difference in samples in which aggregate has been replaced in the sample as shown in the 10% and 12 % samples. However, the 12% sample replacing sand shows a significant drop compared to the other two.

This is surprising since studies have shown that increasing the aggregate volume fraction serves to increase the conductivity of the concrete sample (Kim et al., 2003). However, these studies are typically performed at much lower water to cement ratios, so the excess water content that the biochar demands may have an unexpected impact on the insulating properties. Generally, it is found that the thermal conductivity of a material decreases as the material density increases, which may be the reason why the lowest biochar concentration has the highest thermal resistance (Budaiwi et al., 2002). It is also possible that other heat transfer paths are present within the material such that the biochar does not impede heat transfer across the concrete. This could be a result of improper biochar distribution throughout the material, although this seems unusual as the higher biochar concentrations should negate this effect.

Table 3.10-Temperature dependant thermal conductivity of charcrete samples using BC1

Biochar wt%	*Material Replaced*	*Water to Cement Ratio*	*Mean Temperature (°C)*	*Thermal Conductivity (W/m K)*	*Thermal Resistance (m^2 K/W)*
1 %	Aggregate	0.5	15.03	0.230	0.150
			19.38	0.208	0.165
			24.05	0.210	0.164
			28.78	0.209	0.165
5 %	Sand	0.67	13.31	0.391	0.087
			21.86	0.408	0.083
			25.47	0.444	0.076
			30.83	0.435	0.078
10 %	Aggregate	1.25	15.17	0.283	0.119
			19.31	0.264	0.127
			26.36	0.270	0.125
			31.16	0.274	0.123
12 %	Sand	1.17	15.10	0.236	0.131
			19.34	0.222	0.139
			24.03	0.225	0.137
			28.71	0.227	0.136
12 %	Aggregate	1.46	15.18	0.301	0.105
			19.16	0.283	0.112
			26.26	0.289	0.110
			30.98	0.293	0.108

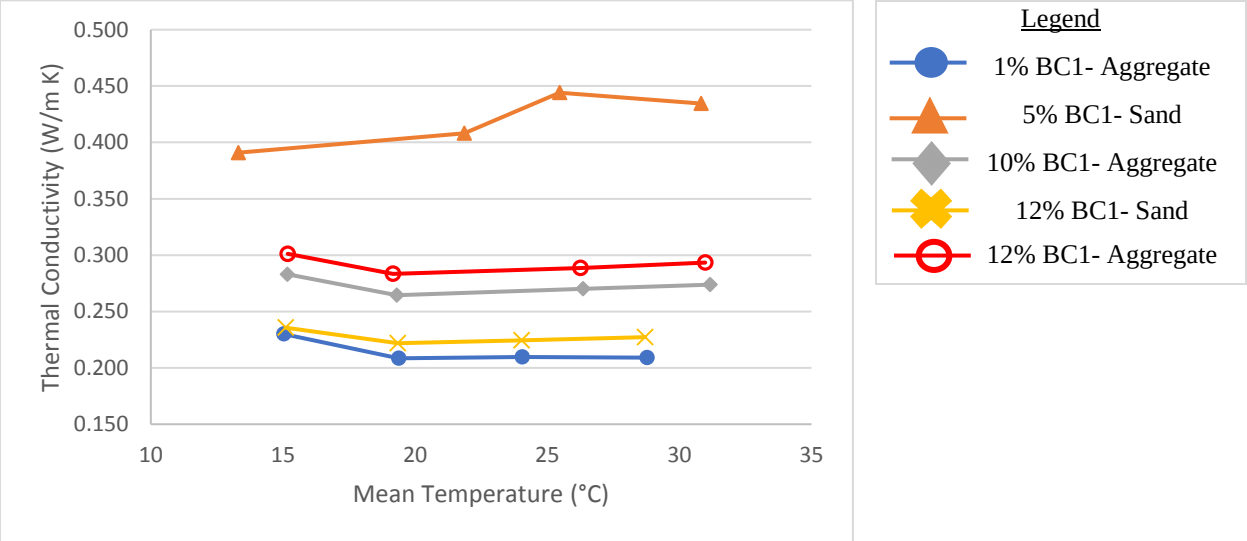

Figure 3.6- Thermal Conductivity as a function of temperature

In terms of improving the insulating properties of concrete, the biochar addition seems to have positive effects on concrete thermal resistance. While it can range depending on a variety of factors, the thermal conductivity of concrete is usually from 0.62 to 3.3 W/m K for standard concrete, or 0.4 to 1.89 W/m K for concrete with lightweight materials (Yun et al., 2013). While this goes against the trend of decreasing conductivity with increasing density, it is likely due to differences in aggregate as other materials may be used to decrease the density of the concrete. For example, a study managed to produce lightweight concrete with a thermal conductivity of 0.23 W/m K, but used diatomite aggregates (Ünal et al., 2007). This shows that biochar addition did manage to improve the thermal resistance of the concrete, even at lower concentrations. However, materials with a conductivity about 0.1 W/m K are typically not named as insulating materials, and most common insulation will have a conductivity in the range of 0.03 to 0.05 W/m K (Berardi & Naldi, 2017). This means that insulation would still need to be used in building applications with the charcrete, but the decreased thermal conductivity would still improve thermal efficiency of buildings.

3.4 Conclusions

Biochar was added as an inert filler to concrete in the place of either sand or coarse aggregate to produce charcrete. The addition of 15 % biochar by weight to the concrete resulted in a concrete density as low as 1454 kg/m^3, falling into the lightweight concrete category, at the expense of very brittle concrete. The maximum amount that could be added to have any sort of integrity was 12% by weight, but the addition of biochar showed a linear decrease in concrete density. Activated carbon was successfully added at up to 30% by weight, but only lowered the density to 1370 kg/m^3.

The addition of both biochar and activated carbon showed a positive increase in the sound absorption coefficient across the frequency range from 200-2000 Hz. Both sets of carbon materials showed the same coefficient despite differences in concentrations, implying that there was no need increase in sound absorption with increasing biochar concentration. Additionally, the Noise Reduction Coefficient of the charcrete at 10% and 15% by weight was 0.45, falling above the threshold of materials considered to have sound absorption properties.

The charcrete also showed improvements in thermal insulation properties compared to standard concrete. The largest reduction in thermal conductivity was present in the charcrete with 1% biochar by weight, with the temperature dependant conductivity ranging from 0.208 to 0.230 W/m K in the measured temperature rage. While this does not fall within the range of conductivity by which a material would be considered insulating, it shows an improvement in the insulating properties of concrete which would help to improve the energy efficiency of buildings which would employ concrete with other insulating materials. At higher biochar concentrations within the concrete, a slight decrease in thermal resistance was found. This could be due to the drastic decrease in material density that was found in these charcrete samples, indicating that lower biochar concentrations are ideal for insulation purposes.

The compressive strength of the charcrete was determined to see if the biochar addition had any negative effects on the concrete. While no clear trend became obvious, there was a slight increase in the compressive strength of the charcrete compared to standard concrete. While a maximum of 21.9 MPa was reached for 3 wt% charcrete (compared to the 17.1 MPa standard), a minimum was also found 11.3 MPa with 1 wt% charcrete. While any differences are likely insignificant, the most important take-away is that biochar has no detrimental effects on the most compressive strength of the concrete. This means that the other investigated advantages of charcrete can be pursued with compromising the concrete integrity in the applications through which it is used.

One negative consequence observed throughout the experiments was the excess water requirement for charcrete. In the standard charcrete production, it was found that 978 mL of excess water was required per kg of biochar added to the recipe in order to have a workable paste, and in the absence of aggregate or sand, 530 mL per kg biochar was required. While increasing the water to cement ratio usually has the impact of decreasing the compressive strength of the concrete, this was not the case. This implies that the excess water is not part of the cement mixture, and is absorbed by the biochar during mixing. Despite that, from an environmental standpoint, the increase in water usage for charcrete is not desirable.

Based on the results of the various testing performed on the concrete, it seems that low levels of biochar in charcrete may be favourable. The thermal conductivity of the charcrete was more

favourable at 1% by weight, and the water usage was still minimized in this range. The compressive strength was not compromised at biochar concentrations up to 3% by weight, however the charcrete became increasingly brittle as more biochar was added. Finally, the sound absorption coefficient showed no further increases with increasing carbon content, implying that large quantities of biochar is not required to show acoustical insulation enhancement. More work still needs to be done to analyze the charcrete properties in the lower biochar concentration ranges. It will also be important to further analyze how biochar properties can be influenced to further enhance the properties of the charcrete.

Chapter 4

4 Production of polymer/ biochar composites with improved electrical and electromagnetic characteristics

This chapter covers the application of biochar for the purpose of creating materials with improved electrical conductance and shielding characteristics. The analytical techniques used to characterize the carbon microstructure and the electrical conductivity of the biochar will be discussed. The electrical permittivity of epoxy composites with electrically conductive biochar will be determined. In addition, a proposed method for predicting biochar distribution in polymer composites will be investigated.

4.1 Introduction

As discussed in Chapter 1, the current reliance of society for oil and gas for energy and petroleum based products has created major issues such as an imbalance in the natural carbon cycle (Schmidt, 2012b). One method of combatting this issue is through the usage of renewable and organic material as a filler in composite materials. Biochar has recently gained researchers attention in this aspect due to its effect of carbon sequestration and waste management, combined with its ability to improve characteristics and potentially replace carbon black (Das, Sarmah, & Bhattacharyya, 2015).

One common property of composites that can be altered is the electrical conductance. Polymer based conductors have several advantages over metallic ones, in that they are light, have corrosion resistance, and can be easily shaped at a lower cost (Ahmetli et al., 2013). High carbon materials can exhibit many forms such as graphene and amorphous phases, and the presence of sp^2 hybridised carbon leads to good electrical properties of the material (Ahmetli et al., 2013; Giorcelli et al., Savi, & Berruti, 2016). Therefor, these conductive carbon materials allow for the tuning of composites to have properties ideal for applications such as pressure sensors, capacitors, and batteries (Nan et al., 2015).

Additionally, conductive polymers have been investigated for their use as microwave absorbing materials (Bhattacharya et al., 2015). The growth of the telecommunications market has lead to a drastic increase in electromagnetic waves (EMWs) pollution, and harmful electromagnetic

interference (EMIs) (Saib et al., 2006). Increased exposure to these radiation is hazardous to human health and increases the risk of tumour growth, with studies showing people with long term exposure to electromagnetic radiation having elevated risk of brain tumours (Beall et al., 1996; Thomas et al., 1987). Thus, it is important that materials with microwave absorption capabilities are investigated and developed.

A material's microwave absorption properties will rely on key factors such as its permeability, permittivity, and conductivity. However, a material with very high conductivity can lead to reflection, whereas a good absorbing material needs to allow the EMW to penetrate into a region where the electrical field can be reduced (Bhattacharya et al., 2015). Through this, materials with appropriate conductivity, dielectric properties, and magnetism will interact with electromagnetic radiation and dissipate the electrical and magnetic fields. Carbonaceous materials have been found to perform well in microwave absorption, such as graphene, due to the formation of carbon sheets within the material and its high electrical conductivity (Bhattacharya & Das, 2013). Carbon nanotubes (CNTs) have been found to be very successful when used in composites due to their high conductivity and high-aspect ratio which allow for the formation of conductive networks (Bhattacharya et al., 2015; Saib et al., 2006). Typically, carbon nanotubes (CNT) and multi-wall carbon nanotubes (MWCNT) are the most common forms of sp^2 carbon used for the purpose of conductive composites, but less-expensive and renewable recycled materials have been gaining ground, such as biochar (Quaranta et al., 2016).

Biochar has several characteristics that can lead to an increased electrical conductance, but the degree of aromatic condensation is one of the most important. With increasing pyrolysis temperature, the original organic matter of biochar continuously breaks down, leaving behind a highly carbonaceous, aromatic structure (Schimmelpfennig & Glaser, 2012). When comparing this to carbon blacks, which are often used for their electrically conductive properties in polymers, it has been found that the electrical conductivity increases with increasing polyaromatic content. Additionally, it has been found that carbon black conductivity increases with decreasing levels of oxygen containing surface functional group (Pantea et al., 2001). Since biochar also shows a decrease in the content of certain oxygen containing surface groups with increasing pyrolysis temperature, this shows high temperature biochar can have similar electrical properties to carbon black (Kloss et al., 2011).

Raman spectroscopy is a commonly used method to define the microstructure of the carbon in biochars. While similar to FTIR, it can be used to identify the sp^2 bonded carbon in aromatic rings and the sp^3 disordered carbon structures (Quaranta et al., 2016). Two main peaks are commonly identified in biochar: the first is the G-band, which comes from in-plane vibrations of sp^2 bonded carbon in graphite layers. The second, the D-band, comes from defects in sp^2 carbon, coming from disorders in highly ordered carbon materials (Mohanty et al., 2013; L. Zhao et al., 2013). Both bands come from different aromatic structures, where the G-band comes from aromatic ring breathing, and the D-band from aromatics with no less than six rings from low-grade fuels (Keown et al., 2008). While the science behind Raman spectroscopy is quite complex, a higher I_D/I_G ratio implies high amounts of disordered sp^2 carbon (Chia et al., 2012). While this development is often studied to determine the development of the carbon structure, some studies have shown no correlation between the intensity of these bands and electrical conductance, though carbon black typically as a high I_D/I_G ratio (Pantea et al., 2001).

Some studies have begun to investigate the electrical conductivity of biochar and the effect of biochar structure as it plays a role. The conductivity of biochar from wood and Miscanthus treated at 500 °C was found to be relatively low. There were very little changes between materials, and the researchers found that the biochar had not developed enough of a crystalline structure to have strong conductivity (Behazin et al., 2016). This is backed up by research showing that low temperature biochar retains its cellulose crystallinity. As temperature increased, more turbostatic crystalline structures are formed, as more graphene sheets are formed at the expense of amorphous carbon (Keiluweit et al., 2010).

This corresponds with a study that had shown very little changes in the I_D/I_G ratio of biochar produced within the range of 350 to 650 °C, as the change in microstructure was negligible (L. Zhao et al., 2013). As temperature increases to the range of 700-900 °C, the D-band intensity can be seen to increase due to the growth of large aromatic structures (>= 6 fused rings) throughout the biochar, and possibly the loss of oxygen surface groups (Keown et al., 2008). Consequently, studies have shown the biochar produced at high temperatures have shown an increase in electrical conductivity with increasing carbon contents, with improvements seen from 83-98% carbon by weight (Gabhi et al., 2017; Jiang et al., 2013). The authors concluded that these biochars have potential for application in electrical products such as supercapacitors. In a

study using biochar in poly(vinyl alcohol) (PVA) composites, it was found that biochar with a fixed carbon 61.8 % was able to provide the composite with similar conductive properties as one prepared with CNTs and graphene (Nan et al., 2015). The same authors found that biochar worked suitably in PVA composites as a pressure sensor, giving another large potential application (Nan & DeVallance, 2017).

This study aims to analyze the carbon microstructure of various North American biomass feedstocks to investigate the change in arrangement with different pyrolysis conditions. The electrical conductivity of the biochar is analyzed in order to determine whether or not the carbon material will be effective in the generation of electrically shielding composites. A method has also been developed for predicting how well biochar will disperse in a polymer composite. As composite production is time consuming and requires expensive extrusion equipment, this study aims to utilize a low-cost method for quickly analyzing how different biochar will behave in polymers.

4.2 Materials and Methods

Biochar Used

For this set of experiments, 11 different biochar samples were analyzed. The first 8 biochar samples were those produced from the continuous pyrolysis experiments highlighted in Chapter 2. The proximate characteristics for these samples are shown in Table 2.12, and the elemental composition and metal contents shown in Table 2.16 and Table 2.21 respectively. The last three biochar samples were produced using CO_2 activation in the ICFAR Jiggle-Bed Reactor (JBR) at three different temperatures, from the Miscanthus harvested in Drumbo, Ontario. The proximate characteristics and elemental composition of the biochar samples can be seen in Table 4.1 and Table 4.2, respectively.

Table 4.1- Proximate characteristics of high temperature Miscanthus biochar

BIOCHAR	VOLATILE MATTER (WT%)	FIXED CARBON (WT%)	ASH CONTENT (WT%)
MISC 650	11.3	81.1	7.6
MISC 700	8.3	80.9	10.9
MISC 750	8.2	79.0	12.9

Table 4.2- Elemental composition of high temperature Miscanthus biochar

BIOCHAR	C (WT%)	H (WT%)	O (WT%)	N (WT%)	O/C	H/C
MISC 650	78.6	1.8	11.6	0.4	0.11	0.27
MISC 700	80.2	1.6	7.0	0.3	0.07	0.24
MISC 750	79.7	1.2	5.8	0.4	0.05	0.18

The volatile matter content in the biochar shows the same decreasing trend from the MS, Drumbo biochar in Chapter 2, and while the fixed carbon shows an increase from the levels seen when produced at 550 °C, it seems to level off around 80%. The elemental composition also shows the expected trends, with the elemental carbon also seemingly plateauing at 80%. Additionally, both the atomic O/C and H/C ratios continue to decrease at higher temperatures, showing that the biochar has had more drastic carbonization effects through pyrolysis. Additionally, the metal content of the biochar samples is shown in Table 4.3, the results of which show no unexpected inorganics appearing within the biochar, with calcium and potassium being the most clearly dominant metals.

Raman Spectroscopy

The raman spectroscopy was performed by the DISAT at the Politecnico di Torino, Italy. The equipment used was a Renshaw Ramascope Microraman, equipped with an Argon green laser (excitation at 514.5 nm at 50 mW). Measurements were taken at different points, with 50 x objective used for the analysis. The signal intensity was taken as a function of the Raman shift, as shown in Figure 4.1.

Table 4.3- Metal content of high temperature Miscanthus biochar

	Miscanthus		
Misc	650	700	750
Ash (mg/kg)	76000	109000	129000
Al	160	275	293
Ca	3390	4306	10316
Cu	3.14	3.09	1.86
Fe	262	442	312
K	2775	3055	4113
Mg	1056	1134	1263
Mn	30.5	47.6	47
Na	257	318	324
Ni	5.22	3.48	8.11
P	1032	1004	543
Pb	0	0	0
S	64.5	75.3	120
Si	328	315	574
Zn	4.98	7.4	3.39

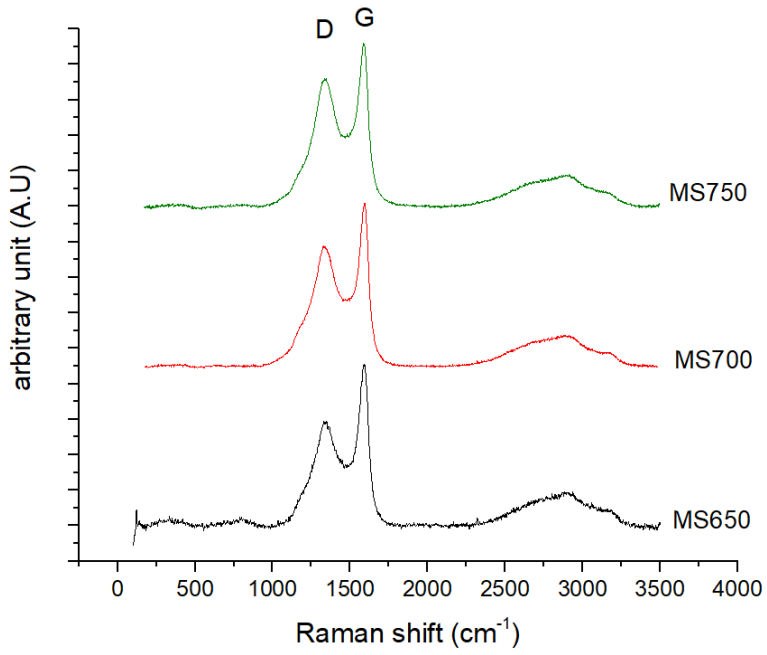

Figure 4.1- Graph of band intensity as a function of the Raman shift

Each Raman spectra was fitted using Gaussian curves able to fit each peak. For each curve, areas were calculated that in turn were used to calculate the ratios. In particular, the intensity of the two peaks at 1360 cm^{-1} (the D band) and at 1580 cm^{-1} (the G band) are then used to calculate the I_D/I_G ratio.

Electrical Conductivity

The electrical conductivity of the biochar was measured at the Politecnico di Torino in Torino, Italy along with the carbon microstructure. The instrument setup is shown in Figure 4.2. Two solid copper cylinders (30 mm diameter, 5 mm length) were connected to a hollow Plexiglass cylinder (30 mm internal diameter) to create an internal chamber between the copper where the biochar could be positioned. Insulators were positioned between the copper cylinders and the load surfaces.

The resistance of the biochar sample was measured using an Agilent 34401A multimeter. The conductivity of the samples was calculated from the resistance across a sample of known size as shown in the equation below:

$$\sigma = \left(\frac{R * A}{L}\right)^{-1}$$

Where σ is the conductivity in S/m, *R* is the resistance in ohms, *A* is the constant contact surface area (m^2) and *L* is the sample thickness (m) that decreases with increasing load. The electrical resistance of the sample was recorded once a stable value was available. The electrical conductivity was measured with increasing pressure applied to the biochar powder. Compression was applied using a hydraulic press (Specac Atlas Manual Hydraulic Press 15T) capable of applying 15 tonnes to the sample surface area, *A*.

Epoxy Resin Composite Preparation

Epoxy resin was used to create the composite material for electrical permittivity characterization, and were cast at the Politecnico di Torino, Italy. Three different biochar samples were used to produce the composites (Misc 650, Misc 700, and Misc 750), and were ground using a

mechanical grinder to produce a powder in the size range of tens of microns. The commercial epoxy resin (Cores LPL) is a low viscosity, transparent resin with reduced crystallization density.

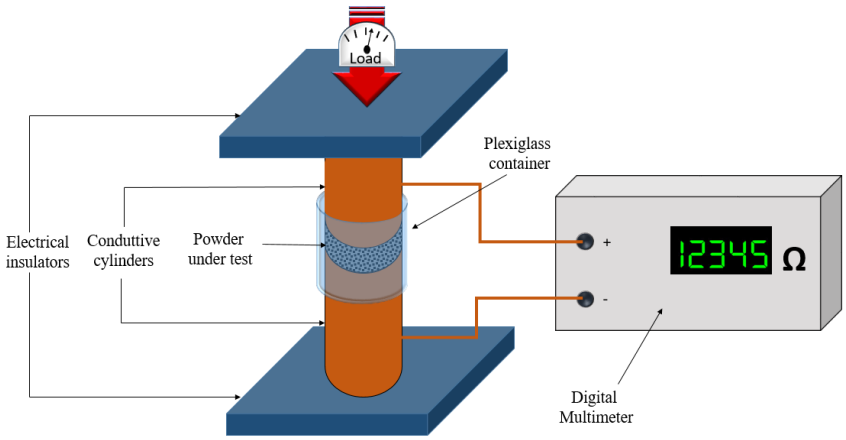

Figure 4.2- Experimental set-up for compressive electrical resistance measurements

The samples were prepared in the following manner:

1. Biochar, in powder form, and Epoxy were weighed via a digital balance and mixed together with a metallic spatula.
2. Composite, in liquid form, was delicately mixed for 20 minutes by mechanical mixer in order to avoid air bubble formation.
3. Composite was further mixed for 5 min using an Ultraturrax® mixer, able to achieve appropriate mixing of small size particles.
4. Curing agent was added to the mixture in the ratio indicated by the producer and 10 minutes of mechanical stirring was performed.
5. The mixture was slowly poured in cubic silicon moulds, carefully avoiding the formation of air bubbles.
6. The composites were degassed in a vacuum chamber for 20 minutes in order to remove possible residual microscopical air bubbles and obtain a uniform material.
7. Final products were dried in oven for 4 hours at 50°C.
8. After an overnight rest, samples were delicately removed from their silicon moulds.

The produced samples can be seen in Figure 4.3

Electrical Permittivity

The interaction between an electric field and a material is described by the complex relative permittivity.

Figure 4.3- Composite for electrical characterization (square) and for other characterizations (cylindrical)

$$\varepsilon_r = \varepsilon_r{}' - j\varepsilon_r{}''$$

Where ε_r is the relative permittivity, with $\varepsilon_r{}'$ representing the real part of the permittivity, and $\varepsilon_r{}''$ the imaginary part. The real aspect of the permittivity is related to the polarizability of the material, or the interaction of the electromagnetic field with the bound charges. The imaginary part describes the total power adsorption or loss (dielectric loss or loss by ionic conduction), arising from interaction with free electrons (Giorcelli et al., 2013):

$$\varepsilon_r{}'' = \varepsilon^{"}{}_d + \frac{\sigma}{2\pi\varepsilon_0 f}$$

Which is simplified further with negligible dielectric losses:

$$\sigma = \omega\varepsilon_0\varepsilon_r{}''$$

Where ω is the angular frequency of the wave (rads/s), ε_o the free space permittivity, and σ the conductivity (S/m). Through this, a charge polarization effect causes an increase in the real part of the complex permittivity, and an increase in the electrical conductivity increases the imaginary part.

The complex permittivity of the epoxy composites was measured in the frequency range of 1-12 GHz. Samples were measured using a commercial open-ended coaxial sensor (Agilent 85070D) and a Network Analyzer (E8361A). This measurement system is used as it allows for wide-band characterization and can be used on samples with small dimensions. On the other hand, free-space measurements require large samples to be used, and the waveguide method needs

waveguides of various dimensions being required to cover a wide frequency range (Giorcelli et al., 2013).

Polyester Resin Composite Production

The polyester resin composite samples were prepared using TAP Clear-Lite casting resin from TAP Plastics. The casting resin is a low exotherm polyester, which cures with the addition of a Methyl Ethyl Ketone Peroxide (MEKP) catalyst. When used on its own, the resin has a water clear colour, a viscosity of 450-600 cps, and a specific gravity of 1.10-1.12.

The samples were prepared by first weighing out the amounts of resin and biochar to be added to the solution. TAP solid white pigment was then added to the resin and mixed in, in order to make an opaque, white material. The biochar was then slowly added to the white resin and stirred thoroughly to ensure the biochar was well distributed. After the biochar was completely mixed in, the MEKP catalyst was added, and the mixture was stirred for 60 seconds. The solution was poured into a 12 cm x 5 cm flexible silicon mould, which was tilted slightly for proper coverage. The composite was allowed to cure for two days before being removed from the mold. The recipe used for composite production is shown in Table 4.4, and it is worth noting that the recipe was produced through trial-and-error.

Table 4.4-Recipe for production of polyester resin/ biochar composites

Material	**Amount**
TAP Clear-Lite Resin	21.99 grams
TAP Opaque White Pigment	3 drops
Biochar	1.41 grams (6 wt%)
MEKP Catalyst	16 drops

Two different sets of experiments were performed to determine the distribution effect of biochar in the polyester resin. The first was using biochar produced at a range of different temperatures to determine if any difference was present when using biochar with different characteristics. The biochar used in this set of experiments was from the unmodified pyrolysis experiments and the slow pyrolysis experiments discussed in Chapter 2, and are shown again in Table 4.5.

Table 4.5- Biochar used in first polyester resin experiments

BIOCHAR	VOLATILE MATTER (WT%)	FIXED CARBON (WT%)	ASH CONTENT (WT%)
MS, DRUMBO 550	18.4	71.3	10.4
MS, DRUMBO 500	22.5	67.8	9.8
MS, DRUMBO 450	32.1	59.9	8.0
MS, AWF 500	24.1	62.8	13.1
MS, AWF 450	28.8	59.2	12.0
MS, AWF 400	31.0	56.5	12.5
MS, AWF 350	47.2	45.5	7.3
MS, SLOW 500	7.5	81.4	11.0
MS, SLOW 480	6.9	81.3	11.7
MS, SLOW 350	13.9	75.2	10.8
MS, SLOW 327	17.8	72.5	9.7

The second set of experiments performed was to determine the reproducibility of polyester resin materials. Three sets of four composite samples were produced using three different biochar samples to determine the reproducibility of the polyester resin samples, and that the differences in materials were significant. The three selected biochar sets had a wide range of characteristics that could influence distribution. The biochar used is shown in Table 4.6.

Table 4.6- Biochar used in second polyester resin experiments

BIOCHAR	PYROLYSIS METHOD	VOLATILE MATTER (%)	FIXED CARBON (%)	ASH CONTENT (%)
MS, DR 500	Unmodified	22.5	67.8	9.8
MS, SLOW 500	Slow	7.5	81.4	11.0
DDG 400	Continuous	54.7	35.0	10.4

Digital Image Analysis

In order to analyze the effectiveness of biochar distribution throughout the material, an image analysis program was prepared using Simulink. The software analyzes an image pixel by pixel, giving each pixel a RGB intensity value on a scale of 0 to 256 (with 0 being completely black, and 256 being completely white). From this, the software calculates both the average intensity

across the pixels to give the average shade, as well as the variance in intensity across the pixels to show how well the material is distributed. Using this software, a perfectly distributed material could have any intensity, but would have a variance of 0.

Three photos were taken of each mould, on the left and right side, and one in the middle. The moulds were all photographed in the same spot, and care was taken to make sure that the lighting was the same between samples, as the intensity values could change depending on the brightness of the lights in the room. Each image was analysed using the software, to determine both the average and the variance in the intensity, from which the coefficient of variance could be calculated. The final values for each sample was then calculated as the average of all three images.

Polyester Resin Composite Density

The density of each sample was calculated using the mass, measured using a laboratory scale, and the volume, found by water displacement.

4.3 Results and Discussion

Raman Spectroscopy

The I_D/I_G ratio of the Miscanthus biochar can be seen in Figure 4.4 as a function of treatment temperature. The development of D-band and G-band peaks shows the beginning of aromatic carbon formation within the biochar at lower temperatures. The I_D/I_G ratio for the low temperature Miscanthus sits between 0.73 and 0.78, showing very little change in that temperature range which is consistent with other studies (L. Zhao et al., 2013). While these ratios are slightly lower than what has been found with similar feedstocks with the same fixed carbon levels, the small differences could be down to lack of peaks in general. At higher temperatures, the I_D/I_G ratio increases drastically, reaching a peak of 2.51 at 700 °C. This increase is consistent in what is found in literature for higher temperature pyrolysis (Keown et al., 2008), and shows more disordered carbon being formed. This is likely due to increased aromaticity of the biochar, with different crystalline structures forming, and oxygen containing functional groups leaving the carbon rings (Keiluweit et al., 2010; Mohanty et al., 2013). The

slight decrease in the I_D/I_G ratio at 750 °C may be negligible, but could possibly come from more ordered graphite carbon forming, or perhaps melting of large aromatic rings.

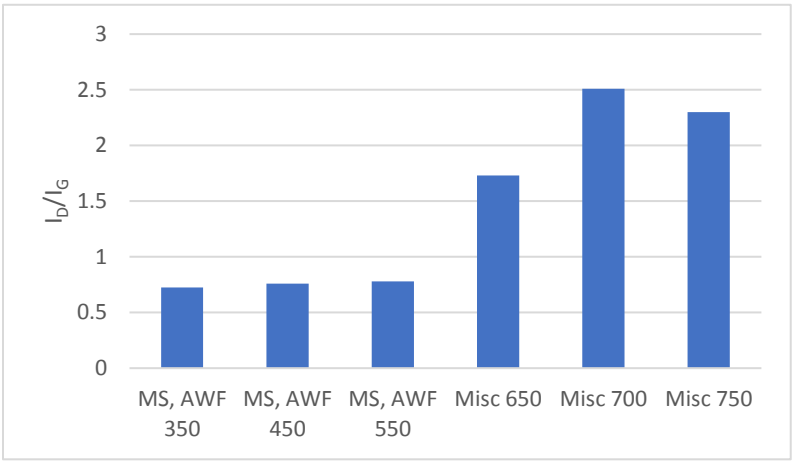

Figure 4.4- I_D/I_G Ratio for Miscanthus biochar

Figure 4.5 shows the same low values for the I_D/I_G ratio as the lower temperature Miscanthus, with very little change with increasing peak temperature. While the ratio is slightly higher for the wood biochar, it is likely non-significant, but could come down to increased aromaticity coming from the differences in feedstock of the carbon.

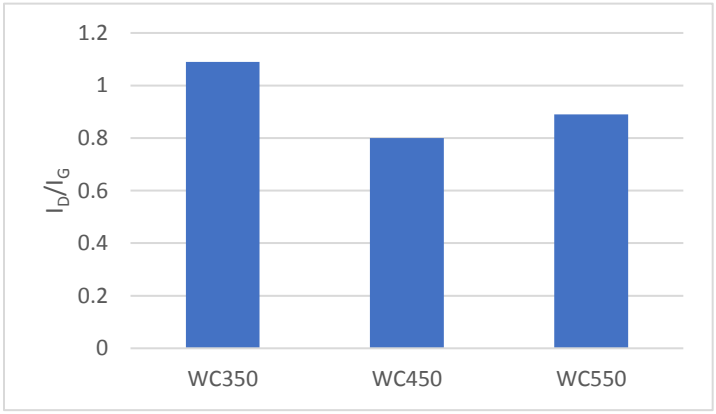

Figure 4.5- ID/IG Ratio for Wood Chip biochar

The Raman shift for the distiller's grain showed no identifiable peaks within the material as shown in Figure 4.6. This implies that the DDG char has no aromatic or graphitic carbon throughout the material, which coincides with the results of the proximate and elemental analysis discussed in Chapter 2. DDG is not a conventional lignocellulosic feedstock, in that its carbon content comes in the form of the large fat and protein content of the starch material. The Raman

spectroscopy confirms that the carbon content, while reaching 60 wt%, has very little fixed, aromatic carbon which forms. This coincides with the SEM imagery of the DDG char in Chapter 2, which shows no pore formation across the material, which likely means the DDG char has no crystalline structure, and may not present any electrical advantages.

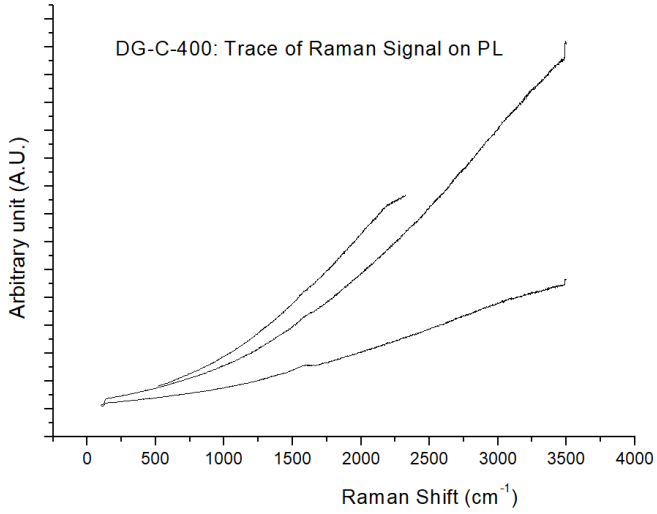

Figure 4.6- Raman shift for distiller's grain biochar

Biochar Conductivity

Figure 4.7 shows the electrical conductivity of the biochar derived from Miscanthus between 650 and 750 °C. The Miscanthus biochar activated at higher temperature had a drastic increase in electrical conductivity with increasing pyrolysis temperature. This could be due to the decrease in volatile matter, or perhaps the increase in the I_D/I_G ratio as identified by electrical conductivity. Both the fixed carbon and elemental carbon are similar across all three samples, which implies that the change in carbon microstructure could have a large impact on the conductive properties of the biochar. This is reinforced further as the commercially available biochar MSP700 (produced by the UK Biochar Research Centre), also produced from Miscanthus at 700 °C, has a significantly lower conductivity. The two samples have near identical carbon, oxygen, and ash contents, which leads to the conclusion that the CO_2 activation is the major difference which would result in a different pore structure and consequently a carbon structure.

This also shows that the activated Miscanthus biochar shows a heavily improved conductivity over two commercially available biochar produced from Miscanthus (MSP700) and oil seed rape straw (OSR700). However, even the higher conductivity samples exhibit conductivities in the

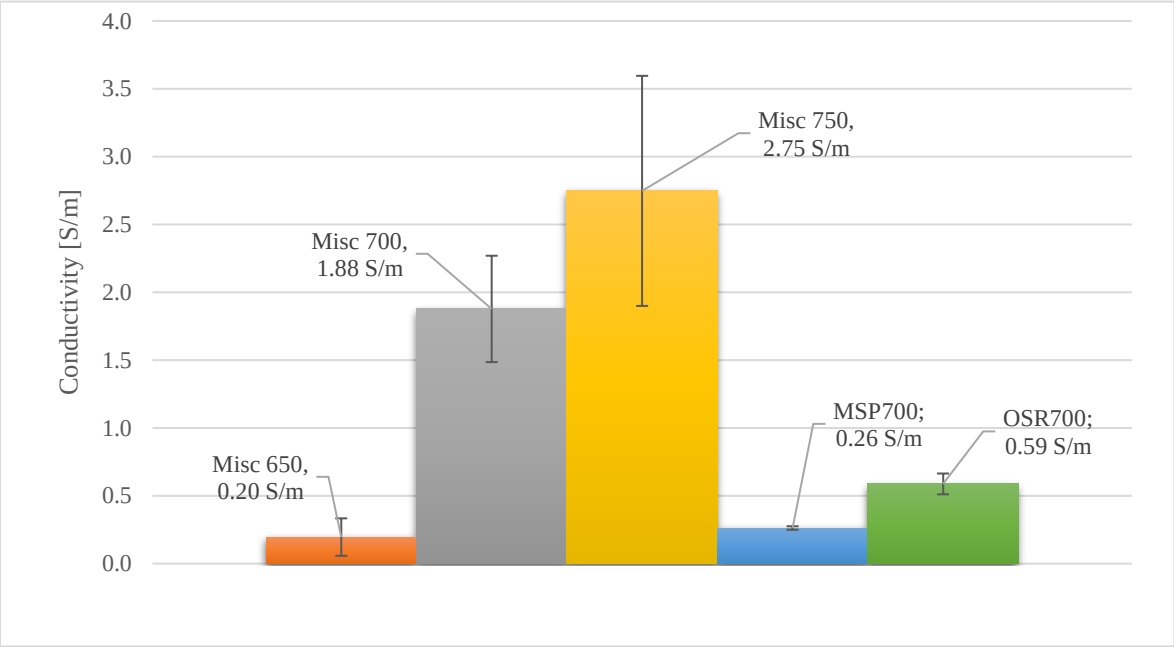

Figure 4.7- Biochar conductivity of tested ICFAR biochar (Misc 650, Misc 700, and Misc750), and of commercially available biochar (MSP700, and OSR700)

lower range of those exhibited by carbon black, which can be in the range of 10-100 S/m (Pantea et al., 2001). The lower temperature biochar showed insignificant electrical conductivities, with MS, AWF 550 and DDG500 having conductivities of 4.2 $x10^{-7}$ S/, and 4.7 $x10^{-7}$ S/m, respectively. This could be due to the lesser extent of carbonization exhibited in the continuous pyrolysis experiments, and the little carbon microstructure displayed by all the samples. This is consistent with research on various biochar, where lower temperature biochar (~500 °C) has little displayed conductivity (Behazin et al., 2016), whereas improving the carbon content through thermal treatment can improve the conductivity into the range of 50-400 S/m (Gabhi et al., 2017).

Electrical Permittivity

Figure 4.8 shows the results of the permittivity measurements of the epoxy resin samples.

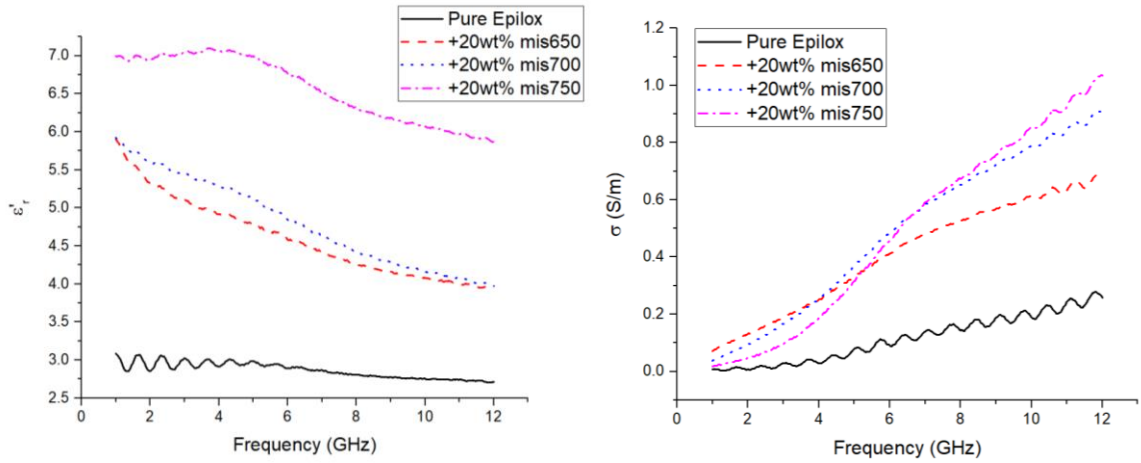

Figure 4.8- Composite permittivity measurements: Real part (left) and conductivity (right) in the frequency range of 1-12 GHz.

The addition of biochar increased the real part of the complex permittivity of the epoxy composites. As expected, Misc 750 shows the greatest increase, which implies it would be the best suited for electromagnetic absorbing properties as it displays the best dielectric properties. At higher frequencies, the addition of 20 % biochar by weight also improves the electrical conductivity of the composite, showing that the high temperature biochar shows potential for use in absorbing and supercapacitor materials. However, when compared to MWCNT's, which are commonly used in these applications, analogue epoxy resin with only 5 % MWCNT's by weight shows a permittivity around double that of the biochar (Giorcelli et al., 2013).

Polyester Resin Composites

In the first set of experiments, three sets of polyester resin composites were used to determine the distribution effect of biochar addition into the resin. Figure 4.9 shows the RGB Intensity as a function of the pyrolysis temperature for the three sets of produced biochar. A slight increase in RGB intensity can be seen for all set of data. This means that the average colour tends to be whiter at higher pyrolysis temperatures, however, in this case the colour is more of a grey. This could be due to more spread of the biochar throughout the material. In order to get a better idea of the biochar distribution, the coefficient of variance in RGB Intensity across the material is shown in Figure 4.10.

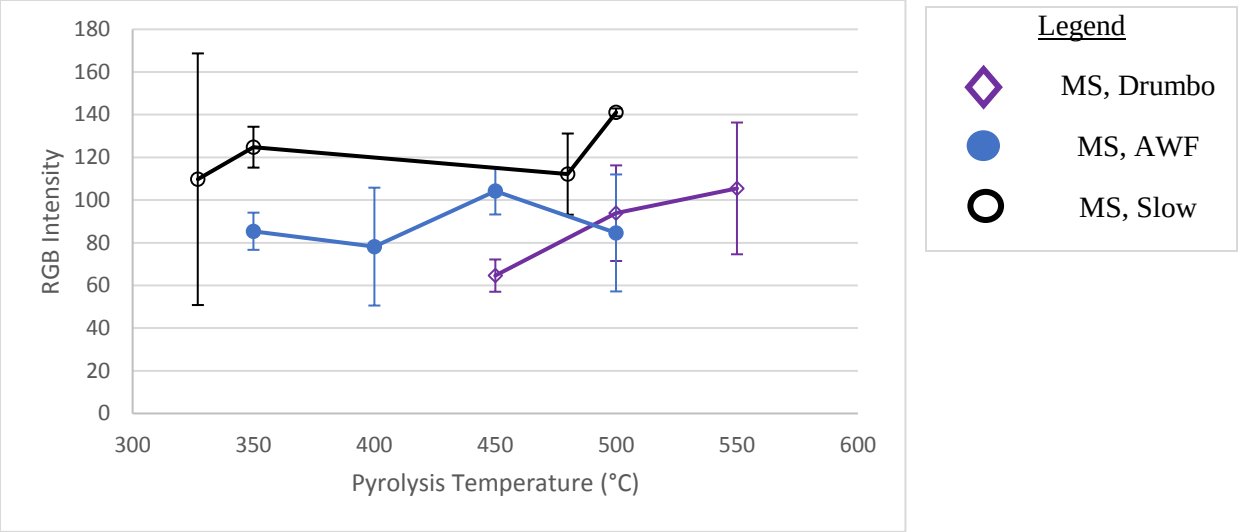

Figure 4.9- RGB Intensity as a function of pyrolysis temperature

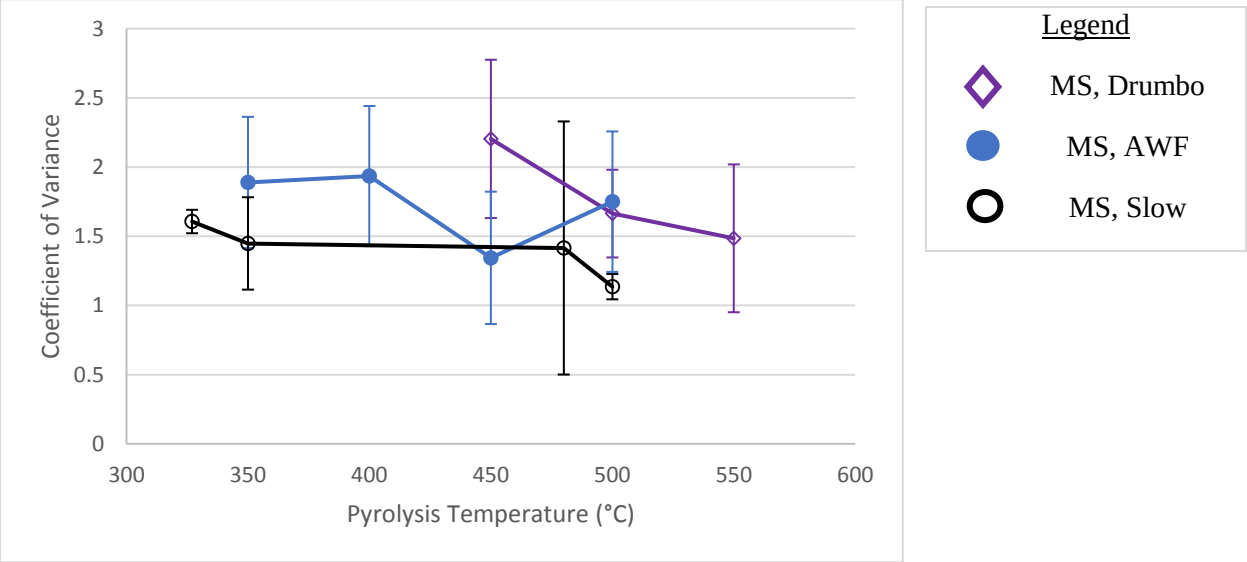

Figure 4.10- Coefficient of Variance for RGB Intensity as a function of biochar pyrolysis temperature

This shows a general decrease in the coefficient of variance of the polyester resin composites with increasing biochar production temperature. Firstly, this corresponds well with the first graph, in that less variance in the intensity of the composite would result in a grey appearance. Secondly, this implies that the biochar is being distributed more evenly throughout the resin when it is produced at higher pyrolysis temperature.

For the second set of experiments, the results can be seen in Table 4.4, with an example of each composite shown in Figure 4.7. From this, it can be seen that there are little differences in the density of each set of composites, with the DDG composite likely being higher due to the

increased density of the biochar. The 95% confidence interval for each composite is relatively low in terms of both intensity and variance. However, a statistical analysis of the results shows that the difference in intensity between Runs 1 and 3 is non-significant, with a 9.7% chance that the first biochar gives an intensity higher than that of the third. The same issue arises with the coefficient of variance between Run 2 and 3, with an 8.9% chance that DDG 400 gives a higher coefficient than MFR MS 500. Despite that, the rest of the comparisons shows significant difference, and once again shows that while a material might have the lower RGB intensity (Run 2), this results in a high variance between the samples. Looking at Figure 4.11, it also appears that the middle image has the best distribution, which is confirmed by the low variance of 1.132 given by the analysis.

Table 4.7- Results of reproducibility experiments on biochar/ polyester resin composites

RUN	BIOCHAR USED	RGB INTENSITY	COEFF. OF VARIANCE	DENSITY (g/L)
1	MS, Drumbo 500	139.7 ± 11.3	1.132 ± 0.085	1220 ± 84
2	MS, Slow 500	125.3 ± 13.8	1.579 ± 0.265	1221 ± 40
3	DDG 400	145.2 ± 3.4	1.440 ± 0.196	1293 ± 69

Figure 4.11- Examples of composites produced during reproducibility experiments, MFR MS 500 (left), MS DRUMBO 500 (middle), and DDG 400 (right)

While these experiments have shown that a slight trend, and relationship, can be seen in the overall intensity and variation in RGB intensity, the detectable changes were small for the composites produced with biochars with different chemical and physical characteristics. However, the second experiment has shown reproducibility in the produced composites, and that significant differences can be seen. It also shows that differences in visible variations are quantifiable using computer software.

Further research in this method should further investigate physical properties of biochar and the effect this biochar has on composites. For example, as particle size is widely considered to be a key characteristic, the intensity and variance should be analyzed over a range of particle sizes.

As well, more sets of data performed on biochar produced over a wide range of temperatures would serve to prove whether or not the detectable trends as shown in experiment one are important or random chance.

4.4 Conclusion

In this study, the carbon microstructure of biochar produced from three different feedstocks at various pyrolysis temperatures were studied. The biochar produced in the continuous pyrolysis experiments from Miscanthus, wood chips, and dried distiller's grain at lower temperatures showed little change in I_D/I_G band ratios. This implies that these biochar samples had not developed any aromatic carbon structure or crystalline structure. Miscanthus biochar activated with CO_2 at higher temperatures exhibited an increase in the I_D/I_G ratio, which is attributed to disordered carbon being more abundant than the carbon found in graphene sheets. This is commonly associated with the development of crystalline structures found in higher temperature biochar.

These biochar samples with a more developed carbon microstructure exhibited a much higher electrical conductivity, with the biochar activated at 750 °C having a conductivity of ~2.75 S/m. This was significantly higher than the conductivity found in commercially available biochar produced in the same temperature range, implying that the activation provided the biochar with different electrical properties. While the conductivity is much lower than that which can be found in carbon blacks, the more sustainable nature of biochar makes it more favourable for use. The addition of biochar also improved the dielectric and conductive properties of epoxy resin, with Misc 750 also showing the biggest increases. This implies that it is most favourable for use in electromagnetic absorbing materials. While the dielectric properties and conductivity of the biochar are much less pronounced than those of carbon nanotubes, the lower cost of production and the environmental factors of biochar means that the potential of the material should be further investigated.

Finally, the addition of biochar as well as a contrasting white dye into polyester resin allowed for digital image analysis to be used in order to analyze the dispersion of the biochar. The variance in black and white colour was found to decrease with increasing pyrolysis temperature of the biochar analyzed. This lower variance means that there was a more uniform colour distribution

across the material which would come from improved dispersions. Despite visible differences, when a statistical analysis was performed on composites produced using biochar with varying characteristics, the differences in RGB intensity and variance were found to be insignificant. However, the chances that the differences were due to chance were very low, and a more pronounced difference could be found with more replicate samples. More samples need to be processed in order to further identify patterns and trends, and more epoxy resins need to be produced and characterized to identify correlations between RGB variance and electrical properties.

Chapter 5

5 Conclusions and Recommendations

In this study, three different pyrolysis reactors were used to produce biochar: the unmodified pyrolysis pilot plant, the modified pyrolysis pilot plant for continuous operation, and the small mechanically fluidized reactor. Additionally, thermal treatment using a modified muffle furnace was performed. The biochar yield was similar for both the modified and unmodified pyrolysis experiments, but the small MFR had slightly higher yields, ranging from 22.4 to 27.5 wt %. However, the processing capability of the MFR is much lower than that of the continuous pyrolysis pilot plant, making the latter more favourable for large scale biochar production. The continuous modification allowed for 1500 to 2000 grams of biomass to be processed per day.

Biochar was produced from Miscanthus, waste wood from construction and demolition projects, and dried distiller's grain. The Miscanthus biochar produced continuously showed the largest increase in fixed carbon (71.8 %) and elemental carbon (76.5 %) while maintain an expected ash content (10.2 %). Also, when produced under slow pyrolysis conditions, the fixed carbon of the Miscanthus biochar increased further (81.4 %), which potentially corresponded to the drastic increase in the specific surface area of 350 m^2/g. Additionally, the slow pyrolysis biochar showed a much larger reduction in atomic O/C and H/C than the continuously produced biochar, implying that the longer residence time was important in the reduction of volatile surface groups on the biochar.

The recycled wood was largely dominated by insoluble silica present within the initial feedstock. Silica is commonly used in the construction industry, for purposes such as concrete and insulation, implying that the wood had been contaminated by some source. This showed heavily within the wood biochar, as the ash content escalated with increasing pyrolysis temperature up to 43.8%, with reductions in the fixed carbon and elemental carbon occurring at higher temperatures. The high amount of silica dominating the biochar limits its potential for uses in applications such as soil amendment and composite production.

The dried distiller's grain displayed non-typical behaviour with increasing pyrolysis temperature. The fixed carbon of the DDG biochar reached 47.4 % at 500 °C, and an average of 65.9 % with

further treatment to 600 °C. However, the elemental carbon did not increase with further treatment up to 600 °C, reaching a peak around 60 %. This implies that there is no real fixed carbon content within the grain, likely since it is composed mostly of protein and fat. The SEM imagery of the DDG biochar confirmed this, as there was no pore structure formation within the material, whereas both the wood and Miscanthus showed the development of a pore structure at higher temperatures.

The incorporation of DDG biochar into concrete (charcrete) showed drastic reductions in the density of the concrete. At up to 15 % biochar by weight, the concrete density could be decreased to below 1500 kg/m^3 falling into the classification of lightweight biochar. However, the charcrete becomes very brittle at these levels. Despite this, the same trends in concrete density can be seen with lower levels of biochar addition, although less pronounced. The compressive strength of the concrete showed a slight upward trend with increasing levels of biochar, particularly between the 2 and 3 wt % samples. However, the trends are not conclusive and consistent enough to say with certainty that the charcrete had improved mechanical properties, but the most important take-away is that the biochar did not negatively impact the compressive strength.

Charcrete also showed strong improvements in sound absorption compared to standard concrete across the frequency range of 200 to 2000 Hz. It appears there is little importance in which filler was replaced in the concrete (sand or aggregate) as different samples showed near identical sound absorption coefficients with different concentrations of fillers. Additionally, the addition of activated carbon in concrete recipes showed no further improvement in the sound absorption when compared to biochar, while increasing biochar concentration also showed no improvements. While the addition of porous materials showed an increased in the porosity of concrete layers, it appears that a maximum may be present in the porosity that can be provided, and subsequently the sound absorption through carbon addition. Despite that, the addition of activated carbon and biochar in varying concentrations resulted in a Noise Reduction Coefficient of 0.45 for all three mixtures. This is not only an improvement in the NRC of 0.25 for standard concrete, but puts the charcrete above the 0.35 threshold for materials considered to be sound absorbers.

The addition of biochar also proved to improve the thermal insulation properties of the concrete. Where the thermal conductivity of most industrial concrete can range anywhere from 0.4 to 3.3 W/m K, the addition of 1% biochar by weight resulted in the charcrete having a temperature dependant thermal conductivity as low as 0.209 W/m K. However, increasing the biochar concentration within the concrete did not have the desired effect of further improving the thermal resistance, and instead increased the thermal conductivity, albeit by a small amount. This could be down to several reasons, one of which is that the decrease in concrete density associated with the addition of biochar counteracted the insulating effects of the biochar. It is also possible the higher concentrations were poorly dispersed, such that other heat transfer paths are available throughout the concrete. Despite that, the addition of low levels of biochar still resulted in concrete with improved thermal insulation. While the conductivity of the concrete was not low enough to fall into the region of materials typically used for thermal insulation (< 0.1 W/m K), the application of charcrete in building applications would still serve to improve the energy efficiency of the building.

Based off of the results of the concrete experiments, it is concluded that biochar could be added to concrete at low levels (1 or 2 % by weight) to create a charcrete with improved characteristics without compromising the compressive strength. This would allow for a concrete which could be used in residential building or applications not requiring high strength in order to improve insulation and sound absorption. Additionally, the incorporation of lower levels of biochar did not significantly increase the amount of water required for workable concrete. While the density can be drastically reduced with larger volumes of biochar, the charcrete can become extremely brittle, with no noticeable improvements in heat resistance.

The results of the Raman spectroscopy showed little change in the carbon microstructure of both the Miscanthus and wood chip biochar produced between 350 and 550 °C. However, Miscanthus biochar activated with CO_2 at temperatures between 650 and 750 °C showed significant increases in the D/G band ratios, implying the development of disordered carbon structures, implying increased aromaticity of the carbon, and oxygen functional groups having left the carbon rings. The dried distiller's grain biochar showed no carbon microstructure through Raman spectroscopy, which is likely due to the differences in feedstock composition (starch) compared to the other feedstocks (lignocellulosic).

The conductivity of the produced biochar samples was measured to determine which materials would be favourable for production of electromagnetic shielding composites. The biochar produced in the continuous pyrolysis experiments had insignificant conductivity, but the Miscanthus biochar activated with CO_2 at higher temperatures had conductivities reaching 2.75 S/m. This is likely due to the increased aromaticity which was evident from the Raman spectroscopy, and the biochar samples was even more conductive than commercially available biochar produced in the same temperature range. When incorporated into epoxy resins, the biochar increased the dielectric properties of the composite as expected, implying that biochar is more susceptible to be polarized by an electric field. The increased permittivity and conductivity means that biochar has potential for electromagnetic shielding or supercapacitor applications. While the biochar does not display the same dielectric and conductive properties as graphene, CNT's, or carbon black, the low cost and sustainability associated with biochar make it more favourable for different applications.

The digital image analysis of the produced polyester resin/ biochar composites showed slight changes in intensity with different biochar added. A slight upward trend in RGB intensity could be seen using biochar from the same feedstock produced in higher temperatures, which implies that the composite is whiter on average. The slow pyrolysis biochar showed the highest RGB intensity, and consequently the lowest coefficient of variance of the three biochar samples tested implying the least variability in colour across the composite. In the other two samples, a slight downward trend could be seen with increasing pyrolysis temperature, implying the higher temperatures result in biochar the disperses better throughout the material. While performing reproducibility measurements and to determine if there was a significant difference between different biochar samples, it could be seen that the density of the composite materials changed very little with different biochar. While there was a visible difference in the dispersion of the produced composites, a statistical analysis shows that there is no significant difference between all three of the samples for RGB intensity and coefficient of variance, albeit with small sample sizes. The same relationship had appeared in these samples through, where a lower RGB intensity (blacker) showed higher variance across the material implying less even dispersion. More replicate composite samples should be produced using different biochar to determine if the differences in intensity and variance are random or statistically significant.

It is recommended for future biochar production experiments that slow pyrolysis tests are conducted with each of the feedstocks used in this study to further analyze trends in production. Since the Miscanthus biochar showed a drastic decrease in volatile matter and the presence of measurable surface area, wood chips and distiller's grain should be studies in a similar fashion. Also, since the activated Miscanthus biochar showed excellent electrical conductivity in Chapter 4, an experimental set up should be achieved to more easily modify larger quantities of various feedstocks.

For charcrete production, replicate samples of each recipe should be produced in order to determine whether or not changes in strength or insulation is significant or reproducible. It is recommended that the concrete recipes be produced using a constant water to cement ratio to further understand the changes in compressive strength and porosity with the inclusion of biochar. Plasticizers or water reducers could allow biochar to be incorporated without the consequential excess water requirement. More standardized vibration techniques should be used to guarantee that all concrete is settled properly. It is also recommended that biochar from different feedstock be incorporated into charcrete to identify if changes in carbon microstructure plays a role in the material characteristics. As highlighted in Chapter 4, the DDG biochar showed significant difference from Miscanthus and wood biochar in terms of carbon microstructure. Therefor, different biochar compositions should be tested to further understand the interaction between separate properties and the resultant charcrete characteristics.

Finally, it is recommended that more slow pyrolysis biochar is analyzed for its carbon microstructure and dielectric properties. The activated biochar showed the best electrical conductivity and electromagnetic insulation when added to epoxy resin. Since the slow pyrolysis biochar produced in the Mechanically Fluidized Reactor showed a similar extent of pyrolysis to the activated carbon, it is reasonable to expect that the slow pyrolysis biochar could show similar dielectric properties. The ease at which slow pyrolysis biochar is produced means that more feedstocks could be analyzed for electromagnetic shielding properties. As well, more epoxy and polyester composites need to be produced in order to find a connection between the biochar characteristics, dispersion in materials, and electrical properties. The limited sample size of produced composites makes it difficult to identify any correlation between the RGB coefficient of variance and electrical conductivity. Since the statistical analysis of the digital image analysis

showed that the differences between biochar samples could be non-significant, a larger sample size could also provide more insight into whether the measured differences are due to chance or not.

References

Ahmad, S., Khushnood, R. A., Jagdale, P., Tulliani, J. M., & Ferro, G. A. (2015). High performance self-consolidating cementitious composites by using micro carbonized bamboo particles. *Materials and Design*, *76*, 223–229. http://doi.org/10.1016/j.matdes.2015.03.048

Ahmetli, G., Kocaman, S., Ozaytekin, I., & Bozkurt, P. (2013). Epoxy composites based on inexpensive char filler obtained from plastic waste and natural resources. *Polymer Composites*, *34*(4), 500–509. http://doi.org/10.1002/pc.22452

Amin, F. R., Huang, Y., He, Y., Zhang, R., Liu, G., & Chen, C. (2016). Biochar applications and modern techniques for characterization. *Clean Technologies and Environmental Policy*, *18*(5), 1457–1473. http://doi.org/10.1007/s10098-016-1218-8

Anuar Sharuddin, S. D., Abnisa, F., Wan Daud, W. M. A., & Aroua, M. K. (2016). A review on pyrolysis of plastic wastes. *Energy Conversion and Management*, *115*, 308–326. http://doi.org/10.1016/j.enconman.2016.02.037

Arenas, C., Leiva, C., Vilches, L. F., Cifuentes, H., & Rodríguez-Galán, M. (2015). Technical specifications for highway noise barriers made of coal bottom ash-based sound absorbing concrete. *Construction and Building Materials*, *95*, 585–591. http://doi.org/10.1016/j.conbuildmat.2015.07.107

ASTM Int. (2015). C518-15: Standard Test Method for Steady-State Thermal Transmission Properties by Means of the Heat Flow Meter Apparatus. *ASTM International*. http://doi.org/10.1520/C0518-10.2

Beall, C., Delzell, E., Cole, P., & Brill, I. (1996). Brain tumors among electronics industry workers. *Epidemiology (Cambridge, Mass.)*, *7*(2), 125–130. http://doi.org/10.1097/00001648-199603000-00004

Behazin, E., Ogunsona, E., Rodriguez-Uribe, A., Mohanty, A. K., Misra, M., & Anyia, A. O. (2016). Mechanical, chemical, and physical properties of wood and perennial grass biochars for possible composite application. *Bioresources*, *11*(1), 1334–1348. http://doi.org/10.15376/biores.11.1.1334-1348

Berardi, U., & Naldi, M. (2017). The impact of the temperature dependent thermal conductivity of insulating materials on the effective building envelope performance. *Energy and Buildings*, *144*, 262–275. http://doi.org/10.1016/j.enbuild.2017.03.052

Berruti, F. M. (2013). *Development and applications of a novel intermittent solids feeder for pyrolysis reactors*. Electronic Thesis and Dissertation Repository, University of Western Ontario.

Bhattacharya, P., & Das, C. K. (2013). Investigation on microwave absorption capacity of nanocomposites based on metal oxides and graphene. *Journal of Materials Science: Materials in Electronics*, *24*(6), 1927–1936. http://doi.org/10.1007/s10854-012-1036-7

Bhattacharya, P., Dhibar, S., Kundu, M. K., Hatui, G., & Das, C. K. (2015). Graphene and MWCNT based bi-functional polymer nanocomposites with enhanced microwave absorption and supercapacitor property. *Materials Research Bulletin*, *66*, 200–212. http://doi.org/10.1016/j.materresbull.2015.02.040

Braun, D., Cherdron, H., Rehahn, M., Ritter, H., & Voit, B. (2013a). Functional Polymers. In *Polymer Synthesis: Theory and Practice: Fundamentals, Methods, Experiments* (5th ed., pp. 375–395). Berlin: Springer-Verlag Berlin Heidelberg. http://doi.org/10.1007/978-3-642-28980-4

Braun, D., Cherdron, H., Rehahn, M., Ritter, H., & Voit, B. (2013b). Introduction. In *Polymer Synthesis: Theory and Practice: Fundamentals, Methods, Experiments* (5th ed., pp. 1–32). Berlin: Springer-Verlag Berlin Heidelberg. http://doi.org/10.1007/978-3-642-28980-4

Brewer, C. E., & Brown, R. C. L. D. a. (2012). *Biochar characterization and engineering*. Graduate Thesis and Dissertations, Iowa State University. http://doi.org/12284

Brewer, C. E., Schmidt-Rohr, K., Satrio, J. A., & Brown, R. C. (2009). Characterization of biochar from fast pyrolysis and gasification systems. *Environmental Progress and Sustainable Energy*, *28*(3), 386–396. http://doi.org/10.1002/ep.10378

Bridgwater, A. V. (2003). Renewable fuels and chemicals by thermal processing of biomass. *Chemical Engineering Journal*, *91*(2–3), 87–102. http://doi.org/10.1016/S1385-8947(02)00142-0

Bridgwater, A. V. (2012). Review of fast pyrolysis of biomass and product upgrading. *Biomass and Bioenergy*, *38*, 68–94. http://doi.org/10.1016/j.biombioe.2011.01.048

Bridgwater, A. V., & Peacocke, G. (2000). Fast pyrolysis processes for bomass. *Renewable & Sustainable Energy Reviews*, *4*(4), 1–73.

Briens, C., Piskorz, J., & Berruti, F. (2008). Biomass Valorization for Fuel and Chemicals Production -- A Review. *International Journal of Chemical Reactor Engineering*, *6*(May 2008), 1–49. http://doi.org/10.2202/1542-6580.1674

Brosse, N., Dufour, A., Meng, X., Sun, Q., & Ragauskas, A. (2012). Miscanthus: a fast growing crop for biofuels and chemicals production. *Biofuels, Bioproducts and Biorefining*, *6*, 580–598. http://doi.org/10.1002/bbb

Budaiwi, I., Abdou, A., & Al-Homoud, M. (2002). Variations of thermal conductivity of insulation materials under different operating temperatures : Impact on envelope-induced cooling load. *Journal of Architectural Engineering*, *8*(December), 125–132. http://doi.org/10.1061/(ASCE)1076-0431(2002)8:4(125)

Canabarro, N., Soares, J. F., Anchieta, C. G., Kelling, C. S., & Mazutti, M. a. (2013). Thermochemical processes for biofuels production from biomass. *Sustainable Chemical Processes*, *1*(1), 22. http://doi.org/10.1186/2043-7129-1-22

Cather, B. (2003). Concrete and Fire Exposure. In J. Newman & B. S. Choo (Eds.), *Advanced Concrete Technology, Volume 2* (p. 10/1-10/13). Oxford: Elsevier Ltd.

CertainTeed Corporation. (2011). Noise control for buildings: Guidelines for acoustical problem solving. Retrieved December 8, 2017, from https://www.certainteed.com/resources/30-29-121.pdf

Cha, J. S., Park, S. H., Jung, S. C., Ryu, C., Jeon, J. K., Shin, M. C., & Park, Y. K. (2016). Production and utilization of biochar: A review. *Journal of Industrial and Engineering Chemistry*, *40*, 1–15. http://doi.org/10.1016/j.jiec.2016.06.002

Chia, C. H., Gong, B., Joseph, S. D., Marjo, C. E., Munroe, P., & Rich, A. M. (2012). Imaging of mineral-enriched biochar by FTIR, Raman and SEM-EDX. *Vibrational Spectroscopy*, *62*, 248–257. http://doi.org/10.1016/j.vibspec.2012.06.006

Choi, W. C., Yun, H. Do, & Lee, J. Y. (2012). Mechanical properties of mortar containing bio-char from pyrolysis. *Journal of the Korean Institute for Structural Maintenance and Inspection*, *16*(3), 67–74.

Colomba, A. (2015). *Production of activated carbons from pyrolytic char for environmental applications*. Electroninc Thesis and Dissertation Repository, University of Western Ontario.

Das, O., & Sarmah, A. K. (2015). The love-hate relationship of pyrolysis biochar and water: A perspective. *Science of the Total Environment*, *512–513*, 682–685. http://doi.org/10.1016/j.scitotenv.2015.01.061

Das, O., Sarmah, A. K., & Bhattacharyya, D. (2015). A novel approach in organic waste utilization through biochar addition in wood/polypropylene composites. *Waste Management*, *38*(1), 132–140. http://doi.org/10.1016/j.wasman.2015.01.015

DeArmitt, C. (2011). Functional Fillers for Plastics. In M. Kutz (Ed.), *Applied Plastics Engineering Handbook- Processing and Materials* (1st ed., pp. 455–468). Oxford: William Andrew. http://doi.org/http://dx.doi.org/10.1016/B978-1-4377-3514-7.10026-1

Di Blasi, C. (2008). Modeling chemical and physical processes of wood and biomass pyrolysis. *Progress in Energy and Combustion Science*, *34*(1), 47–90. http://doi.org/10.1016/j.pecs.2006.12.001

Donaldson, E. C., Alam, W., & Begum, N. (2013). Hydraulic Fracturing Explained. In *Hydraulic Fracturing Explained: Evaluation, Implementation, and Challenges* (pp. 1–22). Houston: Elsevier Ltd. http://doi.org/10.1016/B978-1-933762-40-1.50010-6

Downie, A., Crosky, A., & Munroe, P. (2009). Physical properties of biochar. In J. Lehmann & S. Joseph (Eds.), *Biochar for Environmental Management: Science and Technology* (First, pp. 13–32). Sterling: Earthscan. http://doi.org/10.4324/9781849770552

Dufour, A., Castro-Díaz, M., Marchal, P., Brosse, N., Olcese, R., Bouroukba, M., & Snape, C.

(2012). In situ analysis of biomass pyrolysis by high temperature rheology in relations with 1 H NMR. *Energy & Fuels*, *26*(10), 6432–6441. http://doi.org/10.1021/ef301310x

FAO. (2009). *Assessment of the status of the development of the standards for the terrestrial essential climate variables: biomass*. *GTO System, Version 10*. Rome.

Ferro, G. A., Ahmad, S., Khushnood, R. A., Restuccia, L., & Tulliani, J. M. (2014). Improvements in self-consolidating cementitious composites by using micro carbonized aggregates. *Frattura Ed Integrita Strutturale*, *30*, 75–83. http://doi.org/10.3221/IGF-ESIS.30.11

Fowler, P. A., Hughes, J. M., & Elias, R. M. (2006). Biocomposites: Technology, environmental credentials and market forces. *Journal of the Science of Food and Agriculture*. http://doi.org/10.1002/jsfa.2558

Fröhlich, J., Niedermeier, W., & Luginsland, H. D. (2005). The effect of filler-filler and filler-elastomer interaction on rubber reinforcement. *Composites Part A: Applied Science and Manufacturing*, *36*(4), 449–460. http://doi.org/10.1016/j.compositesa.2004.10.004

Fryda, L., & Visser, R. (2015). Biochar for soil improvement: Evaluation of biochar from gasification and slow pyrolysis. *Agriculture*, *5*(4), 1076–1115. http://doi.org/10.3390/agriculture5041076

Gabhi, R. S., Kirk, D. W., & Jia, C. Q. (2017). Preliminary investigation of electrical conductivity of monolithic biochar. *Carbon*, *116*, 435–442. http://doi.org/10.1016/j.carbon.2017.01.069

Giorcelli, M., Khan, A. A., Tagliaferro, A., Savi, P., & Berruti, F. (2016). Microwave characterization of polymer composite based on biochar: A comparison of composite behaviour for biochar and MWCNTs. In *Proceedings - International NanoElectronics Conference, INEC* (Vol. 2016–Octob). http://doi.org/10.1109/INEC.2016.7589387

Giorcelli, M., Savi, P., Delogu, A., Miscuglio, M., Yahya, Y. M. H., & Tagliaferro, A. (2013). Microwave absorption properties in epoxy resin multi walled carbon nanotubes composites. In *2013 International Conference on Electromagnetics in Advanced Applications (ICEAA)* (pp. 1139–1141). http://doi.org/10.1109/ICEAA.2013.6632420

Gray, M., Johnson, M. G., Dragila, M. I., & Kleber, M. (2014). Water uptake in biochars: The roles of porosity and hydrophobicity. *Biomass and Bioenergy*, *61*, 196–205. http://doi.org/10.1016/j.biombioe.2013.12.010

Gupta, S., & Kua, H. W. (2017). Factors determining the potential of biochar as a carbon capturing and sequestering construction material: Critical review. *Journal of Materials in Civil Engineering*, *29*(9), 4017086. http://doi.org/10.1061/(ASCE)MT.1943-5533.0001924

Hammes, K., Smernik, R. J., Skjemstad, J. O., Herzog, A., Vogt, U. F., & Schmidt, M. W. I. (2006). Synthesis and characterisation of laboratory-charred grass straw (Oryza sativa) and chestnut wood (Castanea sativa) as reference materials for black carbon quantification.

Organic Geochemistry, *37*(11), 1629–1633. http://doi.org/10.1016/j.orggeochem.2006.07.003

Hamza, U. D., Nasri, N. S., Amin, N. S., Mohammed, J., & Zain, H. M. (2015). Characteristics of oil palm shell biochar and activated carbon prepared at different carbonization times. *Desalination and Water Treatment*, *3994*(January 2016), 1–8. http://doi.org/10.1080/19443994.2015.1042068

Hertz, K. D. (2003). Limits of spalling of fire-exposed concrete. *Fire Safety Journal*, *38*(2), 103–116. http://doi.org/10.1016/S0379-7112(02)00051-6

Hulet, C., Briens, C., Berruti, F., & Chan, E. W. (2005). A review of short residence time cracking processes. *International Journal of Chemical Reactor Engineering*, *3*. http://doi.org/10.2202/1542-6580.1139

International Organization for Standardization. (2001). ISO 10534-2, Acoustics- Determination of Sound Absorption Coefficient and Impedance in Impedance Tubes. *International Standard*. http://doi.org/ISO 10534-2:1998(E)

Jahirul, M. I., Rasul, M. G., Chowdhury, A. A., & Ashwath, N. (2012). Biofuels production through biomass pyrolysis- A technological review. *Energies*, *5*(12), 4952–5001. http://doi.org/10.3390/en5124952

Jancar, J. (1998). Structure-property relationships in thermoplastic matrices. *Advances in Polymer Sciences*, *139*, 67–107. http://doi.org/10.1007/3-540-69220-7_1

Jiang, J., Zhang, L., Wang, X., Holm, N., Rajagopalan, K., Chen, F., & Ma, S. (2013). Highly ordered macroporous woody biochar with ultra-high carbon content as supercapacitor electrodes. *Electrochimica Acta*, *113*, 481–489. http://doi.org/10.1016/j.electacta.2013.09.121

Jindo, K., Mizumoto, H., Sawada, Y., Sanchez-Monedero, M. A., & Sonoki, T. (2014). Physical and chemical characterization of biochars derived from different agricultural residues. *Biogeosciences*, *11*(23), 6613–6621. http://doi.org/10.5194/bg-11-6613-2014

Jung, S. H., & Kim, J. S. (2014). Production of biochars by intermediate pyrolysis and activated carbons from oak by three activation methods using CO2. *Journal of Analytical and Applied Pyrolysis*, *107*, 116–122. http://doi.org/10.1016/j.jaap.2014.02.011

Kan, T., Strezov, V., & Evans, T. J. (2016). Lignocellulosic biomass pyrolysis: A review of product properties and effects of pyrolysis parameters. *Renewable and Sustainable Energy Reviews*, *57*, 126–1140. http://doi.org/10.1016/j.rser.2015.12.185

Keiluweit, M., Nico, P. S., Johnson, M., & Kleber, M. (2010). Dynamic molecular structure of plant biomass-derived black carbon (biochar). *Environ. Sci. Technol.*, *44*(4), 1247–1253. http://doi.org/10.1021/es9031419

Keown, D. M., Li, X., Hayashi, J. ichiro, & Li, C. Z. (2008). Evolution of biomass char structure

during oxidation in O2 as revealed with FT-Raman spectroscopy. *Fuel Processing Technology*, *89*(12), 1429–1435. http://doi.org/10.1016/j.fuproc.2008.07.002

Kim, K.-H., Jeon, S.-E., Kim, J.-K., & Yang, S. (2003). An experimental study on thermal conductivity of concrete. *Cement and Concrete Research*, *33*(3), 363–371. http://doi.org/10.1016/S0008-8846(02)00965-1

Kinney, T. J., Masiello, C. A., Dugan, B., Hockaday, W. C., Dean, M. R., Zygourakis, K., & Barnes, R. T. (2012). Hydrologic properties of biochars produced at different temperatures. *Biomass and Bioenergy*, *41*, 34–43. http://doi.org/10.1016/j.biombioe.2012.01.033

Kloss, S., Zehetner, F., Dellantonio, A., Hamid, R., Ottner, F., Liedtke, V., … Soja, G. (2011). Characterization of slow pyrolysis biochars: Effects of feedstocks and pyrolysis temperature on biochar properties. *Journal of Environmental Quality*, *41*(4), 990–1000. http://doi.org/10.2134/jeq2011.0070

Kwapinski, W., Byrne, C. M. P., Kryachko, E., Wolfram, P., Adley, C., Leahy, J. J., … Hayes, M. H. B. (2010). Biochar from biomass and waste. *Waste and Biomass Valorization*, *1*(2), 177–189. http://doi.org/10.1007/s12649-010-9024-8

Lee, Y., Eum, P. R. B., Ryu, C., Park, Y. K., Jung, J. H., & Hyun, S. (2013). Characteristics of biochar produced from slow pyrolysis of Geodae-Uksae 1. *Bioresource Technology*, *130*, 345–350. http://doi.org/10.1016/j.biortech.2012.12.012

Lee, Y., Park, J., Ryu, C., Gang, K. S., Yang, W., Park, Y. K., … Hyun, S. (2013). Comparison of biochar properties from biomass residues produced by slow pyrolysis at 500°C. *Bioresource Technology*, *148*, 196–201. http://doi.org/10.1016/j.biortech.2013.08.135

Lehmann, J. (2007). Bio-energy in the black. *Frontiers in Ecology and the Environment*, *5*(7), 381–387. http://doi.org/10.1890/1540-9295(2007)5[381:BITB]2.0.CO;2

Lehmann, J. (2008). Energy Balance and Emissions Associated with Biochar Sequestration and Pyrolysis Bioenergy Production. *Environmental Science and Technology*, *42*(11), 2–8.

Lehmann, J., & Joseph, S. (2009). Biochar for Environmental Management : An Introduction. In J. Lehmann & S. Joseph (Eds.), *Biochar for Environmental Management: Science and Technoogy* (First, Vol. 1, pp. 1–12). Sterling: Earthscan. http://doi.org/10.1016/j.forpol.2009.07.001

Li, Z. (2011a). Introduction to concrete. In *Advanced Concrete Technology* (pp. 1–22). Hoboken: John Wiley & Sons, Inc.

Li, Z. (2011b). Materials for Making Concrete. In *Advanced Concrete Technology* (pp. 23–93). Hoboken: John Wiley & Sons, Inc. http://doi.org/10.1002/9780470950067.ch2

Li, Z. (2011c). The Future and Development Trends of Concrete. In *Advanced Concrete Technology* (pp. 476–490). Hoboken: John Wiley & Sons, Inc. http://doi.org/10.1002/9780470950067.ch9

Liu, K. (2011). Chemical composition of distillers grains, a review. *Journal of Agricultural and Food Chemistry*, *59*(5), 1508–1526. http://doi.org/10.1021/jf103512z

Lucchini, P., Quilliam, R. S., DeLuca, T. H., Vamerali, T., & Jones, D. L. (2014). Increased bioavailability of metals in two contrasting agricultural soils treated with waste wood-derived biochar and ash. *Environmental Science and Pollution Research*, *21*(5), 3230–3240. http://doi.org/10.1007/s11356-013-2272-y

Manyà, J. J. (2012). Pyrolysis for biochar purposes: A review to establish current knowledge gaps and research needs. *Environ. Sci. Technologies*, *46*, 7939–7954. http://doi.org/10.1021/es301029g

Meyer, C. (2009). The greening of the concrete industry. *Cement and Concrete Composites*, *31*(8), 601–605. http://doi.org/10.1016/j.cemconcomp.2008.12.010

Mimmo, T., Panzacchi, P., Baratieri, M., Davies, C. A., & Tonon, G. (2014). Effect of pyrolysis temperature on miscanthus (Miscanthus x giganteus) biochar physical, chemical and functional properties. *Biomass and Bioenergy*, *62*, 149–157. http://doi.org/10.1016/j.biombioe.2014.01.004

Mitchell, P. J., Dalley, T. S. L., & Helleur, R. J. (2013). Preliminary laboratory production and characterization of biochars from lignocellulosic municipal waste. *Journal of Analytical and Applied Pyrolysis*, *99*, 71–78. http://doi.org/10.1016/j.jaap.2012.10.025

Mohanty, P., Nanda, S., Pant, K. K., Naik, S., Kozinski, J. A., & Dalai, A. K. (2013). Evaluation of the physiochemical development of biochars obtained from pyrolysis of wheat straw, timothy grass and pinewood: Effects of heating rate. *Journal of Analytical and Applied Pyrolysis*, *104*, 485–493. http://doi.org/10.1016/j.jaap.2013.05.022

Moir, G. (2003). Cements. In J. Newman & B. S. Choo (Eds.), *Advanced Concrete Technology, Volume 1* (p. 1/4-1/22). Oxford: John Wiley & Sons, Inc.

Murphy, J. (2001). Modifying specific properties: Mechanical properties — fillers. In *Additives for Plastic Handbook* (2nd ed., pp. 19–35). Oxford: Elsevier Science Ltd. http://doi.org/10.1111/j.1600-0447.1951.tb04141.x

Nan, N., & DeVallance, D. B. (2017). Development of poly(vinyl alcohol)/wood-derived biochar composites for use in pressure sensor applications. *Journal of Materials Science*, *52*(13), 8247–8257. http://doi.org/10.1007/s10853-017-1040-7

Nan, N., Devallance, D. B., Xie, X., & Wang, J. (2015). The effect of bio-carbon addition on the electrical , mechanical , and thermal properties of polyvinyl alcohol / biochar composites. *Journal of Composite Materials*, *0*(0), 1–8. http://doi.org/10.1177/0021998315589770

Nanda, S., Dalai, A. K., Berruti, F., & Kozinski, J. A. (2016). Biochar as an Exceptional Bioresource for Energy, Agronomy, Carbon Sequestration, Activated Carbon and Specialty Materials. *Waste and Biomass Valorization*, *7*(2), 201–235. http://doi.org/10.1007/s12649-015-9459-z

Nanda, S., Mohanty, P., Pant, K. K., Naik, S., Kozinski, J. A., & Dalai, A. K. (2013). Characterization of North American lignocellulosic biomass and biochars in terms of their candidacy for alternate renewable fuels. *Bioenergy Research*, *6*(2), 663–677. http://doi.org/10.1007/s12155-012-9281-4

National Hog Farmer. (2017). Vomitoxin found across the Corn Belt. Retrieved December 4, 2017, from http://www.nationalhogfarmer.com/animal-health/vomitoxin-found-across-corn-belt

National Ready Mix Concrete Association. (2003). CIP 35 -Testing Compressive Strength of Concrete. Retrieved November 19, 2017, from https://www.nrmca.org/aboutconcrete/cips/35p.pdf

Natural Resources Canada. (2006). *An analysis of resource recovery opportunities in Canada and the projection of greenhouse gas implications*. Retrieved from https://www.nrcan.gc.ca/sites/www.nrcan.gc.ca/files/mineralsmetals/pdf/mms-smm/busi-indu/rad-rad/pdf/rrd2-eng.pdf

Neves, D., Thunman, H., Matos, A., Tarelho, L., & Gomez-Barea, A. (2011). Characterization and prediction of biomass pyrolysis products. *Progress in Energy and Combustion Science*, *37*(5), 611–630. http://doi.org/10.1016/j.pecs.2011.01.001

Pantea, D., Darmstadt, H., Kaliaguine, S., Sümmchen, L., & Roy, C. (2001). Electrical conductivity of thermal carbon blacks: Influence of surface chemistry. *Carbon*, *39*(8), 1147–1158. http://doi.org/10.1016/S0008-6223(00)00239-6

Peterson, S. C. (2012a). Evaluating corn starch and corn stover biochar as renewable filler in carboxylated styrene-butadiene rubber composites. *Journal of Elastomers and Plastics*, *44*(1), 43–54. http://doi.org/10.1177/0095244311414011

Peterson, S. C. (2012b). Utilization of low-ash biochar to partially replace carbon black in styrene-butadiene rubber composites. *Journal of Elastomers and Plastics*, *45*(5), 487–497. http://doi.org/10.1177/0095244312459181

Qian, K., Kumar, A., Zhang, H., Bellmer, D., & Huhnke, R. (2015). Recent advances in utilization of biochar. *Renewable and Sustainable Energy Reviews*, *42*, 1055–1064. http://doi.org/10.1016/j.rser.2014.10.074

Quaranta, S., Savi, P., Giorcelli, M., Khan, A. A., Tagliaferro, A., & Jia, C. Q. (2016). Biochar-polymer composites and thin films: Characterizations and applications. *2016 IEEE 2nd International Forum on Research and Technologies for Society and Industry Leveraging a Better Tomorrow, RTSI 2016*, 3–6. http://doi.org/10.1109/RTSI.2016.7740554

Ranzi, E., Cuoci, a, Faravelli, T., Frassoldati, a, Migliavacca, G., Pierucci, S., & Sommariva, S. (2008). Chemical kinetics of biomass pyrolysis. *Energy and Fuels*, *22*(6), 4292–4300. http://doi.org/10.1021/ef800551t

Restuccia, L., & Ferro, G. A. (2016). Promising low cost carbon-based materials to improve

strength and toughness in cement composites. *Construction and Building Materials*, *126*, 1034–1043. http://doi.org/10.1016/j.conbuildmat.2016.09.101

Roberts, K., Gloy, B., Joseph, S., Scott, N. R., & Lehmann, J. (2010). Life cycle assessment of biochar systems: Estimating the energetic, economic, and climate change potential. *Environmental Science and Technology*, *44*, 827–833. http://doi.org/10.1021/es902266r

Ronsse, F., van Hecke, S., Dickinson, D., & Prins, W. (2013). Production and characterization of slow pyrolysis biochar: Influence of feedstock type and pyrolysis conditions. *GCB Bioenergy*, *5*(2), 104–115. http://doi.org/10.1111/gcbb.12018

Rothon, R. N. (2003). *Particulate-Filled Polymer Composites* (2nd ed.). Shawbury: Rapra Technology Ltd. Retrieved from https://app.knovel.com/web/toc.v/cid:kpPFPCE001/viewerType:toc/root_slug:particulate-filled-polymer/url_slug:kt0062Q0M1

Saib, A., Bednarz, L., Daussin, R., Bailly, C., Lou, X., Thomassin, J.-M., … Huynen, I. (2006). Carbon nanotube composites for broadband microwave absorbing materials. *IEEE Transactions on Microwave Theory and Techniques*, *54*(6), 2745–2754. http://doi.org/10.1109/Tntt.2006.0874889

Schimmelpfennig, S., & Glaser, B. (2012). One step forward toward characterization: Some important material properties to distinguish biochars. *Journal of Environment Quality*, *41*(4), 1001–1013. http://doi.org/10.2134/jeq2011.0146

Schmidt, H.-P. (2012a). 55 Uses of Biochar. *Ithaka Journal*, *25*(1/2012), 13–25.

Schmidt, H.-P. (2012b). Biochar- A key technology for the planet. *Ithaka Journal*, (1/2012), 75–79. Retrieved from http://www.ithaka-journal.net/pflanzenkohle-eine-schlusseltechnologie-zur-schliesung-der-stoffkreislaufe?lang=en

Schmidt, H.-P. (2013). The use of biochar as a building material- cities as carbon sinks. *Ithaka Journal*, (1/2013). Retrieved from http://www.ithaka-journal.net/pflanzenkohle-zum-hauser-bauen-stadte-als-kohlenstoffsenken?lang=en

Scott, D. S., Piskorz, J., Bergougnou, M. A., Graham, R., & Overend, R. P. (1988). The role of temperature in the fast pyrolysis of cellulose and wood. *Industrial and Engineering Chemistry Research*, *27*(1), 8–15. http://doi.org/10.1021/ie00073a003

Scurlock, J. M. O. (1999). *Miscanthus: A review of European experience with a novel energy crop* (Vol. ORNL/TM-13). Oak Ridge. Retrieved from http://bioenergy.ornl.gov/reports/miscanthus/toc.html%5Cnfile://c/Documents and Settings/Danie/My Documents/Reference Manager/231 A review of European energy crops.pdf

Shaaban, A., Se, S. M., Dimin, M. F., Juoi, J. M., Mohd Husin, M. H., & Mitan, N. M. M. (2014). Influence of heating temperature and holding time on biochars derived from rubber wood sawdust via slow pyrolysis. *Journal of Analytical and Applied Pyrolysis*, *107*, 31–39.

http://doi.org/10.1016/j.jaap.2014.01.021

Shaw, M. T. (2012). Introduction. In *Introduction to Polymer Rheology* (pp. 1–14). Hoboken: John Wiley & Sons, Inc.

Shin, K., Lee, S., & Kim, Y. Y. (2015). Role of fine aggregates on mechanical properties of mortar Role of fine aggregates on mechanical properties of mortar. *Materials Research Innovations*, *19*. http://doi.org/10.1179/1432891715Z.0000000001778

Srinivasan, P., Sarmah, A. K., Smernik, R., Das, O., Farid, M., & Gao, W. (2015). A feasibility study of agricultural and sewage biomass as biochar, bioenergy and biocomposite feedstock: Production, characterization and potential applications. *Science of the Total Environment*, *512–513*, 495–505. http://doi.org/10.1016/j.scitotenv.2015.01.068

Suliman, W., Harsh, J. B., Abu-Lail, N. I., Fortuna, A. M., Dallmeyer, I., & Garcia-Perez, M. (2016). Influence of feedstock source and pyrolysis temperature on biochar bulk and surface properties. *Biomass and Bioenergy*, *84*, 37–48. http://doi.org/10.1016/j.biombioe.2015.11.010

Sweatman, M. B., & Quirke, N. (2001). Characterization of Porous materials by gas adsorption: Comparison of nitrogen at 77 K and carbon dioxide at 298 K for activated carbon. *Langmuir*, *17*(16), 5011–5020. http://doi.org/10.1021/la010308j

Thomas, T. L., Stolley, P. D., Stemhagen, A., Fontham, E. T., Bleecker, M. L., Stewart, P. A., & Hoover, R. N. (1987). Brain tumor mortality risk among men with electrical and electronics jobs: a case-control study. *Journal of the National Cancer Institute*, *79*(2), 233–238. http://doi.org/10.1093/jnci/79.2.233

Todd, D. B. (2010). Mixing of Fillers with Plastics. In M. Xanthos (Ed.), *Functional Fillers for Plastics: Second, updated and enlarged edition* (2nd ed., pp. 43–60). Weinheim: Wiley VCH. http://doi.org/10.1002/9783527629848.ch3

Tripathi, M., Sahu, J. N., & Ganesan, P. (2016). Effect of process parameters on production of biochar from biomass waste through pyrolysis: A review. *Renewable and Sustainable Energy Reviews*, *55*, 467–481. http://doi.org/10.1016/j.rser.2015.10.122

Ünal, O., Uygunoğlu, T., & Yildiz, A. (2007). Investigation of properties of low-strength lightweight concrete for thermal insulation. *Building and Environment*, *42*(2), 584–590. http://doi.org/10.1016/j.buildenv.2005.09.024

United States Department of Energy. (n.d.). Insulation Materials. Retrieved November 21, 2017, from https://energy.gov/energysaver/insulation-materials

Wang, K., & Brown, R. C. (2017). Prospects for fast pyrolysis of biomass. In R. C. Brown & K. Wang (Eds.), *Fast Pyrolysis of Biomass: Advances in Science and Technology* (pp. 1–11). Cambridge: Royal Society of Chemistry.

Wang, L., & Dibdiakova, J. (2014). Characterization of ashes from different wood parts of

Norway Spruce tree. *Chemical Engineering Transactions*, *37*, 37–42. http://doi.org/10.3303/CET1437007

Wei, H., Deng, S., Hu, B., Chen, Z., Wang, B., Huang, J., & Yu, G. (2012). Granular bamboo-derived activated carbon for high CO2 adsorption: The dominant role of narrow micropores. *ChemSusChem*, *5*(12), 2354–2360. http://doi.org/10.1002/cssc.201200570

Wood, C., Rosentrater, K. A., & Muthukumarappan, K. (2014). Pyrolysis of ethanol coproducts. *Industrial Crops and Products*, *56*, 118–127. http://doi.org/10.1016/j.indcrop.2014.02.039

Wypych, G. (2009). Sources of Fillers , Their Chemical Composition , Properties , and Morphology. In *Handbook of Fillers - A Definitive User's Guide and Databook (2nd ed.)* (Second, pp. 15–61). Toronto: ChemTec Publishing.

Xanthos, M. (2010a). Modification of Polymer Properties with Functional Fillers. In *Functional Fillers for Plastics: Second, updated and enlarged edition* (2nd ed., pp. 19–42). Weinheim: Wiley VCH. http://doi.org/10.1002/9783527629848.ch2

Xanthos, M. (2010b). Polymers and Polymer Composites. In *Functional Fillers for Plastics: Second, updated and enlarged edition* (2nd ed., pp. 2–18). Weinheim: Wiley VCH. http://doi.org/978-3-527-32361-6

Xie, T., Reddy, K. R., Wang, C., Yargicoglu, E., & Spokas, K. (2014). Characteristics and applications of biochar for environmental remediation: A review. *Critical Reviews in Environmental Science and Technology*, *45*(June), 939–969. http://doi.org/10.1080/10643389.2014.924180

Xu, R., Ferrante, L., Hall, K., Briens, C., & Berruti, F. (2011). Thermal self-sustainability of biochar production by pyrolysis. *Journal of Analytical and Applied Pyrolysis*, *91*(1), 55–66. http://doi.org/10.1016/j.jaap.2011.01.001

Yun, T. S., Jeong, Y. J., Han, T. S., & Youm, K. S. (2013). Evaluation of thermal conductivity for thermally insulated concretes. *Energy and Buildings*, *61*, 125–132. http://doi.org/10.1016/j.enbuild.2013.01.043

Zelinka, S. L., & Stone, D. S. (2011). Corrosion of metals in wood: Comparing the results of a rapid test method with long-term exposure tests across six wood treatments. *Corrosion Science*, *53*(5), 1708–1714. http://doi.org/10.1016/j.corsci.2011.01.039

Zhang, J., & Wang, Q. (2016). Sustainable mechanisms of biochar derived from brewers' spent grain and sewage sludge for ammonia-nitrogen capture. *Journal of Cleaner Production*, *112*, 3927–3934. http://doi.org/10.1016/j.jclepro.2015.07.096

Zhao, C., Wang, P., Wang, L., & Liu, D. (2014). Reducing railway noise with porous sound-absorbing concrete slabs. *Advances in Materials Science and Engineering*, *2014*. http://doi.org/10.1155/2014/206549

Zhao, L., Cao, X., Masek, O., & Zimmerman, A. (2013). Heterogeneity of biochar properties as

a function of feedstock sources and production temperatures. *Journal of Hazardous Materials, 256–257*, 1–9. http://doi.org/10.1016/j.jhazmat.2013.04.015

Zhao, M. Y., Enders, A., & Lehmann, J. (2014). Short- and long-term flammability of biochars. *Biomass and Bioenergy, 69*, 183–191. http://doi.org/10.1016/j.biombioe.2014.07.017

Appendix

A. Supplementary Data for Biochar Characterization and Concrete Characterization

The following data represents the biochar that was characterized from different pyrolysis experiments, where the results were presented as an average of what is shown below.

Table A.1- Full list of proximate characteristics of biochar form unmodified pyrolysis experiments

Run	*Feedstock*	*Temperature (°C)*	*Volatile Matter (wt%)*	*Fixed Carbon (wt%)*	*Ash Content (wt%)*
1	MS, Drumbo	550	17.4	71.9	10.7
2	MS, Drumbo	550	19.4	70.6	10.0
3	MS, Drumbo	500*	30.5	60.3	10.2
4	MS, Drumbo	500	22.5	67.8	9.8
5	MS, Drumbo	500**	27.7	64.2	8.1
6	MS, Drumbo	450	32.1	32.1	8.0
7	MS, AWF	500	24.1	62.8	13.1
8	MS, AWF	450	28.9	59.2	12.0
9	MS, AWF	400	31.0	56.5	12.5
10	MS, AWF	350	47.2	45.5	7.3

* This material was not used in the average value as it appeared to have not undergone complete pyrolysis.

**This material was not used in the average due to a line rupturing mid experiment.

Table A.2- Full set of proximate characteristics of biochar from continuous pyrolysis experiments*

Run	*Feedstock*	*Temperature (°C)*	*Volatile Matter (wt%)*	*Fixed Carbon (wt%)*	*Ash Content (wt%)*
1	MS, AWF	550	22.4	68.2	8.9
2	MS, AWF	550	14.5	74.6	10.9
3	MS, AWF	550	18.3	70.7	11.0
4	MS, AWF	450	29.5	59.9	10.6
5	MS, AWF	450	26.3	63.2	10.6
6	MS, AWF	450	32.7	55.8	11.5
7	MS, AWF	350	40.3	54.1	5.5
8	MS, AWF	350	45.6	47.7	6.7
9	Wood Chips	550	21.3	54.9	23.8
10	Wood Chips	550	16.3	29.1	54.6
11	Wood Chips	450	25.0	50.6	24.4
12	Wood Chips	450	23.4	39.5	36.0
13	Wood Chips	350	32.8	57.2	10.0
14	Wood Chips	350	43.5	42.8	13.8
15	DDG	500	35.0	46.5	14.2
16	DDG	500	51.2	38.0	10.93
17	DDG	500	34.9	50.0	15.1
18	DDG	400	56.3	34.1	9.6
19	DDG	400	51.8	36.6	11.7

* The averages reported in the thesis are the weighted averages of all experiments, as all samples from this experiment were mixed.

Table A.3- Full list of concrete densities for all produced shapes

		DENSITY OF CONCRETE SHAPE (kg/m^3)			
SAMPLE	**MATERIAL**	**SHAPE 1**	**SHAPE 2**	**SHAPE 3**	**SHAPE 4**
STD	None	2172	2121	2134	2240
AC-1	AC	1875	1954	1833	N/A
AC-2	AC	1690	1708	1735	N/A
AC-3	AC	2070	2083	1977	N/A
AC-4	AC	2066	2053	1923	N/A
AC-5	AC	1911	1798	1830	N/A
AC-6	AC	1768	1858	1923	N/A
AC-7	AC	N/A	N/A	1370	N/A
AC-8	AC	N/A	1402	1434	N/A
1	BC1	1948	2001	1931	N/A
2	BC1	1954	1978	1967	N/A
3	BC1	1752	1757	1720	N/A
4	BC1	1672	1700	1809	N/A
5	BC1	N/A	1481	1517	N/A
6	BC1	N/A	1434	1474	N/A
7	BC1	1615	N/A	N/A	N/A
8	BC1	1654	N/A	N/A	N/A
9	BC1	2310	2201	2179	2072
10	BC1	2271	2181	2174	2214
11	BC1	2215	2244	2148	2212
12	BC1	2154	2131	2168	2146
13	BC1	2134	2169	2191	2220
14	BC1	2106	2144	2146	2179
15	BC1	2020	2185	2114	N/A
16	BC1	2109	2035	2094	N/A
17	BC3	2145	2083	2000	2215
18	BC2	2177	2128	2186	2204
19	BC2	2153	2101	2201	2191
20	BC2	2097	2010	2199	2162
21	BC2	2198	2161	2085	2209
22	BC2	2155	2120	2105	2106
23	BC2	2160	2107	2136	2118

Curriculum Vitae

Name: Douglas Matthew Cuthbertson

Post-Secondary Education and Degrees:
The University of British Columbia
Vancouver, British Columbia
2010-2014 B.A.Sc

The University of Western Ontario
London, Ontario
2015-2018 M.E.Sc

Honours and Awards:
Graham Somerville Undergraduate Scholarship
Chemical and Biological Engineering Department, The University of British Columbia
Vancouver, British Columbia 2013

Queen Elizabeth II Ontario Graduate Scholarship
School of Graduate and Postdoctoral Studies, The University of Western Ontario
London, Ontario 2015

First Prize Winner, Poster Presentations
14th International Symposium on Bioplastics, Biocomposites, and Biorefining
Guelph, Ontario 2015

Related Work Experience:
Graduate Teaching Assistant
The University of Western Ontario
2014

Undergraduate Laboratory Assistant
The University of British Columbia
2013

Presentations:
"Production of Biochar for Value-Added Composite Materials"
CBE Graduate Seminar Series, The University of Western Ontario
London, Ontario 2017

"Production of Biochar and Development of Predictive Methods for Determining Performance in in Value-Added Composite Materials"
Biochar: Production, Characterization, and Applications
Alba, Italy 2017

"The Production of Biochar from Different Canadian Feedstocks"
Biocarbon Annual Research Meeting
Guelph, Ontario 2017